UNIVERSITY OF MICHIGAN
MAR 28 1956
CHEMISTRY LIBRARY

Journal of Research

of the

National Bureau of Standards

JANUARY 1956

VOLUME 56 NUMBER 1

U. S. DEPARTMENT OF COMMERCE
Sinclair Weeks, Secretary
NATIONAL BUREAU OF STANDARDS
A. V. Astin, Director

JANUARY • 195
VOLUME • 5
NUMBER •

JOURNAL OF RESEARCH
of the
NATIONAL BUREAU OF STANDARDS

PERIODICALS OF THE NATIONAL BUREAU OF STANDARDS
(Published monthly)

The National Bureau of Standards is engaged in fundamental and applied research in physics, chemistry, mathematics, and engineering. Projects are conducted in fifteen fields: electricity and electronics, optics and metrology, heat and power, atomic and radiation physics, chemistry, mechanics, organic and fibrous materials, metallurgy, mineral products, building technology, applied mathematics, data processing systems, cryogenic engineering, radio propagation, and radio standards. The Bureau has custody of the national standards of measurement, and conducts research leading to the improvement of scientific and engineering standards and of techniques and methods of measurement. Testing methods and instruments are developed; physical constants and properties of materials are determined; and technical processes are investigated.

JOURNAL OF RESEARCH

The Journal presents research papers by authorities in the specialized fields of physics, mathematics, chemistry, and engineering. Complete details of the work are presented, including laboratory data, experimental procedures, and theoretical and mathematical analyses. Annual subscription: domestic, $4.00; $1.25 additional for foreign mailing.

TECHNICAL NEWS BULLETIN

Summaries of current research at the National Bureau of Standards are published each month in the Technical News Bulletin. The articles are brief, with emphasis on the results of research, chosen on the basis of their scientific or technologic importance. Lists of all Bureau publications during the preceding month are given, including Research Papers, Handbooks, Applied Mathematics Series, Building Materials and Structures Reports, Miscellaneous Publications, and Circulars. Each issue contains 12 or more two-column pages; illustrated. Annual subscription: domestic, $1.00; 35 cents additional for foreign mailing.

BASIC RADIO PROPAGATION PREDICTIONS

The Predictions provide the information necessary for calculating the best frequencies for communication between any two points in the world at any time during the given month. The data are important to all users of long-range radio communications and navigation, including broadcasting, airline, steamship, and wireless services, as well as to investigators of radio propagation and ionosphere. Each issue, covering a period of one month, is released three months in advance and contains 16 large pages, including pertinent charts, drawings, and tables. Annual subscription: domestic, $1.00; 25 cents additional for foreign mailing.

Order all publications from the Superintendent of Documents
U. S. Government Printing Office, Washington 25, D. C.

The printing of this publication has been approved by the Director of the Bureau of the Budget, May 12, 1953.

Journal of Research of the National Bureau of Standards Vol. 56, No. 1, January 1956 Research Paper 2641

Dielectric Constant of Water from 0° to 100° C

C. G. Malmberg and A. A. Maryott

An equal ratio arm, capacitance-conductance bridge, operated at frequencies below 100 kilocycles per second, was used to measure the dielectric constant of water with an accuracy of better than 0.1 percent at 5-degree intervals over the range 0° to 100° C. At 25° C the dielectric constant was found to have the value 78.30, which is about 0.3 percent lower than that usually accepted. The data fit the equation

$$\epsilon = 87.740 - 0.40008t + 9.398(10^{-4})t^2 - 1.410(10^{-6})t^3,$$

with a maximum deviation of 0.01 unit in dielectric constant. The experimental method and sources of error are considered in some detail.

1. Introduction

Numerous determinations of the dielectric constant of water have been reported in the literature during the past half century.[1] However, much of this work was not conducted with sufficient accuracy to provide data adequate for reference purposes. Several of the more recent investigators [1,2,3,4,5],[2] employing varied experimental techniques in which the accuracy was stated or has been inferred to be of the order of 0.1 percent, report values that are in close agreement at room temperature but not at higher and lower temperatures. Discrepancies amounting to a percent or more exist at higher temperatures.

This investigation was undertaken to redetermine the dielectric constant of water over the range 0° to 100° C with an accuracy better than 0.1 percent. A low-frequency bridge method with a Wagner earth to permit the use of three-terminal dielectric cells was employed. The various methods of measurement, generally some form of bridge or resonance method, are all more or less subject to errors associated with the residual impedances of the network that are enhanced when the medium possesses appreciable conductivity. The present assembly has the advantage of facilitating the minimization, ready control, and accurate evaluation of these residual errors, and of simplifying certain problems regarding the design of cells suitable for accurate absolute measurements.

The values of dielectric constant reported in this investigation are significantly lower than previously assigned values [6], about 0.3 percent at 25°, but the variation of dielectric constant with temperature is substantially the same as reported by Wyman and Ingalls [5] except at the lowest temperatures.

2. Apparatus

The a-c bridge is of the equal-ratio arm, capacitance-conductance type, with a Wagner earth. The Wagner earth permits use of either two- or three-terminal cells, and in conjunction with proper shielding, either eliminates or fixes the influence of ground admittances and interbranch couplings. A schematic diagram of the circuit is shown in figure 1. The basic network and its components, with the exception of the unknown arm and standard capacitor, are substantially the same as those described previously [7].

The unknown arm contains a shielded 3,000-ohm resistor, R, and a small capacitor, C, in parallel with the guarded capacitance, C_x, of the test cell in order to provide convenient "zero" settings for the standards, C_m and R_4, of the measuring arm. The capacitance of the test cell is measured in terms of C_m by connecting the cell in parallel first with C and then with Z_5 of the Wagner earth by means of the switch, K. In the latter case the cell is effectively removed from the main bridge circuit because its earth-potential electrode is connected to ground, and admittances from any corner of the bridge to ground do not affect the conditions of balance.

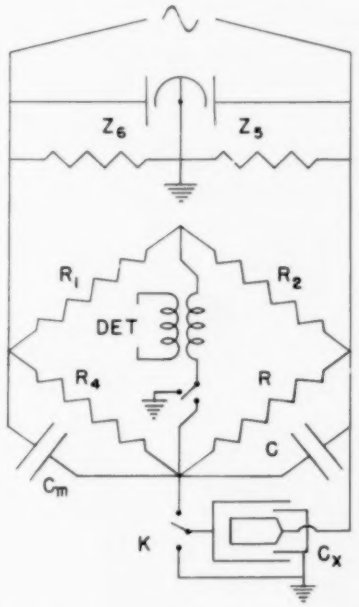

FIGURE 1. *Schematic diagram of the bridge circuit.*

[1] For an extensive compilation and comparison of data prior to 1937, see N. E. Dorsey, Properties of ordinary water substance, ACS Monograph, (Reinhold Publishing Co., New York, N. Y., 1940).

[2] Figures in brackets indicate the literature references at the end of this paper.

The three cells used were designed for "absolute" measurements, the insulating supports being located where they should not affect the desired interelectrode capacitances. Intercomparisons between the three cells, using media of various dielectric constants, indicated that these capacitances varied linearly with the dielectric constant of the medium. Because accurate measurements become increasingly difficult as the conductivity of the medium increases, the materials of construction of the two cells, *A* and *B*, used with water, were selected to minimize electrolytic contamination. Cell *C* was used only for intercomparisons with liquids of lower dielectric constant and conductivity.

Cell *A* is a fixed, three-terminal, cylindrical capacitor. A schematic drawing is shown in figure 2. The base material is copper, with the electrode surfaces coated with pure tin. The central, or high-potential, electrode, *H*, is supported by the grounded guard electrode, *G*. Electrical insulation and a liquid-tight seal are provided by 0.01-in. Teflon gaskets on each side of the silvered copper spacer, *F*, and by a Bakelite bushing on the upper side. The high-potential terminal is electrostatically isolated from the case by the removable shield, *S*. The guard electrode is supported on the outer case, which, in part, serves as the earth-potential electrode *D*, by means of a Pyrex-glass ring and 0.01-inch Teflon gaskets, and held by six bolts insulated from the guard electrode by Bakelite bushings. To prevent the trapping of gas in the annular space between the guard and the earth potential electrodes when the cell is being filled with liquid, four 1-mm holes were drilled through *G* at level *E*. A Pyrex-glass reservoir is attached to a silvered copper tube extending from the bottom of the cell, as shown at the left of figure 3, to facilitate the introduction and manipulation of fluids. Coaxial cable, with the outer conductor grounded, connects the cell to the appropriate bridge terminals. Coupling between the exposed, earth-potential electrode and other components of the network is prevented by proper shielding. As lead, shield, and guard capacitances are all effective directly to ground, only the capacitance between the test electrodes, *D* and *H*, is measured. This capacitance in air is about 34 $\mu\mu$f.

Cell *B*, shown at the right in figure 3, is of the differential type. It was constructed from a General Radio type 568–D variable air capacitor modified in several respects. The number of plates was reduced to give a replaceable capacitance of about 28 $\mu\mu$f, and all metal surfaces were tinned. The steatite insulators were replaced with Pyrex glass and partially shielded to minimize any effect of the insulation on the differential capacitance. The unit was mounted in a gold-plated brass case. The rotor control handle is variable between fixed stops mounted on the cover. The high-potential stator plates bracket the earth-potential rotor plates when interleaved to avoid varying the stray fields through the insulating supports. Both are isolated from the case except when the cell is used as a two-terminal capacitor. Then the rotor plates and the case are connected together. A comparison (table 1) of the values of dielectric constant obtained for a given medium when the cell is used as both a two- and a three-terminal capacitor provides a check of the linearity of its replaceable interval of capacitance with respect to dielectric constant. Any nonlinear effects associated with the insulating supports should differ in the two cases.

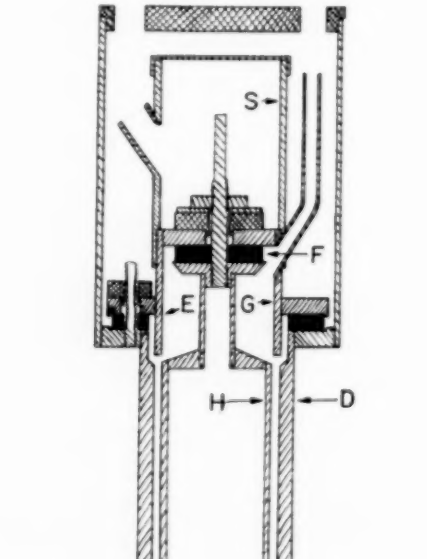

FIGURE 2. *Sectional view of cell A.*

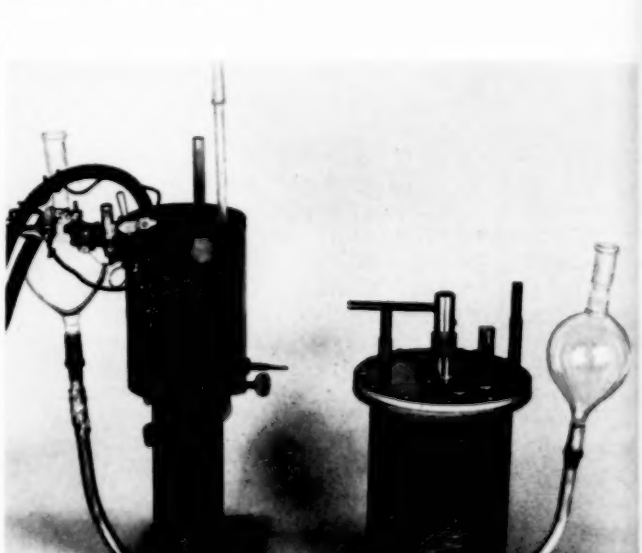

FIGURE 3. *Cell A (left) and cell B (right).*

Cell C is also of the differential type, and similar in design to cell B. It consists of a General Radio type 539–J variable air capacitor, mounted in a brass container, and has a replaceable capacitance of about 500 $\mu\mu$f. Both electrodes are insulated from the case to permit use as either a three- or a two-terminal capacitor.

The standard capacitor, C_m, is a General Radio type 722–D variable precision capacitor with the following modifications: The original wood case, lined with sheet copper, was replaced by a metal case to improve the stability of capacitance; in addition, an external worm and gear drive was mounted on the panel to expand the scale and to allow a precision of setting of 0.01 $\mu\mu$f on the 100 to 1,100 $\mu\mu$f range. The capacity of this interval was assumed to be exact and was calibrated internally in the conventional stepwise manner, using the replaceable air capacitances of cells A and B and other larger and smaller fixed increments. Calibrations made several times during the course of the measurements on water and with the different increments were consistent to 0.05 $\mu\mu$f or better throughout the range of the precision capacitor. The total backlash associated with the setting of this capacitor amounts to about 0.005 $\mu\mu$f on the 100 to 1,100 $\mu\mu$f range and about one-tenth of this value on the 25 to 110 $\mu\mu$f range. Mica capacitors, General Radio type 505, were plugged to the terminals of the precision capacitor to extend its range as needed. These were calibrated in terms of the standard capacitor at the required frequencies, and over a period of a year their capacitances were found to remain constant to better than 0.01 percent.

The apparatus was contained in a constant-temperature room maintained at 23° C. The cells were placed in a grounded oil bath controlled to better than 0.01 deg and the temperatures determined with a platinum resistance thermometer. Cell A was immersed to within 1 inch of the top and the exposed portion provided with adequate thermal shielding. Experimental evidence showed that without such shielding, significant thermal gradients existed within the cell at the higher temperatures. Cells B and C were immersed so that the oil just covered the lids and were used only for measurements at 25° C.

3. Water

Distilled water was obtained as required from the regular supply piped to the laboratory. This supply is free of ammonia and has an average conductivity of 0.5 micromho/cm at 25°, due mainly to dissolved CO_2. Each sample was boiled in the test cell prior to measurement. This procedure was effective in removing dissolved air in order both to eliminate the tendency for bubbles to form between the electrodes and to reduce the CO_2 content, thereby decreasing conductivity. An atmosphere of hydrogen was thereafter maintained in the cell. After thorough cleaning and leaching of the cell, it was possible to keep the conductivity of the water in the range 0.1 to 1.7 micromho/cm at all temperatures and to avoid rapid drifts, which would interfere with the precision of capacitance balance.

4. Procedure and Errors

If C_x is the true interelectrode capacitance of the fixed, guarded cell, A, when filled with a medium of dielectric constant, ϵ_x, then

$$\epsilon_x = C_x/C_v = \epsilon_k C_x/C_k, \tag{1}$$

where C_v is the capacitance in vacuum, C_k the capacitance in air, and ϵ_k the dielectric constant of air. If the residual impedances associated with the bridge network are negligibly small, the interelectrode capacitance is obtained directly as the difference in capacitance of the standard capacitor, $C_m - C_m'$, where C_m and C_m' are the capacitances measured with the cell connected to the appropriate bridge terminals and with the earth-potential electrode connected directly to ground, respectively. In practice, errors that may seriously limit the accuracy of the measurements of dielectric constant can arise from the effects of residual impedances associated with the leads and components of the bridge circuit. Although these errors can be minimized by careful design of the network and the selection of components, by optimum choice of frequency and cell capacitance, and by avoiding excessively high conductivities resulting from electrolytic contamination of the medium, it is often not feasible to reduce these errors to negligible proportions, and procedures must be devised for their evaluation.

If the admittances between each test electrode and the guard electrode of the cell are neglected for the moment, the actual network can be simulated by that shown in figure 4. The effective capacitances of the ratio arms are represented by C_1 and C_2, the self-inductance of the standard condenser and its leads by l_m, the effective series inductance of the

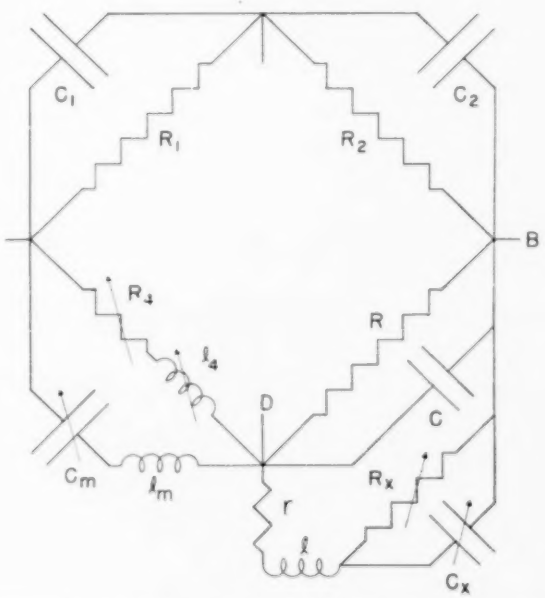

FIGURE 4. *Schematic circuit showing the distribution of residual impedances in the bridge network.*

resistance box by l_4, the cell resistance by R_x, and the inductance and resistance of the leads to the cell by l and r. The residual impedances associated with the fixed 3,000-ohm resistor, R, and small condenser, C, of the unknown arm are neglected, as they do not alter the error analysis to follow. The cell capacitance is given by

$$C_x=(C_m-C_m')+C_a+C_b+C_c+C_d+C_e, \qquad (2)$$

where, neglecting terms of higher order,

$$C_a=(C_1-C_2)(R_1/R_4-R_1/R_4'),$$
$$C_b=l/R_x^2+l_4'/R_4'^2-l_4/R_4^2,$$
$$C_c=-2rC_x/R_x,$$
$$C_d=\omega^2 l_m(C_m'^2-C_m'^2)-\omega^2 l C_x^2\cong\omega^2(l_m-l)C_x^2.$$

C_e, the capacitance due to electrode polarization, varies approximately as ω^{-n}, where ω is the angular frequency and n generally lies between 1.5 and 2 but is virtually constant for a given experiment and temperature. The unprimed symbols refer to the case where the cell is connected in the normal manner, and the primed symbols to the case where the earth-potential electrode is connected directly to ground.

The errors attributable to C_d and C_e, being functions of the frequency, were eliminated in the following manner. In each instance values of C_m were obtained at 3, 6, 12, 24, 48, and 96 kc. A representative plot of such data is shown by the solid line of figure 5. At the lower frequencies the variation of C_m is due predominately to electrode polarization, and the error associated with the lead inductances is negligible or greatly minimized, whereas the converse is true at the higher frequencies. The unbalance in lead inductances, l_m-l, which amounted to 1.2 μh, was determined experimentally and the appropriate correction made, as indicated by the broken line of figure 5. Extrapolation of this latter curve to infinite frequency then gives the cell capacitance, corrected for the frequency-dependent errors. Determinations of l_m-l were made both during the normal course of the measurements on water at the lowest temperatures, where electrode polarization was negligible at all but the lowest frequencies, and by plugging sufficient capacitance in the form of the mica standards across the empty cell and standard condenser to cause a readily measurable change of capacitance balance with frequency. The uncertainty in the value of the dielectric constant of water associated with these corrections is definitely less than 0.01 unit.

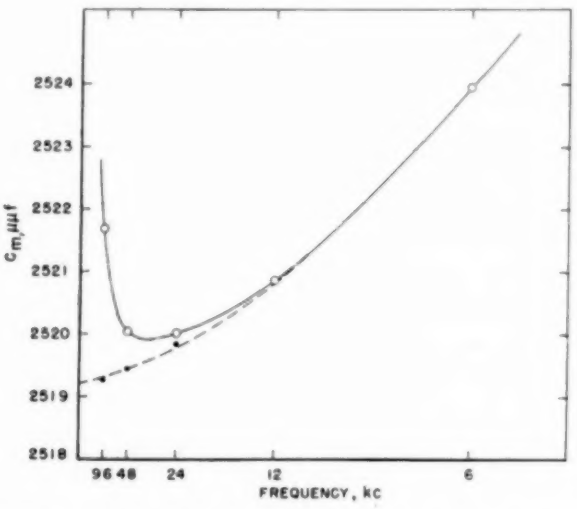

FIGURE 5. *Capacitance C_m plotted on an inverse frequency scale.*

_____ measured values, _ _ _ _ _ after correction for C_d.

Of the remaining terms in eq (2), C_c is not significant in the present case as long as good electric contacts are maintained. The sum of the errors C_a+C_b, which depend upon the resistance balance, was obtained by a modification of the procedure previously described [7]. The dielectric cell was replaced by a conductivity cell of negligible capacitance, with l kept very nearly the same. The resistance of the cell filled with distilled water was then decreased in small steps by the addition of a solution of KCl. The change in C_m required to rebalance the bridge was observed at about 10-ohm intervals. The entire range of R_4 required for the measurements on water, namely, 1,000 to 3,000 ohms, was calibrated in this manner, using a frequency sufficiently high to avoid any effects of electrode polarization. The range 1,000 to 2,600 ohms was also calibrated directly, using cell *A*. In this case the resistance was changed by the addition or removal of small amounts of CO_2. Both calibrations were in satisfactory agreement. The correction for C_a+C_b, which, in the extreme case, amounted to about 0.07 unit in dielectric constant, should not lead to an uncertainty greater than 0.005 unit.

Determination of the replaceable capacitance of the cell when filled with dry air, C_k, was made as part of the procedure employed for calibrating the standard capacitor. Thus, C_k was equal to the total interval of capacitance that could be covered in integral steps of C_k divided by the number of steps. Four determinations of C_k, made at various times during the measurements on water, gave an average deviation of 0.007 percent. The variation of C_k with temperature was obtained from measurements at a number of temperatures in the range 0 to 100°, using the low range of the standard condenser, where a precision of setting of 0.001 $\mu\mu$f was possible. When C_k is corrected to vacuum, using adequate values for the dielectric constant of air [8], the vacuum capacitance, C_v, is given by

$$(C_v)_t=33.76_1[1+1.8_0(10^{-5})(t-25)]\mu\mu\text{f}.$$

The change with temperature is very nearly the same as predicted from the linear coefficient of expansion of copper.

Determinations of the dielectric constant of water were made in cell A at 5-deg intervals, using two or more samples of water at each temperature. As a further check on the correction for C_a+C_b, the use of samples of corresponding conductivity was avoided. Without exception, the values of dielectric constant obtained at each temperature agreed to 0.01 unit or better with respect to their mean.

As an over-all check on the accuracy of the measurements with cell A, some additional experiments were made at 25° C, using auxiliary cells B and C both as two- and as three-terminal cells. The nature of the residual errors and the procedures used in their evaluation are similar to those discussed above for cell A. However, as these cells are of the differential type, they require twice as many measurements of capacitance and associated corrections. The dielectric constant of water was redetermined in cell B, whereas ethylene chloride and 2-ethylhexanol were measured in cell C. The latter materials were of technical grade. The degree of purity was immaterial as the sample was used for intercomparison in cell A. The values of dielectric constant obtained with the three cells are listed in table 1. The differences are quite negligible except in the case of water, where cell B gives a value about 0.03 percent larger than cell A. However, as the experimental uncertainties associated with cell B are at least twice those of cell A, this difference is hardly significant.

TABLE 1. *Intercomparison of values of dielectric constants measured at 25° C with the different cells*

Cell	Dielectric constant		
	Water	$C_5H_{12}O$[a]	$C_2H_4Cl_2$[a]
A	78.30$_1$	6.831$_6$	10.376
B 2-terminal	78.32$_5$		
B 3-terminal	78.32$_7$		
C 2-terminal		6.831$_2$	10.377
C 3-terminal		6.831$_4$	10.378

[a] Technical grade, unpurified.

It was assumed in the previous analysis that the test cell and its leads are adequately represented by the series-parallel combination of r, l, and C_x, and R_x, shown in figure 4, for which the equivalent parallel capacitance is given to a sufficient approximation by

$$C_p=C_x(1+\omega^2 lC_x-2r/R_x)-l/R_x^2. \tag{3}$$

A more rigorous consideration of its properties as a three-terminal impedance with associated leads results in the equivalent circuit of figure 6. D, B, and G are the points of connection to the bridge and to ground, and D', B', and G' are the corresponding electrodes of the cell. Analysis of this circuit was made by using the star-mesh transformation [9]. The equivalent parallel capacitance is given to a sufficient approximation by

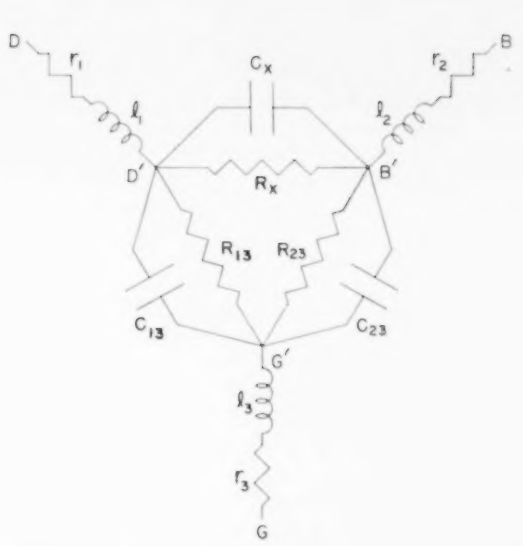

FIGURE 6. *Schematic circuit for the three-terminal cell.*

$$C_p=C_x\left[1+\omega^2 l_2(C_{23}+C_x)+\omega^2 l_1(C_{13}+C_x)-\frac{r_2(R_{23}+R_x)}{R_{23}R_x}\right.$$

$$\left.-\frac{r_1(R_{13}+R_x)}{R_{13}R_x}\right]-\frac{l_2(R_{23}+R_x)}{R_{23}R_x^2}-\frac{l_1(R_{13}+R_x)}{R_{13}R_x^2}-\frac{r_2(C_{23}+C_x)}{R_x}$$

$$-\frac{r_1(C_{13}+C_x)}{R_x}+\frac{r_3(C_{13}R_{13}+C_{23}R_{23})+l_3(1-\omega^2 C_{13}C_{23}R_{13}R_{23})}{R_{13}R_{23}}. \tag{4}$$

It is evident from this relation that significant lead impedances can seriously limit the utility of a three-terminal cell unless the admittances from each of the test electrodes to the guard electrode are kept small compared to the direct admittance between the test electrodes. The procedures described previously for evaluating the residual errors are not entirely valid when the effective capacitance is calculated by eq (4) rather than eq (3). In the present measurements, however, where the admittances to the guard electrode were comparatively small, computations indicate that the use of eq (3) should not lead to an error in dielectric constant greater than 0.01 unit in any case. In fact, if any difficulty had arisen from this simplification, it would have become evident at various stages during the course of the measurements, as, for example, in a discrepancy in the calibrations for C_a+C_b when the conductivity and dielectric cells were used.

5. Results

The values of the dielectric constant of water measured over the range 0.1° to 99° C fit the equation

$$\epsilon=87.740-0.4008t+9.398(10^{-4})t^2-1.410(10^{-6})t^3, \tag{5}$$

where t is the temperature in degrees Celsius. The

values computed from this equation are listed in table 2, together with the differences between these values and those actually measured at each of the specified temperatures. The maximum difference does not exceed 0.01 unit. The last two columns list the values of $d\epsilon/dt$ and the temperature coefficient $(1/\epsilon)(d\epsilon/dt)$. It is interesting to note that the temperature coefficient is remarkably constant over the entire range. In fact, the alternative relation

$$\log_{10}\epsilon = 1.94315 - 0.0019720t, \qquad (6)$$

fits the data nearly as well as eq (5). In this case the maximum deviation is 0.02 and the average deviation 0.01 unit in dielectric constant.

It is estimated that the over-all accuracy of the tabulated values of dielectric constant is ± 0.05 unit or better, and that the temperature coefficient is determined to 1 percent or better at all temperatures.

TABLE 2. *Dielectric constant of water and related data at various temperatures*

t	ϵ eq (5)	ϵ eq (5) $-\epsilon$ obs.	$-d\epsilon/dt$	$-\frac{1}{\epsilon}\frac{d\epsilon}{dt}$
°C				
0	87.740		0.4001	4.560×10^{-3}
0.1	87.700	+0.004		
5	85.763	−.001	.3908	4.557
10	83.832	−.002	.3817	4.553
15	81.946	−.004	.3729	4.550
20	80.103	+.003	.3642	4.547
25	78.304	+.003	.3557	4.543
30	76.546	+.006	.3475	4.539
35	74.828	−.004	.3395	4.537
40	73.151	+.002	.3317	4.534
45	71.512	+.004	.3241	4.532
50	69.910	−.007	.3167	4.530
55	68.345	.000	.3095	4.529
60	66.815	−.005	.3025	4.528
65	65.319	+.002	.2958	4.528
70	63.857	−.002	.2892	4.529
75	62.427	+.009	.2829	4.531
80	61.027	+.008	.2768	4.535
85	59.659	+.001	.2709	4.541
90	58.319	+.005	.2652	4.547
95	57.007	−.001	.2597	4.555
99	55.977	−.008		
100	55.720		.2544	4.566

6. Discussion

A comparison of the present data with those reported, over a wide range of temperature, by certain investigators in the last quarter century is shown in figure 7. The differences between the values of dielectric constant obtained in the earlier work and the present investigation are plotted as a function of the temperature. Smooth curves are shown where the data were fitted to empirical relations. With respect to the variation of dielectric constant with temperature, only the data of Wyman and Ingalls [5], which were obtained in terms of Wyman's [1] value at 25° C, are in satisfactory agreement with the present measurements over an extended interval of temperature. Although their values are consistently higher, the temperature coefficient derived from the two sets of data agrees to better than 1 percent at all temperatures above 20° C.

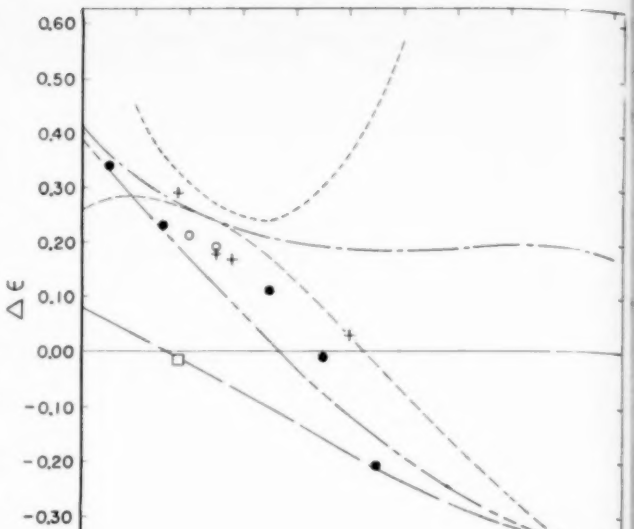

FIGURE 7. *Comparison of the differences in the values of the dielectric constant of water obtained by various workers.*

$\Delta\epsilon = \epsilon$ literature $-\epsilon$ present work.
- Drake, Pierce, and Dow (1930).
- Wyman and Ingalls (1938).
- Wyman (1930).
- Åkerlöf and Oshry (1950). [11].
- Lattey, Gatty, and Davies (1931).
- + Albright (1937).
- ● Albright and Gosting (1946).
- ○ T. T. Jones and R. M. Davies (1939).
- □ Mean of 17 values selected from literature, Lattey, Gatty, and Davies (1931).

Various reported values of the dielectric constant at 25° C are compared in table 3. The value of Lattey, Gatty, and Davies [10] resulted from a survey of the literature prior to 1930. Although this value is closest to that obtained here, the agreement is not significant because of the wide scatter in the individual results (mean deviation ± 0.4 unit). The remaining values, each obtained by a different experimental procedure and considered to have an accuracy of the order of 0.1 percent, are roughly 0.3 percent higher than that reported in this investigation. The close agreement between these earlier values at 25° C would appear to be rather fortuitious in view of the sizable discrepancies existing at other temperatures, as shown by figure 7.

TABLE 3. *Comparison of values of the dielectric constant of water at 25° C*

ϵ_{25}	Method	Frequency	Authors
78.25	Mean of 17 reported values prior to 1930.		Lattey, Gatty, Davies (1931).
[a]78.54	Resonators suspended in medium.	4 to 81 Mc	Wyman (1930).
78.57	Standing waves in coaxial line.	12 to 77 Mc	Drake, Pierce, Dow (1930).
[a]78.48	Bridge	570 kc	Albright (1937).
[a]78.49	Voltage resonance	670 kc	Jones and Davies (1939).
78.30	Bridge	3 to 96 kc	Present work.

[a] Values apparently relative to air rather than to vacuum.

Although the work of Jones and Davies [4] was of high precision and conducted with unusual care and attention to possible sources of error, the method was a comparative one in which benzene was employed as the primary standard. Consequently, any error in the assumed value for the dielectric constant of benzene would result in a percentage error nearly twice as large in the value for water. Furthermore, direct comparisons of water and benzene in the same cell were not feasible, so that additional cells and liquids of intermediate dielectric constant were required. The number of operations upon which the value for water was dependent was thereby increased and the over-all uncertainties of the method somewhat enhanced. In view of these limitations the difference between this and the present work does not appear to be excessively large. In fact, if the data of Jones and Davies are corrected for the value of benzene recently recommended [6], this difference is reduced to about 0.1 percent.

The remaining values in table 3 were obtained by methods essentially absolute in that no standard medium other than air was needed. Because of the lack of experimental detail pertinent to the possible sources of error in the report of Albright [3], no detailed comment on this work is possible. The experimental methods of Wyman [1] and of Drake, Pierce, and Dow [2] were comparatively direct and simple in principle. Although the experimental precision was less than that obtainable with conventional bridge and resonance methods, this disadvantage was seemingly offset by the reduction or avoidance of troublesome residual errors. In both cases the value reported at 25° C was the mean of a number of values obtained at various frequencies which had a spread of more than 0.3 percent.

The method of Wyman involves the determination of the resonant frequencies of fixed, metallic resonators suspended in the medium. Seven resonators of several different designs and of varying frequencies were employed. Exclusive of the value obtained with the resonator of lowest frequency, which was about 5 percent too high, the values of dielectric constant, when corrected to 25° C, ranged from 78.42 to 78.70. It was assumed that these resonators behaved as idealized lumped circuits of inductance L and capacitance C, so that the resonant frequency $f=1/[2\pi(LC)^{1/2}]$. Then $\epsilon=f_0^2/f^2$, where f_0 is the resonant frequency in vacuum, and f is the corresponding frequency in the medium. The strict validity of this relation is questionable because of the effect of conductance of the medium on the properties of resonant circuits and the dependence of the inductance and resistance of metallic conductors upon frequency through the "skin effect." A change in inductance due to the skin effect would lead to a high value for the dielectric constant. Although the magnitude of this error is difficult to evaluate without more specific details regarding the construction of the resonators, estimates based upon simple U-loops, which simulate the form of inductance in some of the resonators, indicate that an error of the order of several tenths of 1 percent is plausible. From a study of the behavior of several resonators when the ionic conductivity of the water was increased by the addition of small amounts of KCl, Wyman showed that the resulting error also gave high values for the dielectric constant, but concluded that the error was not significant in the case of pure water. However, estimates based upon the data presented, after making allowance for the small but significant contribution to the conductivity arising from dielectric loss, indicate a remaining error of the order of 0.1 percent in most instances.

The procedure of Drake, Pierce, and Dow involved, in essence, the determination of the half wavelength of the standing waves set up by a source of known frequency in a 4-m, vertical, coaxial pipe filled with water. Except for factors computed to be of negligible proportions, the dielectric constant was given by $\epsilon=c^2/(f^2\lambda_m^2)$, where f is the frequency, λ_m the wavelength in the medium, and c the velocity of light. The precision obtained in determining the values of dielectric constant was governed primarily by the limitations in measuring half wavelength and temperature, about 0.2 mm and 0.2° C, respectively, and varied from 0.3 to 0.15 percent, depending upon the frequency. Inasmuch as the presence of systematic errors of comparable magnitude would hardly be detected, the difference noted between their value and the present value is not unreasonable.

The magnitude of the disagreement shown in figure 7 indicates that, in general, the accuracy of these data can hardly approach 0.1 percent. This is not too surprising as the reproducibility obtained was only rarely better than 0.1 percent.

For the present investigation, the uncertainty due to any known source of error seems to be limited to ± 0.01 unit. Summation, without regard to sign, of the individual uncertainties associated with the recognized sources of error, leads to a possible uncertainty of ± 0.05 in the values of ϵ or ± 0.1 percent at the highest temperature. The over-all reproducibility of separate determinations at any single temperature, ranging in number from 2 to 10, was such that the largest deviation from the mean for any given temperature was never worse than ± 0.015 unit, which occurred with both cells at 25° C ($4+6=10$ observations); and the average of all 69 deviations from the individual means for 21 temperatures was ± 0.005 unit. This agreement indicates the absence of significant cumulative error and should provide a reasonable basis for an estimation of the accuracy attained. As a consequence, the assignment of an accuracy of ± 0.05 unit to all these data seems entirely justified.

7. References

[1] J. Wyman, Phys. Rev. **35**, 623 (1930).
[2] F. H. Drake, G. W. Pierce, and M. T. Dow, Phys. Rev. **35**, 613 (1930).
[3] P. S. Albright, J. Am. Chem. Soc. **59**, 2098 (1937); P. S. Albright and L. J. Gosting, **68**, 1061 (1946).
[4] T. T. Jones and R. M. Davies, Phil. Mag. **28**, 307 (1939).
[5] J. Wyman and E. N. Ingalls, J. Am. Chem. Soc. **60**, 1182 (1938).
[6] A. A. Maryott and E. R. Smith, Table of dielectric constants of pure liquids, NBS Circular 514 (1951).
[7] C. G. Malmberg and A. A. Maryott, J. Research NBS **45**, 299 (1950) RP2137.
[8] A. A. Maryott and F. Buckley, Tables of dielectric constants and electric dipole moments of substances in the gaseous state, NBS Circular 537 (1953).
[9] B. Hague, Alternating current bridge methods, 5th ed. (Sir Isaac Pitman & Sons, Ltd., London, 1943).
[10] R. T. Lattey, O. Gatty, and W. G. Davies, Phil. Mag. **12**, 1019 (1931).
[11] G. C. Åkerlöf and H. I. Oshry, J. Am. Chem. Soc. **72**, 2844 (1950).

WASHINGTON, October 6, 1955.

Journal of Research of the National Bureau of Standards Vol. 56, No. 1, January 1956 Research Paper 2642

A Calorimeter for Measuring the Power in a High-Energy X-ray Beam*

John McElhinney,[1] Bernard Zendle, and Steve Domen

The design and calibration of a calorimeter to measure the power in X-ray beams having peak energies between 1 and 180 million electron volts are described. The calorimeter included two thermally balanced lead cylinders, 4 centimeters in diameter by 7.5 centimeters long, one irradiated by an X-ray beam. The lead cylinder was large enough to absorb almost completely the X-ray beam. The absorbed energy resulted in an unbalance of temperature of the two cylinders, which was measured by the change in resistance of embedded thermistors.

Calibration of the calorimeter consisted in observing the temperature rise due to a measured quantity of electric energy dissipated in the same cylinder. The results are given for five calibration runs, each using about 70 microwatts of power for approximately 20 minutes. The probable error of the mean was about ±1 percent. Separate reports of measurements of X-ray-beam powers at 1.4 and 36 million electron volts are in preparation.

1. Introduction

The interpretation of physical and medical experiments with high-energy X-rays has been greatly hampered by the uncertainties in the measurement of X-ray-beam power. The conventional method of determining beam power has been to measure the ionization current in the gas of an ionization chamber placed in the X-ray beam. To calculate the relationship between the beam power and the ionization current, one must make various assumptions concerning the spectrum of the incident photons, the production of electrons and positrons by the photons in the chamber walls, the values of the stopping power for these electrons in the wall and the gas, and the energy required for an electron or positron to produce an ion pair in the gas of the ionization chamber. Because these assumptions and quantities are difficult to evaluate, the calculated response of an ionization chamber to X-rays may contain unknown errors of the order of 5 to 10 percent.

In order to avoid these uncertainties, apparatus was constructed at the National Bureau of Standards for measuring the X-ray-beam power calorimetrically. Such measurements were made by comparing the temperature rise of a lead cylinder irradiated by the X-ray beam with the temperature rise of the same cylinder heated by a measured quantity of electric energy. After making suitable corrections for the small proportion of X-ray energy that was not absorbed, an electrical equivalent of X-ray energy could be obtained.

The first published measurements of this type were made by Laughlin et al. [1].[2] His later publication [2] described an improved calorimeter used to measure beam power from a 22.5-Mev betatron and a 400-kev[3] X-ray unit. Laughlin's calorimeter consisted of twin lead cylinders, one of which was irradiated. The resulting temperature difference between the two cylinders was used to determine the total energy absorbed.

Calorimetric measurements of X-ray-beam power were also made by Edwards and Kerst [3] for X-ray peak energies ranging between 150 and 300 Mev. Their calorimeter was similar to Laughlin's in design, but, due to the higher energy X-rays, more consideration had to be given to the power escaping from the cylinders.

One of the projects of the Betatron Section at the National Bureau of Standards was to develop an instrument to measure the power in X-ray beams with peak energies between 1 and 180 Mev. This report describes the construction and operation of a calorimeter designed for this purpose. X-ray-beam power measurements at 1.4 and 36 Mev with this calorimeter have been made, and the results are now being prepared.

2. General Method of Operation of the Calorimeter

The calorimeter consisted, essentially, of two similar lead cylinders, thermally insulated from their surroundings and from each other. The X-ray beam, emerging from an aperture in the shielding wall around the X-ray source, was directed axially into the end of one of the lead cylinders. The X-ray energy absorbed in the cylinder was converted into heat energy, resulting in a rise in temperature of the lead cylinder. The temperature-sensing elements were thermistors embedded in the two cylinders and connected in a Wheatstone-bridge circuit. Thermistors have a large negative temperature coefficient of resistance, thus providing high sensitivity to small temperature changes in the cylinders. Absolute

*This work was conducted under a program of basic instrumentation, research, and development, jointly sponsored by the Office of Naval Research, Office of Scientific Research of the Air Research and Development Command, and the Atomic Energy Commission.

[1] Present address, Naval Research Laboratory, Washington 25, D. C.

[2] Figures in brackets indicate the literature references at the end of this paper.

[3] Mev and kev are energy units referring to "million electron volts" and "thousand electron volts", respectively.

calibrations were made by determining the temperature rise when a measured quantity of electric energy was dissipated in a resistor embedded in the cylinder.

3. Construction of the Calorimeter

Figure 1 shows the vacuum chamber containing the two lead cylinders. The cylinders appearing in the background are reflections in the chrome lining of the chamber. The vacuum chamber was supported in a temperature-regulated water bath. Figure 2 is a schematic front view showing the position of the vacuum chamber in the water bath. A detailed description of the various components follows.

3.1. Cylinders

The absorbing cylinders were made of lead because the absorption per unit heat capacity for high-energy X-rays is greater for a material of high atomic number than for one of low atomic number. The cylinders were 7.5 cm long and 4 cm in diameter. Figures 1 and 2 show their location in the evacuated chamber. The surface of each cylinder was gold plated to limit radiation losses, and the cylinders were suspended by nylon threads to limit conduction losses. The cylinders were cut in planes through their axes to simplify the insertion of the thermistors and calibrating resistors. Figure 3 shows one of the cylinders partly opened. The end of the cylinder that received the irradiation was called the front surface. When X-rays are absorbed by lead the maximum density of energy dissipation is at a position a few millimeters behind the front surface. This position depends upon the energy of the incident X-rays. The resistors for calibrating were, therefore, placed near the front surface. The position of these resistors was not critical because the heat from them was transmitted throughout the lead cylinder in a time that was short compared with the irradiation time. The resistors were located near the end of the cylinder in order to be out of the X-ray beam where they would not affect the absorption of the X-rays by the lead. One resistor was located in each half of the cylinder. Commercial 1,000-ohm ½-w carbon resistors were used. The resistors were coated with a liquid cement, placed in a groove in the lead, and surrounded with Wood's metal. The cement provided electrical insulation, and the Wood's metal filled the air gaps, thus providing better thermal contact.

The thermistors were located near the back surface and near the edge of the cylinder, so that they also were not in the primary X-ray beam. One thermistor was located in each half of the cylinder. They were embedded in the lead in the same manner as the resistors.

Number 43 enameled copper wire was used to connect the thermistors and the calibrating resistors to the outside. The wires were about 10 cm long, and small enough to limit conduction losses to a low value, yet large enough that their resistances were small compared with those of the thermistors and calibrating resistors.

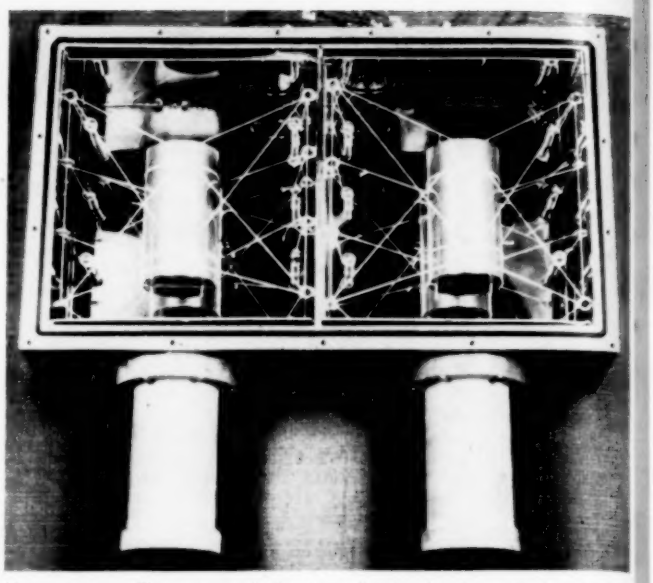

FIGURE 1. *Top view of the twin lead-cylinder calorimeter for measuring X-ray-beam power.*

The lead cylinders in the background are reflections in the chromium-plated surface.

3.2. Vacuum Chamber

The lead cylinders were suspended inside a brass vacuum chamber by means of 16 nylon threads. The chamber had ½-in.-thick walls and ¼-in.-thick bottom and top plates. Its inside dimensions were 6 by 11 in. and 2½ in. high. The inside surface was lined with 1/32-in. plates, the surface of each of which had been chromium plated to limit thermal radiation effects on the cylinders. A chromium-plated metal partition separated the two cylinders. The chamber was evacuated to a pressure of about 10^{-5} mm Hg by means of an oil-diffusion pump and a mechanical forepump. A 1½-in.-diam hole was located just in front of each cylinder to permit the X-ray beam to enter without penetrating the ½-in. wall of brass. These holes were sealed with 0.003-in. brass foil as its absorption for high-energy X-rays is negligible. The electric connections were made through a glass-to-metal seal containing eight small metal tubes. The wires were threaded through but insulated from the tubes and then sealed with a liquid cement.

3.3. Water Bath

As shown in figure 2, the vacuum chamber was immersed in a temperature-controlled water bath. The water container, 15 by 21 by 12 in. high, was made of Bakelite reinforced with angle iron to prevent warping due to water absorption. There was at least 3 in. of water on all sides of the vacuum chamber. Two stirrers, placed diagonally opposite one another, circulated the water. The stirrers were geared to synchronous motors in order to help maintain a constant temperature distribution throughout the water bath. Air-filled Bakelite tubes extended through the water bath in front of the entrance ports of the vacuum chamber in order to

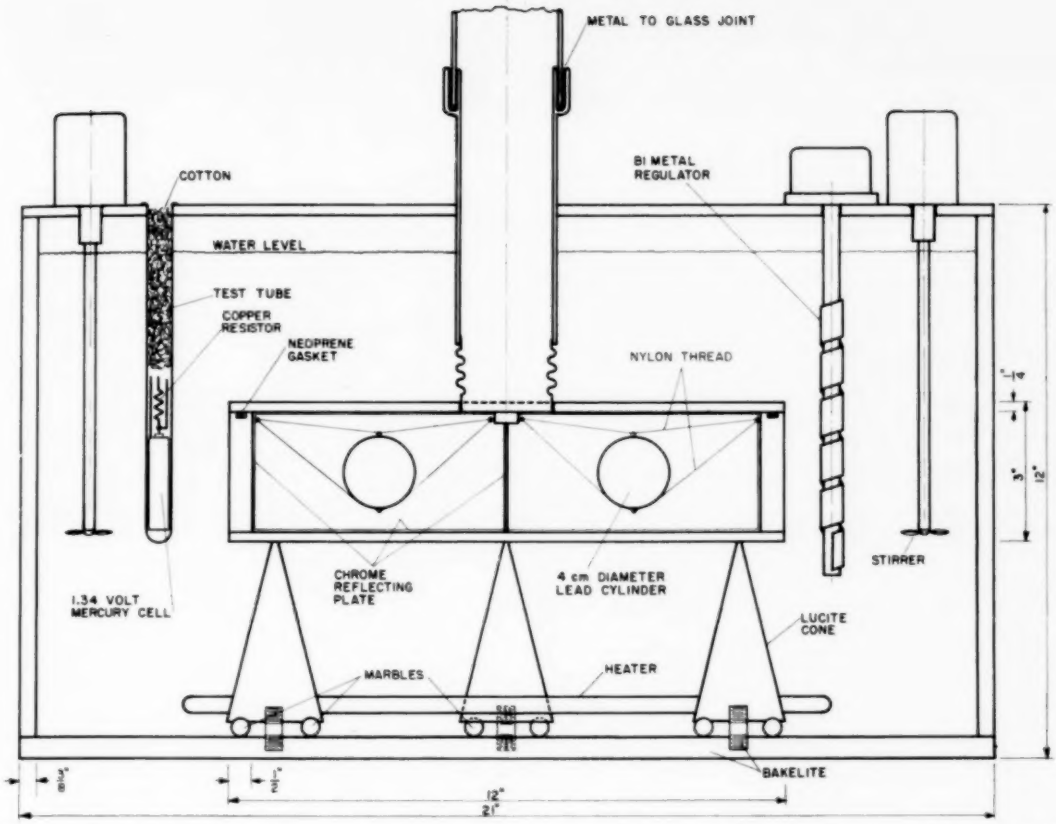

FIGURE 2. *Schematic diagram of a vertical cross section of the calorimeter with the associated water bath and equipment.*

keep the water from absorbing energy from the X-ray beam. A 0.001-in. aluminum foil was placed at the external end of the tubes to limit exchange of heat either by convection of air or by radiation to the inner foil.

The vacuum chamber was supported inside the water bath on the points of three Lucite cones, each of which rested on three marbles. The vacuum connection to the top of the chamber consisted of a 2-in.-diam glass tube on top of a metal sylphon soldered to the vacuum chamber. The purpose of this construction was to provide high insulation between the chamber and the outside, and to provide good thermal contact between the chamber and the water bath, so that outside temperature fluctuations would have as small an effect as possible on the temperature of the vacuum chamber.

The temperature of the water bath was regulated by means of an immersed helical bimetallic strip with an electric contact at one end. The electric current through the contact actuated an electric relay that controlled the "on" and "off" time of the electric heater at the bottom of the water bath. Thermal regulation under optimum conditions was estimated to be ± 0.005 deg C. The heater was operated at 24 w and maintained the temperature at 33.4° C.

It was found necessary to surround the Bakelite box with a larger plywood box to prevent temperature fluctuations due to convection currents in the

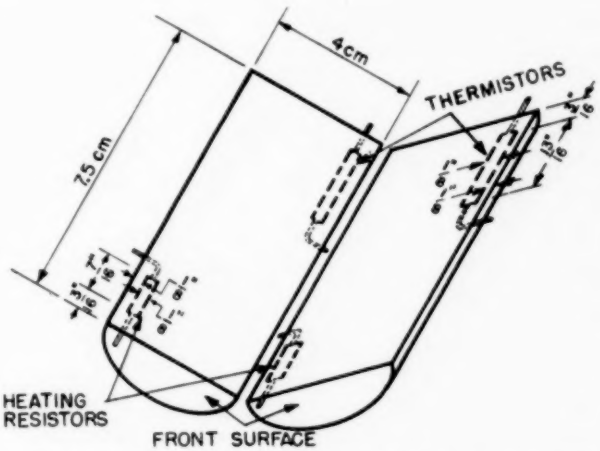

FIGURE 3. *Schematic diagram of one of the lead cylinders split in the plane along its axis to show the location of the thermistors and the heating resistors used for calibration.*
The X-ray beam was incident axially on the front surface.

room. The temperature of the air in the plywood box was controlled by a thermostat to within ± 0.3 deg C of 32.4° C.

The entire calorimeter was mounted on an adjustable hydraulic lift table for convenience in lining up the calorimeter with the beam from the X-ray source.

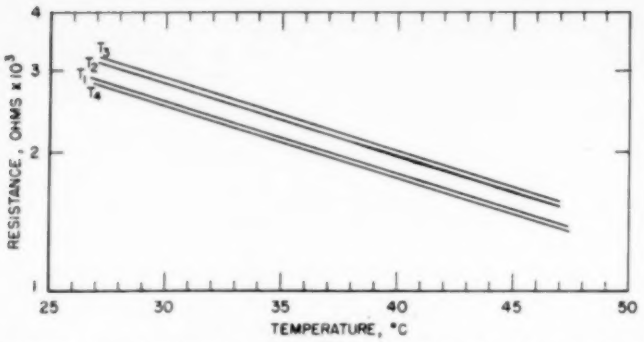

FIGURE 4. *Resistance of thermistors used in the calorimeter as a function of temperature.*

The temperature coefficient of resistance was −0.0363 for all four thermistors.

4. Characteristics of the Thermistors

The temperature-sensing elements in the lead cylinders were Veco 33S1 thermistors, about ⅛ in. in diam by $^{13}/_{16}$ in. long. They were made of a mixture of the oxides of cobalt, manganese, and nickel. Figure 4 shows a plot of their resistance versus temperature over the range of about 30° to 45° C. Over this range the logarithm of the resistance is approximately a linear function of the temperature. Over a large range the resistance, R, at Kelvin temperature T, can be expressed as

$$R = R_0 e^{B(1/T - 1/T_0)},$$

where R_0 is the resistance at temperature T_0 (304° K), and B is a constant of the material. Table 1 shows the characteristics of the four thermistors used.

TABLE 1. *Thermistor characteristics*

Thermistor	R_0	B
	Ohms	° *K*
1	2,479	3,355
2	2,719	3,359
3	2,776	3,362
4	2,420	3,353

5. Wheatstone-Bridge Circuit

Two thermistors were embedded in each lead cylinder and connected in a Wheatstone bridge, as shown in figure 5. The 24-ohm copper resistor compensated for the adjustable resistance of the resistance box and provided an adequate range. A mercury cell supplying 1.34 v was used because of its stable output voltage with time. A variation in the cell voltage would affect the currents in the thermistors. These currents affect the temperatures of the thermistors, which in turn affect their resistances, resulting in a possible unbalance of the Wheatstone bridge. This effect was small because of the similarity of the thermistors, the symmetry of the bridge, and the magnitude of the bridge current used. The compensating copper resistor

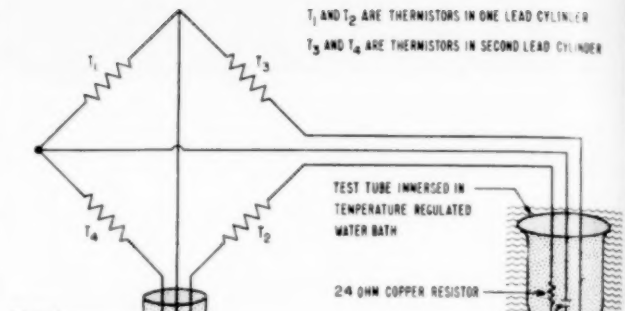
T1 AND T2 ARE THERMISTORS IN ONE LEAD CYLINDER
T3 AND T4 ARE THERMISTORS IN SECOND LEAD CYLINDER
T1
T3
T4
T2
TEST TUBE INMERSED IN TEMPERATURE REGULATED WATER BATH
24 OHM COPPER RESISTOR
1.34 VOLT MERCURY CELL
70 FOOT SHIELDED CABLE TO CONTROL ROOM
RESISTANCE BOX WITH 0.01 OHM STEPS
BREAKER AMPLIFIER
RECORDER

FIGURE 5. *Wheatstone-bridge-circuit diagram showing location of electric components.*

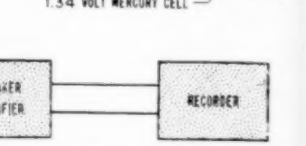

FIGURE 6. *Arrangement of resistors to give 0.01-ohm steps in resistance box and to reduce variations at the output of the bridge circuit due to contact resistances and emf's originating in the switch.*

and the mercury cell were located in a glass tube immersed in the water bath. The tube was stuffed with cotton to inhibit temperature variations due to convection from above. A 0.01 deg C change in temperature of the 24-ohm copper resistor could create the same bridge unbalance as a 5×10^{-6} deg C change in the thermistors in one of the lead cylinders.

The resistance box was a six-decade box with steps of 0.01 ohm. Because of unpredictable variations in contact resistances and emf's originating in the switch, the decade was modified as shown in figure 6, involving a variation of several methods described by Mueller and Wenner [4]. As the contact was moved from one end of the decade to the other, the total resistance changed from 1.00 to 1.10 ohms. Because the variable contact resistance was always in series with a relatively large resistor, it contributed less variation to the over-all resistance.

The four thermistors, selected from a group of 12, had the most similar characteristics. This was desirable in order to reduce drifts and fluctuations at the output of the Wheatstone bridge produced by ambient temperature fluctuations and changes in bridge working currents that affected the temperature and hence the resistance of the thermistors.

For the small temperature changes occurring in these experiments, the first two terms of an expansion of the exponential formula were sufficient, so that R could be expressed as

$$R=R_0[1-(B\{T-T_0\})/(T_0^2)],$$

and the resistance could be assumed to be a linear function of the temperature. The temperature coefficient of resistance was $-0.0363/°$ C for the four thermistors used. As the temperature rise during any set of runs did not exceed 0.01 deg C, the error introduced by assuming linearity and neglecting the next term in the expansion was less than 1 part in 10 million.

Because of the small voltages detected in the Wheatstone bridge (order of microvolts), it is necessary to take every possible precaution to avoid variable voltages due to thermoelectric effects when conductors of different materials are used. Copper connecting wire was used throughout, and a special solder with small thermal electromotive force with respect to copper was used to minimize thermoelectric effects. Difficulty was originally observed with the use of solid metal leads through the glass seal to the vacuum. Although copper wires were attached to both ends, the variable thermal electromotive forces due to temperature differences between the inside and outside of the vacuum chamber were too great to work with. For this reason metal tubes were substituted, and the copper connecting wires were run through the axes and insulated from the metal to form a circuit of copper alone.

About 0.26 ma of current flowing through each arm of the Wheatstone bridge supplied about 0.35 mw of power continuously to each lead cylinder. This caused the equilibrium temperature of the cylinders to be of the order of 0.03 deg C above the surrounding temperature. As long as this temperature difference was constant and all heat losses were approximately linear functions of the temperature difference, this effect could be disregarded.

The detector employed in the bridge circuit was a d-c breaker amplifier. Its input impedance was 1,000 ohms. In the breaker amplifier the d-c input voltage was converted to an 8-cps signal by a mechanical breaker contact. The amplifier, tuned to 8 cps, amplified the signal, which was then converted back to direct current by a second breaker synchronous with the first. In this way the background noise was kept low. The observed noise level (maximum fluctuations peak to peak) corresponded to about 0.1-μv input, and the voltage gain was of the order of 500,000.

The temperature data were taken by either of the following methods: (1) The output of the amplifier was connected to a recording milliammeter. The amplifier and recorder were used as a null detector, so that variations in gain in the amplifier were not of primary importance. As the thermistors changed resistance due to a temperature change of the lead cylinder, the resistance box was adjusted, as required, to bring the bridge back into balance. The required balancing resistance was then plotted against time to provide the data. (2) The second method consisted in connecting the output of the amplifier to a recording d-c potentiometer (0 to 30 mv) with an 11-in.-wide chart and recording the unbalance of the Wheatstone bridge without changing the balancing resistor. Although this system eliminated the transient voltages caused by switching the balancing resistor, it had the disadvantage of depending upon the constancy of the amplifier gain. Periodic checks were made of the amplifier gain by adding a 1-μv signal to the input and observing the deflection; yet no evidence of a change in gain was observed.

6. Operating Characteristics

The smallest short-time signal detectable was limited by the noise level of the output signal. This noise had an over-all amplitude of about 0.0008-ohm equivalent, and corresponded to about 5×10^{-6} °C.

The smallest sustained input power detectable was limited by the long-time drifts in the balance point of the bridge. These could have been due to drifts in the thermistor resistance, drifts in the battery voltage, or changes in the water-bath temperature that affected the bridge output due to asymmetry of the bridge. The observed drift during good operation was less than 0.005 ohm/hr, and corresponded to approximately 3×10^{-5} °C/hr. The temperature rise due to the 100-μw input power in one cylinder was approximately 2×10^{-3} °C/hr and could readily be observed and measured.

7. Heat Losses

It was desirable to keep the heat losses small for several reasons: (1) it put less stringent requirements on the constancy of the water-bath temperature and led to a greater stability of the bridge balance, (2) a larger over-all temperature rise could be accumulated if the time constant were longer, and (3) linear approximations for heat-loss calculations could be used. The associated disadvantage was the long time required for the calorimeter to attain thermal equilibrium. The cooling time constant was determined from data taken of the required balancing resistance versus time before and after the cylinder was heated with 14.03 mw for 10 min. The data are shown in figure 7. Assuming Newton's law of cooling and linearity between R and T, the cooling constant K was determined in the following manner:

$$dR/dt=-K(R-R_e)$$

$$K=-(dR_i/dt-dR_n/dt)/(R_i-R_n),$$

where dR_i/dt and dR_n/dt are the slopes at R_i and R_n, respectively, and R_e is the equilibrium resistance that the exponential curve was approaching. K was determined at five points on the decay curve and found to average about 0.00548 $\pm$0.00002 min^{-1}, when the bath temperature was 33.4° C. This corresponded to about a 3-hr time constant. As is shown below, most of the heat losses were due to radiation. Therefore, this decay constant should

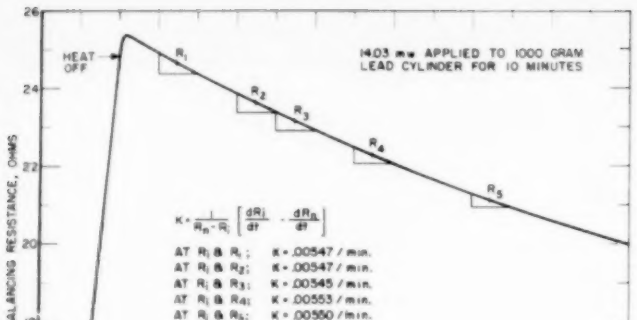
HEAT OFF
14.03 mw APPLIED TO 1000 GRAM LEAD CYLINDER FOR 10 MINUTES
R_1
R_2
R_3
R_4
R_5
$K = \frac{1}{R_0 - R_i}\left[\frac{dR_i}{dt} - \frac{dR_0}{dt}\right]$
AT R_1 & R_1; K = .00547 / min.
AT R_1 & R_2; K = .00547 / min.
AT R_1 & R_3; K = .00545 / min.
AT R_1 & R_4; K = .00553 / min.
AT R_1 & R_5; K = .00550 / min.
5.51 x 10^{-3} °C
HEAT ON
R_1 = 14.813 OHMS
$\frac{dR_1}{dt}$ = .0002 OHM / min.
BALANCING RESISTANCE, OHMS
TIME, MINUTES

FIGURE 7. *Data from which the cooling constant was calculated.*

vary directly as the cube of the absolute temperature of the water bath. Four measurements of the decay constant over a temperature range of 5 deg agreed with the cube-law dependence on the absolute temperature.

The heat capacity of each cylinder was calculated from its dimensions and material to be about 136 j/°C. The heat loss per unit time per degree temperature difference between the cylinder and its surroundings is equal to the product of the cooling constant, K, and the heat capacity. Using these values, one obtains 12.8 mw/°C as the rate of heat loss by the cylinder to its surroundings. This heat loss is believed to be due, primarily, to radiation. Because of the roughness of the gold surface on the cylinders, the emissivity was not known, but must be considerably larger than 0.02, which is the emissivity for a polished gold surface.

The rate of heat loss per degree Celsius due to conduction was calculated and found to be small compared with the observed rate of heat loss. The loss due to conduction along the wires was 0.065 mw/°C, which is only about 0.5 percent of the observed value.

The rate of heat loss per degree Celsius by conduction through the air was 0.017 mw/°C, which is only about 0.1 percent of the observed value. The pressure used in this calculation was 10^{-5}mm Hg, as measured with an ion gage.

Assuming the entire observed rate of heat loss is due to radiation, the effective emissivity of the lead cylinder in the vacuum chamber can be calculated from the formula

$$dQ/dt = cA\epsilon_{eff}(T^4 - T_0^4)$$

where c is the Stefan-Boltzmann constant [5.673×10^{-12} w/cm^2 per (deg K)^4], A is the surface area of the cylinder (120 cm^2), ϵ_{eff} is the effective emissivity of the cylinder in the vacuum chamber, and T and T_0 are the absolute temperatures of the cylinder and surroundings, respectively. Assuming $(T - T_0) \ll T_0$ and solving for ϵ_{eff}, one obtains

$$\epsilon_{eff} = \frac{1}{4cAT_0^3(T - T_0)} \times \frac{dQ}{dt}$$

Substituting the measured value of 12.8 mw/°C for $(1/\{T - T_0\} \times dQ/dt)$, 303° K for T_0, and the above values for c and A, one obtains a value of 0.17 for the effective emissivity. This is a reasonable value, considering the matted appearance of the gold surface of the lead cylinder. It also indicates that a considerable improvement is possible if the gold surface were highly polished.

8. Calibration

The method used for calibrating the calorimeter was to supply a measured quantity of electric energy to the resistors embedded in the lead cylinder and to determine the resulting rise in temperature of the cylinder. The rate of heating and total temperature rise were chosen so as to duplicate as nearly as possible the conditions during the measurement of the X-ray-beam energy. This procedure partially eliminates some of the systematic errors in the calorimetric measurements. A potentiometer with an accuracy of about 0.1 percent was used to measure the voltage across the heating resistor, and a model 622 Weston d-c milliammeter with an accuracy of 0.5 percent of full-scale deflection was used to measure the current. The measurements involved about half-scale deflections, so the accuracy of the current reading was about 1 percent.

Figure 8 is a freehand sketch showing the output voltage of the Wheatstone bridge when method 1, described in section 5, was used. The vertical breaks represent manual changes of the resistance box of 0.01 ohm. The values between breaks indicate the

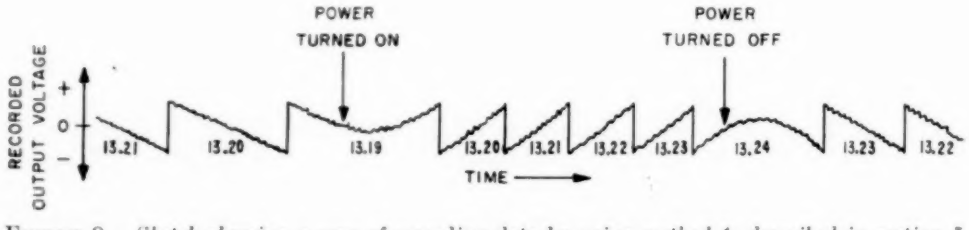

FIGURE 8. *Sketch showing a way of recording data by using method 1, described in section 5.*
The vertical breaks were caused by manual changes in the resistance box of 0.01 ohm. The resistance values are shown between breaks.

resistance of the box at that time. A change in slope of the output versus time in figure 8 follows any change in the power being applied to the cylinder.

The resistance required for exact balance could be determined at any instant by interpolation. This resistance was calculated at the instant before each vertical break in order to minimize the effect of transients that sometimes appeared after a change of resistance. Figure 9 shows a plot of the calculated balancing resistance as a function of time for a 1,400-kev X-ray run. Straight lines were drawn to represent the average data and to simplify the analysis. Linearity between the balancing resistance and temperature was assumed, and the observed temperature rise was calculated to be 4.0×10^{-4} °C.

Figure 10 is a graph of a calibration run, using method 2 described in section 5; 122.6 μw of power was applied for 12 min. Linearity between the bridge unbalance and the temperature was assumed, and the observed temperature rise during the heating period in this example was calculated to be 5.47×10^{-4} °C.

In figures 9 and 10 there is apparent an approximately 45-sec time lag between the application of heat to the cylinder and the detected temperature rise. This time lag was caused by a combination of two phenomena: (1) the time required for diffusion of heat through the lead (most of the heat energy was supplied near the front surface, whereas the thermistors were located near the back surface), and (2) the thermal time constant of the thermistor determined by its heat capacity and its insulation from the surrounding lead. The correction of the observed temperature rise for heat loss was made on the basis of Newton's law of cooling, using the observed curve of temperature as a function of time. This procedure makes the assumption that the average temperature throughout the cylinder is equal to the surface temperature, and that the time lag in the observed temperature is constant. It is recognized that these assumptions may not be strictly true when comparing the heating portion of the curve with the initial- and final-cooling portions. However, it is believed that the error arising from this assumption is small in comparison with the estimated over-all error, and will partially cancel out when comparing X-ray energy with electric energy.

TABLE 2. *Electrical calibration of calorimenter*

Resistance change corresponding to temperature rise	Resistance change corresponding to heat loss	Resistance change corresponding to total energy	Input power	Heating period	Calibration factor [1]
Ohm	*Ohm*	*Ohm*	*μw*	*min*	*Ohm/μw-min*
0.058	0.052	0.110	70.6	20	77.6×10^{-6}
.114	.008	.122	69.9	21	83.2
.095	.028	.123	70.5	22	79.4
.080	.033	.113	70.5	20	80.3
.080	.036	.116	70.7	20	81.9

[1] Average $=80.5\times10^{-6}\pm1.0\times10^{-6}$ ohm/μw-min.

The total energy absorbed by the lead cylinder can be expressed as a sum of two terms, one involving the observed temperature rise and the other involving the energy lost to the surroundings as a result of the temperature difference. The heat lost to the surroundings was calculated from the average of the observed cooling slopes before and after the heating period. Table 2 summarizes the results of five calibration runs over a period of 2 days, using method 1. The heat loss was computed for each run, so it was not necessary to wait each time for complete temperature equilibrium to be attained. It is seen that at times the heat lost through radiation was just about as large as the heat corresponding to the net temperature rise. The average calibration factor of this calorimeter was 80.5×10^{-6} ohm/μw-min, with an rms error of 1.0×10^{-6}.

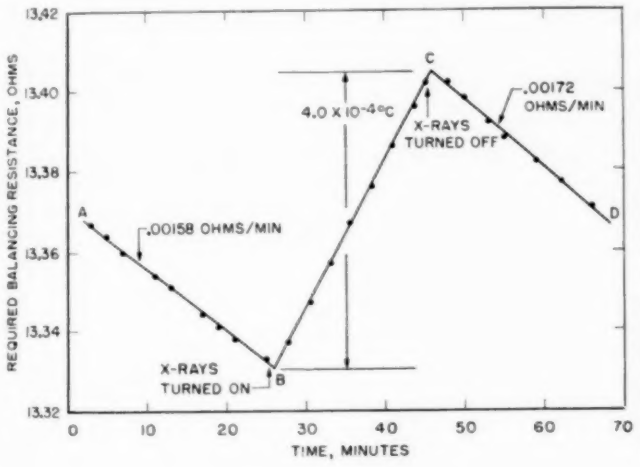

FIGURE 9. *Data calculated from recordings such as in figure 8.* Straight lines were drawn through the points for aid in calculating the total relative heat absorbed.

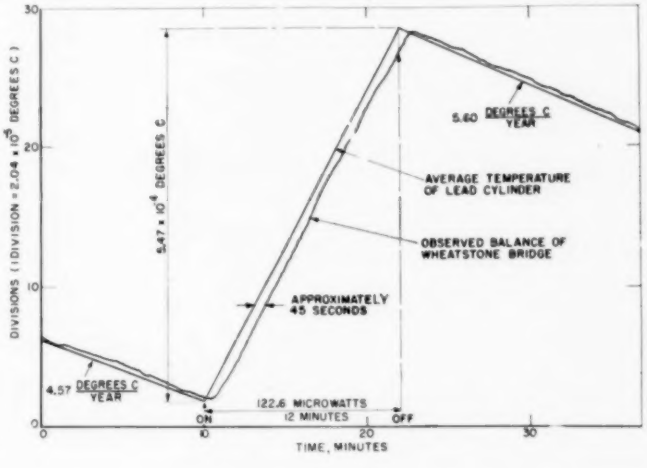

FIGURE 10. *Signal from Wheatstone bridge during a typical heat run when method 2, described in section 5, is used.*

9. Considerations in Measuring X-ray-Beam Power

The described calorimeter was designed for measuring X-ray beams in the range 1 to 180 Mev. The total beam power will be the sum of the power absorbed by the lead cylinder plus that which escapes by transmission, scattering, or by other means. As the escaping energy must be measured by auxiliary experiments, using ionization chambers or scintillation detectors (the very methods whose uncertainties make the calorimeter necessary), it is desirable to select X-ray-beam and lead-cylinder dimensions that limit the escaping energy to less than 10 percent. If an effort is made to reduce the escaping energy further by increasing the dimensions of the lead cylinder, the heat capacity would be increased, and thus the sensitivity would be decreased. To obtain maximum accuracy and sensitivity, a specific size and shape of lead cylinder should be chosen for each application, depending upon the beam power available and the X-ray energy of the source.

The authors express their gratitude to H. W. Koch for his encouragement during the development of the calorimeter. The contributions of Samira M. Aly [4] and Donald Bowers during the initial stages of development are also greatly appreciated.

[4] Fulbright Fellow from the University Fuad I, Cairo, Egypt. Deceased.

10. References

[1] J. S. Laughlin and J. W. Beattie, Calorimetric determination of energy flux of 22.5 Mev X-rays, Rev. Sci. Instr. **22,** 572 (1951).

[2] J. S. Laughlin, J. W. Beattie, W. J. Henderson, and R. A. Harvey, Calorimetric evaluation of the roentgen for 400 kv and 22.5 Mev roentgen rays, Am. J. Roentgenol. Radium Therapy Nuclear Med. **70,** No. 2 (1953).

[3] P. D. Edwards and D. W. Kerst, Determination of photon flux for energies between 150 Mev and 300 Mev, Rev. Sci. Instr. **24,** 490 (1952).

[4] E. F. Mueller and F. Wenner, The Waidner-Wolff and other adjustable electrical-resistance elements, J. Research NBS, **15,** 477 (1935) RP 842.

WASHINGTON, June 1, 1955.

Journal of Research of the National Bureau of Standards Vol. 56, No. 1, January 1956 Research Paper 2643

Pyrochlore-Type Compounds Containing Double Oxides of Trivalent and Tetravalent Ions[1]

Robert S. Roth

A study has been made by X-ray diffraction analyses of the $A_2O_3{:}2BO_2$-type double oxides. It was found that many of these mixed oxides, after appropriate heat treatment, formed compounds of the formula type $A_2B_2O_7$. Most of these compounds crystallized in the cubic system with a face-centered cell similar to that found for the mineral pyrochlore, although some were distorted from the ideal cubic structure.

Indexed X-ray diffraction powder patterns are given for the cubic compounds $Sm_2O_3{\cdot}2TiO_2$, $Gd_2O_3{\cdot}2TiO_2$, $Dy_2O_3{\cdot}2TiO_2$, $Y_2O_3{\cdot}2TiO_2$, $Yb_2O_3{\cdot}2TiO_2$, $La_2O_3{\cdot}2SnO_2$, $Nd_2O_3{\cdot}2SnO_2$, $La_2O_3{\cdot}2ZrO_2$, $Nd_2O_3{\cdot}2ZrO_2$, and for the possible compounds $Y_2O_3{\cdot}2ZrO_2$ and $Nd_2O_3{\cdot}2UO_2$. Unindexed patterns are given for $La_2O_3{\cdot}2TiO_2$, $Nd_2O_3{\cdot}2TiO_2$ and $Bi_2O_3{\cdot}2SnO_2$.

On the basis of the existence of the two compounds $La_2O_3{\cdot}2ZrO_2$ and $Nd_2O_3{\cdot}2ZrO_2$, the phase diagrams for the systems La_2O_3-ZrO_2 and Nd_2O_3-ZrO_2 have been revised.

1. Introduction

A partial survey of the reactions occurring in binary oxide mixtures of the type $A_2O_3{:}2BO_2$ has been conducted as part of a program of fundamental research on ceramic materials. Combinations of simple oxides in this proportion were selected because of the current interest in ferroelectric ceramics. $Cd_2Nb_2O_7$, at room temperature, has the cubic pyrochlore structure, although the ferroelectric form at low temperatures is distorted from this ideal structure [1, 2, 3].[2] The fact that the compound $Cd_2Nb_2O_7$ is known to be ferroelectric at certain temperatures [1] led to the study of other compounds with similar structure.

At the time this work was initiated, no references were known describing a pyrochlore structure that did not contain a pentavalent ion as an essential element of the compound. A ternary compound of this type having the formula $CaO{\cdot}ZrO_2{\cdot}2TiO_2$ or $(Ca_{1.0}Zr_{1.0})\ Ti_2O_7$ was, however, described by Coughanour et al. [4]. Another reference has recently been made by Padrow and Schusterius [5] to pyrochlore phases in the system La_2O_3-SnO_2-TiO_2.

This report is concerned with some combinations of the oxides of trivalent and tetravalent ions which, on the basis of radius ratio, might be expected to form compounds of the pyrochlore type.

2. Materials and Methods

2.1. Materials

The following substances were used as sources of the component oxides in this study:

TiO_2. A rutile of 99.5-percent purity.

SnO_2. Precipitated tin oxide of over 98.5-percent purity.

ZrO_2. Dense zirconia of over 99-percent purity, calcined at 1,450° C.

CeO_2. Calcined cerium dioxide of nominal 99-percent purity.

UO_2. Urania, supplied by the United States Atomic Energy Commission, of over 99.9-percent purity.

La_2O_3. Lanthanum oxide of 98-percent purity, remainder mostly water and CO_2.

Nd_2O_3. Neodymium oxide of over 99-percent purity.

Sm_2O_3. Samarium oxide of nominal 99-percent purity.

Gd_2O_3. Gadolinium oxide of nominal 98-percent purity.

Bi_2O_3. Bismuth trioxide of over 99-percent purity.

$Bi_2O_3{\cdot}3SnO_2{\cdot}5H_2O$. Precipitated hydrous bismuth stannate of at least 98-percent purity.

Y_2O_3. Yttrium oxide of 98- to 99-percent purity, the remainder being rare earths.

Dy_2O_3. Dysprosium oxide of nominal 98-percent purity.

Yb_2O_3. Ytterbium oxide of nominal 98-percent purity.

In_2O_3. Rather impure indium oxide specified "for manufacturing use only."

Sb_2O_3. Antimony trioxide of over 99-percent purity, with 0.2 percent of As_2O_3.

2.2. Sample Preparation

The starting materials, in sufficient quantities to give either a 10.0-g sample or a 1.0-g sample, depending upon the availability of the raw materials, were weighed to the nearest milligram. No corrections were made for the percentage purity of the raw materials, except for loss due to water and carbon dioxide. They were then mixed together with a few drops of distilled water to assure bonding and formed into 1-in. or ½-in.-diam disks at a pressure of 5,000 lb/in.^{2}. The pressed disks were fired for 4 hr at 1,100° C on platinum foil in an air atmosphere, using an electrically heated furnace wound with 80% Pt–20% Rh wire.

[1] This work has been sponsored as part of a program for Improvement of Piezoelectric Ceramics by the Office of Ordnance Research of the Department of the Army.

[2] Figures in brackets indicate the literature references at the end of this paper.

Following the preliminary heat treatment, the disks were ground, using a mullite mortar and pestle, remixed with a few drops of distilled water, and new disks, about ¼ in. high, were formed at 15,000 lb/in.^{2} in either a ½-in. or ¼-in.-diam mold. These specimens were then ready to be used for solid-state reaction studies. Some of the specimens used were prepared by G. R. Shelton of the Bureau during the last 10 years by methods similar to those described here. Most of these specimens were reheated, in the present study, to obtain better crystallinity.

2.3. Study of Solid-State Reactions

In the study of solid-state reactions, a conventional platinum-wound quench furnace was used. The temperature in the furnace was measured with a Pt versus Pt–10-percent-Rh thermocouple and controlled by a modified Roberts-type controller. The quenching technique was used because it has been observed that sharper X-ray patterns are often obtained by very fast cooling of the specimen. Phase transitions in the pyrochlore structure are probably completely reversible and cannot be "frozen in" by quenching. For quench tests, the ½- or ¼-in.-diam disks were placed on a platinum platform, which was then suspended in the furnace. The test temperature ranged from 1,250° to 1,550° C and was maintained constant for a given length of time. Equilibrium conditions were usually reached in less than 3 hr. Equilibrium was believed to have been reached when X-ray patterns of the specimen showed only a single phase, or when the pattern of a two-phase specimen showed no change with successive heat treatment. After this reaction time, the sample was quenched in air by lifting the specimen disk on its platinum platform out of the hot furnace. The specimen cooled to room temperature in less than 2 min. The samples were then examined by X-ray diffraction, using a Geiger counter diffractometer employing nickel-filtered copper radiation.

In the case of specimens containing UO_2, an argon atmosphere was used and the specimens were not quenched. The heating element of the furnace used was a molybdenum-wound stabilized ZrO_2 tube and is similar to the one described by Davenport et al. [6].

3. The Pyrochlore-Structure Type

The structure of the mineral pyrochlore and of related mineral types has been described by several workers [3, 7, 8]. Pyrochlore has the formula $NaCaNbTaO_6F$, in which Na and Ca can be considered the A ions, and Nb and Ta the B ions of an $A_2B_2X_7$ structure. The space group for this cubic compound has been found to be $Fd3m$–O_h^7, with $Z=8$ and a unit cell of 10.35 to 10.40 A.

In the following description of the pyrochlore structure, the cell origin has been taken at a center of symmetry and the sets of positions referred to may be found on page 341 of reference [9]. In this structure type there are 16 A ions in position (c), 16 B ions in position (d), and 8 negative ions in position (a); for the mineral pyrochlore these are the fluorine ions. The remainder of the negative ions (48 oxygen) are in position (f), which contains only one unknown parameter. From a consideration of the spatial requirements in the pyrochlore structure, it is obvious that the value of the unknown parameter must be equal to or very close to ⅜. If the value of ⅜ is used, then all possible *xyz* combinations of ⅛, ⅜, ⅝, and ⅞ are occupied by oxygen, except the eight sites required by the special position (b), which are vacant. In such a structure, if these vacant sites were also occupied, the formula type would be $A_2B_2O_8$ or ABO_4 instead of $A_2B_2O_7$. The pyrochlore-structure type may therefore be compared to a fluorite structure with 1 out of every 8 negative ions missing. From data given by Bystrom [3], the value of x in the oxygen position for $Cd_2Nb_2O_7$ and $Cd_2Ta_2O_7$ can be taken as 0.414 instead of 0.375 for ⅜. It will be seen in the following discussions that the value of x is probably not the same for all of the pyrochlore-type compounds.

In addition to the extinctions to be expected from a face-centered cell, there are two special extinction rules due to the particular positions of the ions in the pyrochlore-type structure:

(1) The positions (a) and (f), filled by negative ions, are such that possible reflections are limited to the type *hkl* where $h+k+l=2n+1$ or $4n$.

(2) The positions (c) and (d), filled by positive ions, are such that possible reflections are limited to planes of the type

$$\left.\begin{matrix} hkl{:}h=2n+1 \\ k=2n+1 \\ l=2n+1 \end{matrix}\right\} \quad \text{or} \quad \left.\begin{matrix} 4n+2 \\ 4n+2 \\ 4n+2 \end{matrix}\right\} \quad \text{or} \quad \left.\begin{matrix} 4n \\ 4n \\ 4n \end{matrix}\right\}.$$

The result is that, in the pyrochlore-type diffraction patterns, certain reflections are always absent. Of those that may be observed, some are due only to metal atom scattering, some only to oxygen atom scattering, and the remainder to both metal and oxygen scattering. Therefore, the intensities of the peaks in the X-ray powder diffraction patterns are characteristic of the pyrochlore structure, and are evidence for the existence of such a structure. Intensity calculations have been made for some of the cubic compounds studied and will be discussed in later sections.

4. Results and Discussion

4.1. General

The X-ray diffraction powder patterns prepared in this study revealed that many of the mixtures formed binary compounds of the type $A_2B_2O_7$. The great majority of the compounds were cubic, essentially isostructural with the mineral pyrochlore. Table 1 lists the indexed X-ray diffraction powder patterns for these cubic compounds. All of the *hkl*

TABLE 1. *X-ray diffraction powder data for the compounds* $Sn_2Ti_2O_7$, $Gd_2Ti_2O_7$, $Dy_2Ti_2O_7$, $Y_2Ti_2O_7$, $Yb_2Ti_2O_7$, $La_2Sn_2O_7$, $Nd_2Sn_2O_7$, $La_2Zr_2O_7$, $Nd_2Zr_2O_7$ *and the possible compounds* $Y_2Zr_2O_7$ *and* $Nd_2U_2O_7$

TABLE 1. *X-ray diffraction powder data for the compounds* $Sm_2Ti_2O_7$, $Gd_2Ti_2O_7$, $Dy_2Ti_2O_7$, $Y_2Ti_2O_7$, $Yb_2Ti_2O_7$, $La_2Sn_2O_7$, $Nd_2Sn_2O_7$, $La_2Zr_2O_7$, $Nd_2Zr_2O_7$ *and the possible compounds* $Y_2Zr_2O_7$ *and* $Nd_2U_2O_7$

hkl	$Sm_2Ti_2O_7$		$Gd_2Ti_2O_7$		$Dy_2Ti_2O_7$		$Y_2Ti_2O_7$		$Yb_2Ti_2O_7$		$La_2Sn_2O_7$		$Nd_2Sn_2O_7$		$La_2Zr_2O_7$		$Nd_2Zr_2O_7$		$Y_2Zr_2O_7$(?)		$Nd_2U_2O_7$(?)	
	d	I^a	*d*	I^a	*d*	I^a	*d*	I^a	*d*	I^a	*d*	I^a	*d*	I^a	*d*	I^a	*d*	I^a	*d*	I^a	*d*	I^a
111	5.91	22	5.86	18	5.80	19	5.79	22	5.77	54	6.18	7	6.08	4	6.21	5	6.14	5	----	----	----	----
200 [b]	----	----	----	----	----	----	----	----	----	----	----	----	----	----	----	----	----	----	----	----	----	----
220	----	----	----	----	----	----	----	----	----	----	----	----	----	----	----	----	----	----	----	----	----	----
311	3.09	22	3.06	11	3.04	15	3.03	9	3.02	63	----	----	3.18	4	----	----	3.21	4	----	----	----	----
222	2.96	[c] 100+	2.94	100	2.91	[c] 100+	2.91	356	2.89	[c] 100+++	3.08	[c] 100+++	3.04	[c] 100+	3.11	[c] 100++	3.07	[c] 100+	3.00	[c] 100++	3.12	[c] 100+
400	2.56	60	2.54	19	2.52	45	2.52	45	2.50	81	2.67	91	2.64	77	2.69	60	2.66	48	2.59	73	2.71	69
331	2.35	36	2.33	16	2.31	32	2.31	62	2.30	78	2.45	7	2.42	7	2.47	11	2.44	8	----	----	----	----
420 [b]	----	----	----	----	----	----	----	----	----	----	----	----	----	----	----	----	----	----	----	----	----	----
422	2.076	4	----	----	----	----	2.056	5	2.044	3	----	----	2.153	3	----	----	2.172	3	----	----	----	----
511/333	1.969	14	1.958	10	1.943	13	1.940	16	1.929	39	2.058	5	2.030	3	2.075	5	2.046	5	----	----	----	----
440	1.809	68	1.799	39	1.785	75	1.782	170	1.772	[c] 100++	1.809	[c] 100++	1.866	100	1.907	[c] 100+	1.882	70	1.837	[c] 100+	1.919	72
531	1.730	11	1.720	8	1.707	10	1.704	7	1.694	42	----	----	1.780	3	----	----	1.799	3	----	----	----	----
600/442 [b]	----	----	----	----	----	----	----	----	----	----	----	----	----	----	----	----	----	----	----	----	----	----
620	----	----	----	----	----	----	1.593	3	----	----	----	----	----	----	----	----	----	----	----	----	----	----
533	1.560	6	----	----	----	----	----	----	1.539	8	----	----	----	----	----	----	1.632	4	----	----	----	----
622	1.543	41	1.535	31	1.522	58	1.520	56	1.511	[c] 100+	1.613	[c] 100+	1.592	84	1.626	88	1.605	63	1.567	73	1.638	69
444	1.477	17	1.469	10	1.458	13	1.456	13	1.447	57	1.544	29	1.524	25	1.557	22	1.537	16	1.501	14	1.569	16
711/551	1.432	6	1.425	3	1.415	5	1.412	4	1.404	14	----	----	----	----	----	----	1.491	3	----	----	----	----
640 [b]	----	----	----	----	----	----	----	----	----	----	----	----	----	----	----	----	----	----	----	----	----	----
642	----	----	----	----	----	----	----	----	----	----	----	----	----	----	----	----	----	----	----	----	----	----
731/553	1.332	8	1.325	3	1.316	5	1.313	5	1.305	14	----	----	----	----	----	----	1.386	2	----	----	----	----
800	1.279	9	1.273	5	1.262	10	1.261	10	1.254	15	1.337	15	1.320	17	1.349	13	1.331	11	1.300	11	1.360	14
733	1.250	4	1.242	3	1.234	5	1.233	5	1.225	8	----	----	1.288	3	1.319	3	1.296	3	----	----	----	----
820/644 [b]	----	----	----	----	----	----	----	----	----	----	----	----	----	----	----	----	----	----	----	----	----	----
822/660	----	----	1.202	3	----	----	1.190	3	1.181	3	----	----	----	----	----	----	----	----	----	----	----	----
751/555	1.182	6	----	----	1.167	5	----	----	1.158	10	----	----	----	----	1.245	3	1.229	4	----	----	----	----
662	1.174	19	1.168	11	1.159	19	1.157	85	1.150	45	1.227	37	1.212	30	1.238	38	1.222	24	1.192	18	1.249	24
840	1.144	19	1.138	9	1.130	13	1.128	17	1.121	37	1.196	29	1.181	25	1.207	28	1.190	16	1.162	11	1.217	20
911/753	1.123	8	1.117	4	1.109	5	1.108	3	1.101	15	----	----	----	----	----	----	1.169	3	----	----	----	----
842 [b]	----	----	----	----	----	----	----	----	----	----	----	----	----	----	----	----	----	----	----	----	----	----
664	----	----	----	----	----	----	----	----	----	----	----	----	----	----	----	----	----	----	----	----	----	----
931	1.073	5	----	----	----	----	----	----	1.051	3	----	----	----	----	----	----	----	----	----	----	----	----
844	1.044	15	1.039	8	1.031	12	1.030	51	1.024	25	1.092	26	1.078	22	1.102	17	1.087	17	1.062	16	1.111	17
933/771/755	1.028	7	1.023	4	1.016	5	1.014	5	1.008	8	----	----	----	----	----	----	1.067	3	----	----	----	----
10, 0, 0/860 [b]	----	----	----	----	----	----	----	----	----	----	----	----	----	----	----	----	----	----	----	----	----	----
10, 2, 0/862	1.003	5	----	----	----	----	----	----	----	----	----	----	----	----	----	----	----	----	----	----	----	----
951/773	0.9895	5	----	----	----	----	0.9757	3	0.9693	4	----	----	----	----	----	----	----	----	----	----	----	----
10, 2, 2/666	.9841	16	0.9797	9	0.9726	13	.9711	12	.9646	23	1.030	28	1.017	22	1.039	20	1.025	15	1.001	12	1.048	19
953	----	----	----	----	----	----	----	----	.9352	3	----	----	----	----	----	----	----	----	----	----	----	----
10, 4, 0/864 [b]	----	----	----	----	----	----	----	----	----	----	----	----	----	----	----	----	----	----	----	----	----	----
10, 4, 2	----	----	----	----	----	----	----	----	----	----	----	----	----	----	----	----	----	----	----	----	----	----
11, 1, 1/775	----	----	----	----	----	----	----	----	.9043	4	----	----	----	----	----	----	----	----	----	----	----	----
880	.9041	13	.9000	5	.8934	7	.8926	4	.8866	12	0.9459	11	0.9340	8	0.9540	7	0.9411	6	0.9192	5	0.9628	8
11, 3, 1/971/955	.8938	6	----	----	.8829	5	.8819	3	.8763	8	----	----	----	----	----	----	.9304	5	----	----	----	----
10, 4, 4/882 [b]	----	----	----	----	----	----	----	----	----	----	----	----	----	----	----	----	----	----	----	----	----	----
10, 6, 0/866	----	----	----	----	----	----	----	----	----	----	----	----	----	----	----	----	----	----	----	----	----	----
11, 3, 3, 973	.8676	5	----	----	----	----	----	----	.8507	4	----	----	----	----	----	----	----	----	----	----	----	----
10, 6, 2	.8644	13	.8605	13	.8541	15	.8530	12	.8477	28	.9045	30	.8932	26	.9122	23	.9000	18	.8793	11	.9208	19
12, 0, 0/884	.8523	17	.8456	8	.8421	12	.8410	35	.8359	21	.8918	21	.8896	18	.8995	14	.8874	13	.8667	7	.9078	12
11, 5, 1/777	.8438	5	----	----	----	----	----	----	.8273	5	----	----	----	----	----	----	----	----	----	----	----	----
12, 2, 0 [b]	----	----	----	----	----	----	----	----	----	----	----	----	----	----	----	----	----	----	----	----	----	----
12, 2, 2/10, 6, 4	----	----	----	----	----	----	----	----	----	----	----	----	----	----	----	----	----	----	----	----	----	----
11, 5, 3/975	.8215	6	.8176	4	.8119	5	.8106	5	.8057	5	----	----	----	----	----	----	----	----	----	----	----	----
12, 4, 0	.8085	16	.8050	7	.7989	7	.7980	7	.7930	15	.8461	18	.8355	15	.8533	11	.8418	12	.8224	7	.8615	11
991	----	----	----	----	----	----	----	----	----	----	----	----	----	----	----	----	----	----	----	----	----	----
12, 4, 2/10, 8, 0/886 [b]	----	----	----	----	----	----	----	----	----	----	----	----	----	----	----	----	----	----	----	----	----	----
10, 8, 2	----	----	----	----	----	----	----	----	----	----	----	----	----	----	----	----	----	----	----	----	----	----
13, 1, 1/11, 7, 1/11, 5, 5/993	.7819	5	----	----	----	----	----	----	----	----	.8161	17	.8059	14	.8230	12	.8119	9	.7932	5	.8310	8
10, 6, 6	.7798	10	.7787	4	----	----	----	----	----	----	.8067	18	.7966	15	.8136	11	.8026	7	.7841	3	.8216	8
12, 4, 4	----	----	----	----	----	----	----	----	----	----	----	----	----	----	----	----	----	----	----	----	----	----
13, 3, 1/11, 7, 3/977	----	----	----	----	----	----	----	----	----	----	----	----	----	----	----	----	----	----	----	----	----	----
12, 6, 0/10, 8, 4 [b]	----	----	----	----	----	----	----	----	----	----	----	----	----	----	----	----	----	----	----	----	----	----
12, 6, 2	----	----	----	----	----	----	----	----	----	----	----	----	----	----	----	----	----	----	----	----	----	----
13, 3, 3/995	----	----	----	----	----	----	----	----	----	----	----	----	----	----	.7788	5	----	----	----	----	.7865	5
888	----	----	----	----	----	----	----	----	----	----	----	----	----	----	----	----	----	----	----	----	----	----

[a] *I* is the measured height of the diffraction peaks. [b] Not allowed because of extinction rules for the point positions of the pyrochlore structure. [c] Too strong to be completely recorded on the X-ray pattern.

TABLE 2. *Heat treatment and structure type of compositions studied*

Composition	Radius [a] of A^{+3}	Radius [a] of B^{+4}	Heat treatment [b]		Structure type	Symmetry	Parameter "a"
			Temperature	Time			
			°C	hr			
$La_2Ti_2O_7$	1.14	0.68	1,550	1	Distorted pyrochlore	Unknown	
$Nd_2Ti_2O_7$	1.04	.68	1,550	1	do	do	
$Sm_2Ti_2O_7$	1.00	.68	1,550	½	Pyrochlore	Cubic	10.228
$Gd_2Ti_2O_7$	0.97	.68	1,550	2	do	do	10.181
$Dy_2Ti_2O_7$	.92	68	1,425	1	do	do	10.106
$Y_2Ti_2O_7$	.92	.68	1,525	½	do	do	10.093
$Yb_2Ti_2O_7$	.86	.68	1,550	2	do	do	10.030
$In_2O_3:2TiO_2$	.81	.68	1,550	3	No compound		
$Sb_2O_3:2TiO_2$	.76	.68	1,475	2	do		
$La_2Sn_2O_7$	1.14	.71	1,550	1	Pyrochlore	Cubic	10.702
$Nd_2Sn_2O_7$	1.04	.71	1,550	1	do	do	10.568
$Bi_2Sn_2O_7$	0.96	.71	1,250	1	Distorted pyrochlore	Unknown	
$La_2Zr_2O_7$	1.14	.79	1,550	3	Pyrochlore	Cubic	10.793
$Nd_2Zr_2O_7$	1.04	.79	1,550	2	do	do	10.648
$Y_2Zr_2O_7$	0.92	.79	1,550	2	do (?)	do	10.402(?)
$In_2O_3:2ZrO_2$	.81	.79	1,550	3	No compound		
$In_2O_3:2CeO_2$	.81	.94	1,350	½	do		
$Nd_2O_3:2UO_2$	1.04	.97	[c] 1,600	1	Fluorite solid solution (?)	Cubic	5.449
$Y_2O_3:2UO_2$	0.92	.97	[c] 1,600	1	No compound		

[a] Radius of the ions taken from Green [10].
[b] All specimens, unless otherwise stated, were quenched from the designated temperature.
[c] These specimens were heated in an argon atmosphere to prevent the oxidation of UO_2 and were not quenched.

values allowed by a face-centered lattice have been listed, up to and including $h^2+k^2+l^2=192$. It may be seen that none of the peaks forbidden by the structural arrangement of the pyrochlore type are observed in the X-ray patterns of any of the compounds studied.

Table 2 lists the lattice parameters of these compounds, together with the composition, heat treatment, and structure identification for all the materials examined. All compounds and mixtures studied have been plotted in figure 1 on the basis of constituent ionic radii. The values for the radii of the ions have been taken from Green's Geochemical Table of the Elements [10]. The radius of the A^{+3} ion is plotted as the ordinate and that of the B^{+4} ion as the abscissa. It can be seen that only the larger A ions with the smaller B ions (the upper left of the diagram) form compounds. In the lower-right portion of the diagram no compounds are indicated. Thus, areas of compound formation and also of symmetry types can be located on this diagram. This is similar to the types of diagrams given by Wood [11] and by Keith and Roy [12] for perovskite structures. Detailed discussion of each of the compounds studied is given in the following sections.

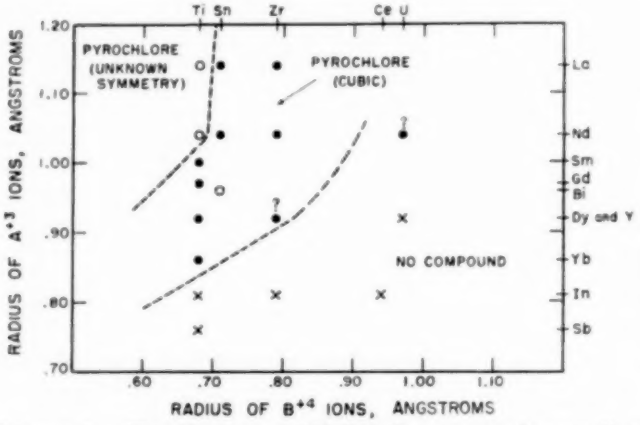

FIGURE 1. *Classification of $A^{+3}{}_2B^{+4}{}_2O_7$ compounds according to the constituent ionic radii.*

○ Pyrochlore (unknown symmetry).
● Pyrochlore (cubic).
?● Single-phase face-centered cubic.
× No compound.

4.2. Titanates

Most of the rare-earth titanates form compounds having the cubic pyrochlore structure; however, $La_2Ti_2O_7$ and $Nd_2Ti_2O_7$ are not cubic. The X-ray diffraction powder data for these two compounds are listed in table 3. The X-ray pattern for $La_2Ti_2O_7$ is very sharp and clear; however, that of $Nd_2Ti_2O_7$ is rather diffuse. These compounds seem to be approximately isostructural with $CaZrTi_2O_7$ [4]. The X-ray patterns of these compounds all have diffraction peaks more or less grouped around the positions that would be expected for a cubic pyrochlore structure. An effort has been made to correlate the structure of these titanates with the orthorhombic form of the $A_2B_2X_7$ compounds exemplified by the mineral weberite, as described by Bystrom [7] for $Ca_2Sb_2O_7$ and other antimonates. The titanates reported in the present study do not seem to have the same structure as that reported for the compounds studied by Bystrom, and the X-ray patterns strongly suggest distortions of the pyrochlore type.

The other four rare-earth titanates studied here have the cubic pyrochlore structure, as does yttrium titanate (table 1). These compounds all give very sharp X-ray patterns, with relatively strong additional lines for the *hkl* peaks required by the pyrochlore structure as compared to the fluorite structure.

TABLE 3. *X-ray diffraction powder data for the compounds* $La_2O_3 \cdot 2TiO_2$ *and* $Nd_2O_3 \cdot 2TiO_2$

$La_2O_3 \cdot 2TiO_2$			$Nd_2O_3 \cdot 2TiO_2$		
2θ	d	I[a]	2θ	d	I[a]
13.75	6.4	20	13.79	6.4	9
17.37	5.10	6	------	------	------
21.14	4.20	43	21.35	4.16	39
23.00	3.86	12	23.43	3.79	11
24.98	3.56	5	------	------	------
26.24	3.39	13	26.40	3.37	9
27.70	3.22	[b] 100++	27.73	3.21	48
28.11	3.17	33	28.61	3.12	25
28.64	3.11	14	29.01	3.07	15
29.79	3.00	[b] 100+	30.26	2.95	100
32.16	2.78	71	32.30	2.77	30
32.24	2.77	70	32.76	2.73	35
32.96	2.72	71	33.42	2.68	49
33.43	2.68	35	33.75	2.65	21
34.82	2.57	9	35.10	2.55	5
------	------	------	35.95	2.50	6
37.24	2.41	5	------	------	------
38.53	2.33	8	38.65	2.33	9
38.97	2.31	7	39.90	2.26	5
39.96	2.25	30	40.65	2.218	22
41.23	2.188	7	41.92	2.153	10
42.09	2.145	39	42.15	2.142	11
42.36	2.132	25	42.77	2.112	13
43.01	2.101	36	43.45	2.081	26
43.64	2.072	26	44.28	2.044	15
45.14	2.007	15	45.40	1.996	16
45.29	2.001	20			
46.38	1.956	47	47.32	1.919	31
47.12	1.927	31	47.73	1.904	20
48.16	1.888	48	48.55	1.873	23
49.54	1.838	8	49.55	1.838	7
49.68	1.833	7			
51.52	1.772	24	52.12	1.753	15
51.68	1.767	21	52.37	1.745	15
52.40	1.745	10	------	------	------
54.00	1.697	15	54.35	1.686	11
54.47	1.683	13	54.76	1.675	11
54.90	1.671	32	55.72	1.648	15
56.00	1.641	17	56.90	1.617	11
57.59	1.599	33	58.80	1.569	24
57.98	1.589	25			
58.72	1.571	8	60.04	1.539	8
59.81	1.545	18	61.62	1.504	10
61.26	1.512	16	62.80	1.478	9
62.26	1.490	12	64.49	1.444	6
64.44	1.445	10	65.21	1.429	6
65.14	1.431	26	66.14	1.412	13
66.85	1.398	7	67.69	1.383	7
67.50	1.386	8	68.62	1.366	6
67.92	1.379	9	69.08	1.358	9
68.59	1.367	12	------	------	------
69.10	1.358	10	70.14	1.341	7
70.30	1.338	4			
71.70	1.315	4	73.02	1.295	5
72.50	1.303	5	73.55	1.287	5
73.18	1.292	3	74.26	1.276	5
73.55	1.286	14	75.05	1.264	7
73.84	1.282	12	------	------	------
74.15	1.277	10	------	------	------
74.43	1.273	9	------	------	------
75.76	1.255	9	77.25	1.234	8
76.28	1.247	5	77.50	1.231	7
76.80	1.240	5	------	------	------
77.40	1.232	9	78.94	1.212	5
77.64	1.229	8	------	------	------
78.26	1.221	5	------	------	------
78.90	1.212	10	79.66	1.203	6
80.10	1.197	4	82.00	1.174	6
80.80	1.188	4	82.28	1.171	6
81.65	1.178	4	------	------	------
82.47	1.168	6	83.59	1.156	6
82.65	1.166	7			
------	------	------	85.05	1.139	5
85.15	1.138	3	------	------	------
85.83	1.131	8	87.49	1.114	5
86.26	1.127	8	87.90	1.110	6
86.57	1.123	7	------	------	------
87.37	1.115	5	88.90	1.100	4
89.87	1.090	5	91.51	1.075	6
90.15	1.088	4	91.80	1.073	6

TABLE 3. *X-ray diffraction powder data for the compounds* $La_2O_3 \cdot 2TiO_2$ *and* $Nd_2O_3 \cdot 2TiO_2$—Continued

$La_2O_3 \cdot 2TiO_2$			$Nd_2O_3 \cdot 2TiO_2$		
2θ	d	I[a]	2θ	d	I[a]
91.25	1.078	5	------	------	------
91.57	1.075	7	------	------	------
92.50	1.066	9	94.06	1.053	6
93.69	1.056	13	95.57	1.040	7
------	------	------	96.72	1.031	6
95.13	1.044	5	97.20	1.027	7
96.15	1.035	7	97.82	1.022	6
98.04	1.020	4	------	------	------
98.98	1.013	3	100.70	1.000	5
100.45	1.002	6	103.12	0.9834	5
100.83	0.9995	5			
103.96	.9777	5	106.02	.9643	4
			106.60	.9607	7
104.88	.9717	3	107.70	.9539	5
105.22	.9694	4			
108.40	.9497	4	110.79	.9358	4
110.25	.9388	9	112.13	.9284	5
111.93	.9294	6	------	------	------
113.31	.9221	7	116.45	.9061	7
113.84	.9192	8	116.87	.9040	2
------	------	------	119.03	.8938	5
------	------	------	120.40	.8876	6
120.70	.8863	7	124.02	.8723	6
123.15	.8758	4	------	------	------
124.08	.8720	4	------	------	------
124.68	.8696	4	------	------	------
125.32	.8671	4	------	------	------
128.35	.8557	3	------	------	------
128.81	.8540	3	------	------	------
130.14	.8494	5	------	------	------
130.82	.8471	5	------	------	------
133.35	.8388	8	139.41	.8212	6
135.10	.8334	5	------	------	------
135.80	.8313	6	------	------	------
137.80	.8256	4	149.87	.7976	5
147.10	.8031	6	------	------	------
148.02	.8012	5	------	------	------
149.92	.7976	5	------	------	------
150.45	.7966	8	158.45	.7841	6
151.65	.7944	7	------	------	------
152.90	.7923	5	------	------	------

[a] I is the observed height of the diffraction peaks.
[b] These peaks were too strong to be completely recorded on the X-ray pattern.

Table 4 shows the intensity values calculated for a few representative planes of $Sm_2Ti_2O_7$ and other compounds. The intensity valves were calculated, using the formula

$$I_{calc.} \approx F^2 \rho \frac{1+\cos^2 2\theta}{\sin^2 \theta \cdot \cos \theta},$$

where

F=the structure amplitude as given in reference [9, p. 519].

ρ=multiplicity factor, and the balance of the equation refers to the polarization and Lorenz factors for powder patterns.

These intensities were then recalculated on the basis of 100 for the strongest peak. Table 4 shows the individual contribution of the ions in the structure and the final intensity valves compared with the measured peak heights. It can be seen that both the 0.375 value and the 0.414 value of the x parameter for 48 oxygen give poor agreement between observed peak heights and calculated intensity for $Sm_2Ti_2O_7$ although the agreement of the zirconates and stannates is fair for 0.414. It must be concluded that the oxygen parameter for the titanate compounds is slightly different than that reported by Bystrom [3] for the niobates and tantalates.

TABLE 4. *Calculated versus observed intensities for some of the diffraction peaks of typical* $A_2^{+3}B_2^{+4}O_7$ *compounds*

hkl	$f\times16$ A^{+3}	$f\times16$ B^{+4}	$f\times8$ O	$f\times48$ O		Calculated I [a]		Observed I [a]
				$x=0.375$	$x=0.414$	$x=0.375$	$x=0.414$	
				$Sm_2Ti_2O_7$				
111	−445	126	−48	0	70	50.6	33.1	22
222	829	242	0	0	0	100.0	100.0	[b] 100+
400	805	232	−22	−269	−150	26.1	35.1	60
331	392	−112	30	0	66	9.6	21.7	36
511/333	−720	589	52	0	31	0.9	0.3	14
				$Nd_2Zr_2O_7$				
111	−432	273	−48	0	70	10.5	4.6	5
222	814	514	0	0	0	100.0	100.0	[b] 100+
400	786	501	−23	−274	−153	26.7	33.6	48
331	384	−245	31	0	68	1.2	5.8	8
511/333	−725	458	53	0	31	4.1	3.0	5
				$Y_2Zr_2O_7$				
111	−271	274	−48	0	70	0.9	0.3	0
222	499	512	0	0	0	100.0	100.0	[b] 100+
400	482	496	−23	−274	−153	24.6	34.1	73
331	238	−246	31	0	68	0.1	1.5	0
511/333	−442	454	53	0	31	.2	0.8	0
				$Nd_2Sn_2O_7$				
111	−432	350	−48	0	70	3.3	0.9	4
222	811	661	0	0	0	100.0	100.0	[b] 100+
400	782	642	−23	−274	−153	31.5	38.6	77
331	382	−313	31	0	68	0.8	2.2	7
511/333	−720	589	53	0	31	.4	0.2	3

[a] I is the height of the diffraction peaks.
[b] These peaks were too strong to be completely recorded on the X-ray pattern.

Neither indium nor antimony oxides form compounds with titania. The X-ray patterns for the mixtures In_2O_3:2TiO_2 and Sb_2O_3:2TiO_2 show only the presence of TiO_2. The specimens had contracted and lost weight, indicating that the other oxide had volatilized and had not combined with titania. It was found that, if In_2O_3 or Sb_2O_3 reacts with a second oxide to yield a true compound, little or no material is lost in volatilization under the heating conditions used in these experiments.

4.3. Stannates

Both of the rare-earth oxides, lanthana and neodymia, form cubic compounds with stannic oxide. There are only a few small peaks in the X-ray diffraction powder patterns (table 1) that cannot be indexed on the basis of a fluorite-type structure with a unit-cell size of approximately 5 A. However, these additional lines indicate that the true structure is that of the pyrochlore type with a cell size of approximately 10 A. The diminished intensity of these excess lines, as compared to those of the titanates, is due to the small difference in the scattering power of the two metal ions, as shown in table 4 for $Nd_2Sn_2O_7$. No other rare-earth stannates have been studied, but it is probable that many of them form cubic pyrochlore compounds. Also, it is evident, from the work of Padrow and Schusterius [5] that solid solutions of the rare-earth titanates and stannates can occur.

TABLE 5. *X-ray powder diffraction data for the compound* $Bi_2O_3.2SnO_2$

d	I [a]	*d*	I [a]	*d*	I [a]
6.2	25	1.496	7	1.028	15
3.77	14	1.428	5	1.006	4
3.61	46	1.425	6	0.9964	4
3.22	27	1.419	10	.9924	4
3.08	[b] 100++++	1.394	7	.9814	3
2.78	21	1.391	9	.9756	3
2.67	[b] 100+++	1.372	4	.9641	4
2.47	15	1.349	8	.9446	5
2.45	22	1.336	17	.9338	6
2.39	8	1.328	6	.9315	5
2.35	13	1.296	6	.9277	5
2.240	10	1.259	4	.9200	4
2.181	5	1.253	8	.9168	4
2.090	5	1.235	7	.9067	6
2.065	7	1.226	30	.9033	14
2.057	11	1.205	9	.8905	9
1.993	6	1.195	25	.8817	4
1.888	[b] 100++	1.175	7	.8765	4
1.868	8	1.173	7	.8705	4
1.812	21	1.166	6	.8645	5
1.807	16	1.161	5	.8584	5
1.780	11	1.148	6	.8480	6
1.763	14	1.139	4	.8449	8
1.717	16	1.122	5	.8374	5
1.690	8	1.110	6	.8346	5
1.629	9	1.091	15	.8242	3
1.610	[b] 100+	1.075	5	.8171	8
1.597	12	1.054	4	.8149	7
1.542	32	1.045	4	.8054	6
1.531	13	1.033	9	.7987	8

[a] I is the observed height of the diffraction peaks.
[b] These peaks were too strong to be completely recorded on the X-ray pattern.

The reaction between Bi_2O_3 and SnO_2 has been studied extensively by Coffeen [13, 14], who indicated that the hydrous bismuth stannate, $Bi_2(SnO_3)_3 \cdot 5H_2O$, fired at 1,149° C, formed the compound $Bi_2(SnO_3)_3$. The present study indicates that the Bi_2O_3:3SnO_2 mixture contains a new compound plus free SnO_2, and that the composition $Bi_2O_3 \cdot 2SnO_2$ contains no free SnO_2. It had been reported by Aurivillius [15] that the system Bi_2O_3-TiO_2 contained a compound, $Bi_4Ti_3O_{12}$, that was pseudotetragonal, actually orthorhombic; therefore, the analogous compound $2Bi_2O_3$:3SnO_2 was looked for in the Bi_2O_3-SnO_2 system. The reported structure could not be correlated with the compound found in the Bi_2O_3-SnO_2 system. It must therefore be concluded that the Bi_2O_3-SnO_2 compound is not isostructural with $Bi_2Ti_3O_{12}$, but has a distorted pyrochlore-type structure with a ratio of Bi_2O_3:2SnO_2.

The X-ray pattern of the $Bi_2O_3 \cdot 2SnO_2$ compound given in table 5 resembles very strongly those of the cubic pyrochlores. All of the cubic peaks for a 10.68 A cubic pyrochlore structure can be found in this pattern, although there are other peaks present. A cubic unit cell of 21.37 A could account for most of these excess peaks, but some would be still unexplained. Although the pattern is very strongly pseudo-cubic, it must be concluded that the true symmetry is other than cubic.

It may be seen in figure 1 that the radius of the Bi^{+3} ion is close to that of Gd^{+3} and, on the basis of radius ratio only, could be expected to form a cubic pyrochlore structure with SnO_2. However, the electronic polarization of the Bi^{+3} ion is probably different from that of the rare earths and may be

related to the distortion from cubic symmetry. This notion of electronic polarization has been very valuable in explaining the distortion from cubic symmetry in the perovskite structures [16].

4.4. Zirconates

Specimens of La_2O_3:$2ZrO_2$ and Nd_2O_3:$2ZrO_2$ were carefully examined by X-ray diffraction powder analysis because previous work by Brown and Duwez [17] indicated that no compounds existed in these two systems. Table 1 shows that several extra lines of relatively low intensity were found in both patterns, which could be indexed only on the basis of a cubic pyrochlore-type compound. In table 4 the intensities calculated for $Nd_2Zr_2O_7$, using an oxygen parameter of 0.414, agree very well with the observed peak heights. A compound at a composition of La_2O_3:$2ZrO_2$ was suggested by Trombe and Foex [18]. From the data presented it must be concluded that the compounds $La_2Zr_2O_7$ and $Nd_2Zr_2O_7$ do indeed exist and probably have a wide solid-solution range. They would fall in the middle of the stabilized cubic zirconia solid-solution regions, shown in the phase diagrams of the systems La_2O_3-ZrO_2 and Nd_2O_3-ZrO_2, proposed by Brown and Duwez [17] and reproduced here as figures 2 (a) and 3 (a). These compounds are indicated in the proposed revision of the two phase diagrams, figures 2 (b) and (c), and 3 (b). The compounds La_2O_3·$2ZrO_2$ and Nd_2O_3·$2ZrO_2$ have been indicated as melting congruently in figures 2 (b) and 3 (b) for the purpose of simplicity of the phase diagram, although no information is available on the melting points. If the compound melted incongruently, there could be no field of $La_2Zr_2O_7$ (or $Nd_2Zr_2O_7$) solid solution on the high ZrO_2 side of the compound. This would not agree with the observed widening of the single-phase cubic solid-solution area shown by Brown and Duwez [17]. Figure 2 (c) indicates the phase equilibria in the La_2O_3-ZrO_2 system if the pyrochlore compound actually melted incongruently.

It might be thought possible to have both a compound and a cubic ZrO_2 solid solution in the phase diagrams. Such a situation would demand that the diffraction peaks in the X-ray patterns of the fluorite-type solid-solution phases coincided with the strong peaks of the pyrochlore compound, so as to agree with the observed single-phase solid solution. A highly complex diagram of this sort could be drawn for either a congruently or an incongruently melting compound. As a complexity of such a nature is unlikely, it is thought that the phase diagrams, figures 2 (b) and 3 (b), best fit all of the observed data.

It has been claimed by Ruff and Ebert [19], and Duwez, Brown, and Odel [20] that Sc_2O_3, Sm_2O_3, Gd_2O_3, and Y_2O_3 all form cubic zirconia solid solutions. These conclusions have been quoted by Dietzel and Tober [21]. In the present study, only the Y_2O_3:$2ZrO_2$ composition has been examined. This specimen is apparently that of a single-phase fluorite material with no additional lines observable.

It is possible that the Y_2O_3:$2ZrO_2$ composition is a true pyrochlore compound in which the faint

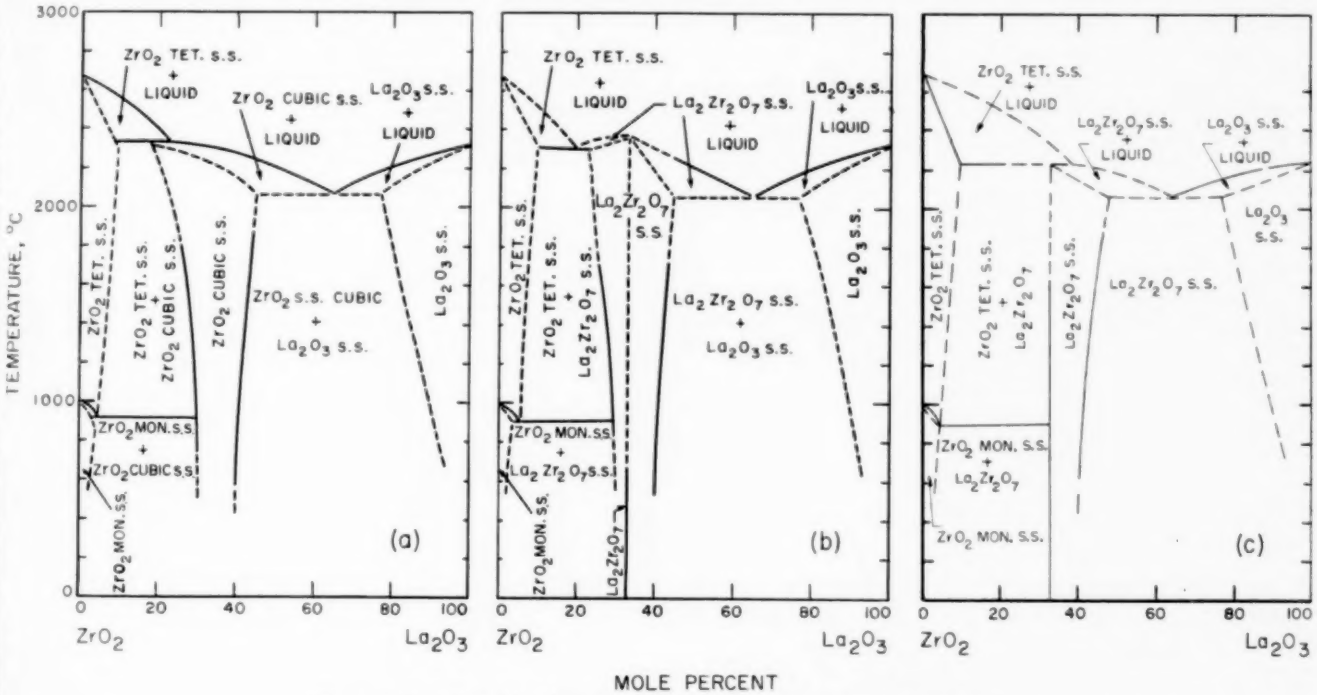

FIGURE 2. *Possible phase equilibria in lanthana-zirconia system.*

(a) Phase equilibria in the system lanthana-zirconia according to Brown and Duwez [17]. (b) Postulated phase equilibria in the system lanthana-zirconia showing the compound $La_2Zr_2O_7$ melting congruently with solid solution on both sides of the compound. (c) Possible phase equilibria in the system lanthana-zirconia showing the compound $La_2Zr_2O_7$ melting incongruently with solid solution only on the high La_2O_3 side of the compound.

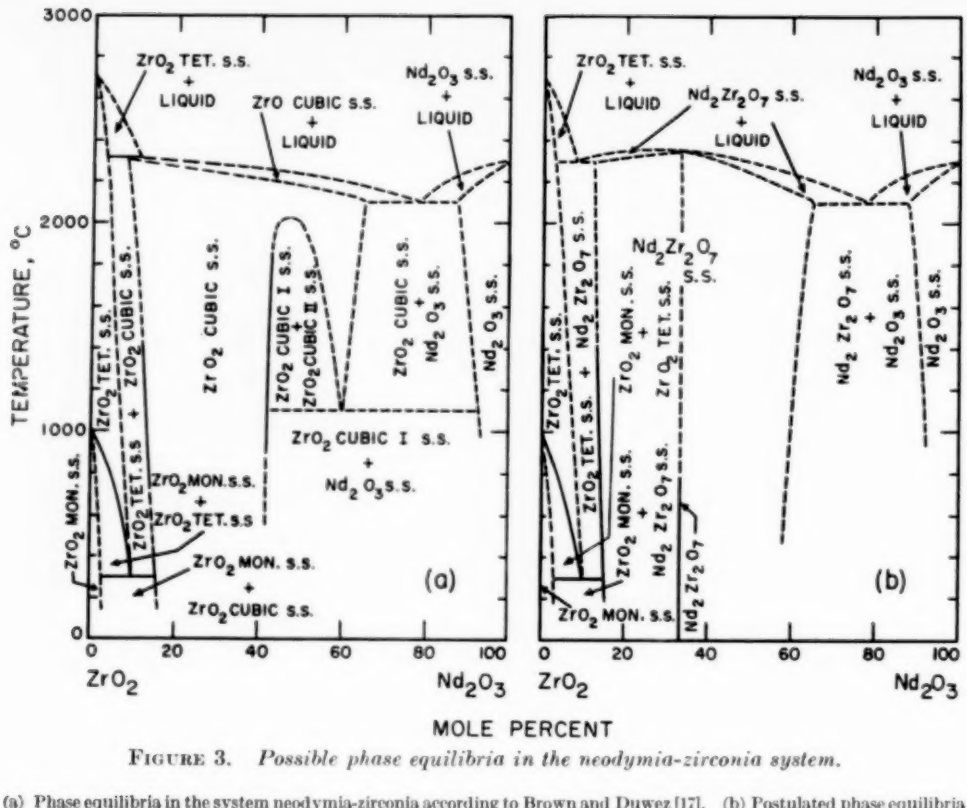

FIGURE 3. *Possible phase equilibria in the neodymia-zirconia system.*

(a) Phase equilibria in the system neodymia-zirconia according to Brown and Duwez [17]. (b) Postulated phase equilibria in the system neodymia-zirconia showing the compound $Nd_2Zr_2O_7$ melting congruently with solid solution on both sides of the compound.

lines characteristic of pyrochlore are too weak to be observed. As shown in table 4, the intensity of these lines is almost entirely due to the difference in the scattering power of the A and B ions. The relative intensity of the additional peaks should be very small as the scattering factors of Y^{+3} and Zr^{+4} are almost exactly equal and the intensities depend almost entirely on the oxygen ions. The observed peak heights and the calculated intensities of $Y_2Zr_2O_7$ show good correlation. Although it cannot be unequivocally decided whether the Y_2O_3:$2ZrO_2$ composition is a fluorite solid solution or a pyrochlore-type compound, the latter is more probable, and it is not surprising that the excess lines cannot be seen on the X-ray diffraction powder patterns. It is, therefore, proposed that no stabilized cubic ZrO_2 solid solutions exist in mixtures of ZrO_2 and the larger trivalent ions. All such reported occurrences would than be solid solutions of $A_2B_2O_7$ pyrochlore compounds, as shown in figures 2 (b) and 3 (b).

The In_2O_3:$2ZrO_2$ composition also shows only a single cubic fluorite-type phase in the X-ray diffraction powder pattern. As the In_2O_3-ZrO_2 system is known to contain two phases in this area [22], and the present specimen contracted considerably and lost weight, it is assumed that the excess In_2O_3 was volatilized and that a cubic ZrO_2 solid solution was actually found in this case.

A general rule can now be given for the reaction of ZrO_2 with various oxides of trivalent metals:

Solid-state reactions of ZrO_2 with oxides of the smaller trivalent ions, for example In_2O_3, yield cubic ZrO_2 solid solutions; however, the larger trivalent ions probably result in $A_2B_2O_7$ pyrochlore-type solid solutions.

4.5. Cerates and Uranates

a. Cerates

The only cerate composition examined in this study was In_2O_3:$2CeO_2$. The X-ray pattern showed only CeO_2 with no solid-solution or compound formation. The In_2O_3 was believed to have volatilized.

b. Uranates

Only two compositions containing UO_2, applicable to the present work, Nd_2O_3:$2UO_2$ and Y_2O_3:$2UO_2$ were examined. These preparations have been described elsewhere [23] and will be reviewed briefly here. The Y_2O_3:$2UO_2$ composition was definitely two phases, showing partial solid solution of both components. The X-ray pattern of the Nd_2O_3:$2UO_2$ composition showed a single phase apparently a fluorite-type solid solution (table 1). In this case the characteristic lines of the pyrochlore structure should easily have been observed, as Nd

has an atomic number of 60, whereas U is 92. When the oxygen positions were shifted considerably from those of the other pyrochlores in an attempt to account for the zero intensity of the additional peaks, improbable uranium to oxygen bond lengths resulted. It must be concluded, therefore, that a compound of the type $Nd_2U_2O_7$ probably does not exist and that the composition $Nd_2O_3{:}2UO_2$ is a single-phase fluorite-type solid solution with an oxygen deficiency.

5. Summary

X-ray diffraction powder data have been presented to show that many $A_2O_3{:}2BO_2$ compositions yield pyrochlore-type compounds when heated to the appropriate temperatures to give solid-state reactions. Oxides of the largest A^{+3} ions with TiO_2 give distorted pyrochlore structures, whereas most of the oxides of the large A^{+3} ions form cubic pyrochlore compounds with the tetravalent ions. Oxides of the smaller A^{+3} ions do not form compounds. This information is shown in a plot of the radius of the A^{+3} ions versus that of the B^{+4} ions. Here it can be seen that certain areas of this diagram enclose certain structural types of compounds, although exceptions may be found.

Because of the discovery of small peaks characteristic of the pyrochlore structure in the X-ray diffraction powder patterns of $La_2O_3 \cdot 2ZrO_2$ and $Nd_2O_3 \cdot 2ZrO_2$, these compositions have been called pyrochlore-type compounds. The presence of these compounds necessitates a revision of the published phase diagrams for these systems, and such revisions have been shown.

6. References

[1] W. R. Cook and H. Jaffe, Phys. Rev. **88,** 1426 (1952).
[2] W. R. Cook and H. Jaffe, Phys. Rev. **89,** 1297 (1953).
[3] A. Bystrom, Arkiv Kemi, Mineral. Geol. [A] **18** (1945).
[4] L. W. Coughanour, R. S. Roth, S. Marzullo, and F. E. Sennett, J. Research NBS **54,** 191 (1955) RP2580.
[5] N. N. Padrow and C. Schusterius, Ber. deut. keram. Ges. **31,** 391 (1954).
[6] W. H. Davenport, S. S. Kistler, W. N. Wheildon, and O. T. Whittemore, J. Am. Ceram. Soc. **33,** 333 (1950).
[7] H. R. Gaertner, Jahrb. Min. Beil. Bd. [1] **61,** (1930).
[8] O. Rosen and A. Westgren, Geol. Fören. Förh. **60,** 226 (1938).
[9] International tables for X-ray crystallography, vol. 1. (Kynoch Press, Birmingham, England, 1952).
[10] J. Green, Bul. Geol. Soc. Am. **64,** 1001 (1953).
[11] E. A. Wood, Acta Cryst. **4,** 353 (1951).
[12] M. L. Keith and R. Roy, Am. Mineralogist **39,** 1 (1954).
[13] W. Coffeen, J. Am. Ceram. Soc. **36,** 207 (1953).
[14] W. Coffeen (personal communication).
[15] B. Aurivillius, Ark. Kem. Sverige. **1,** 499 (1950).
[16] S. Roberts, Phys. Rev. **76,** 1217 (1949).
[17] F. H. Brown, Jr. and P. Duwez, J. Am. Ceram. Soc. **38,** 95 (1955).
[18] F. Trombe and M. Foex, Compt. rend. **233,** 254 (1951).
[19] O. Ruff, and F. Ebert, Z. anorg. u allgem. Chem. **180,** 19 (1929).
[20] P. Duwez, F. H. Brown, Jr., and F. Odell, J. Electrochem. Soc. **38,** 356 (1951).
[21] A. Dietzel and H. Tober, Ber. deut. keram. Ges. **30,** 71 (1953).
[22] C. Schusterius and N. N. Padrow, Ber. deut. keram. Ges. **30,** 235 (1953).
[23] S. M. Lang, F. P. Knudsen, R. S. Roth, and C. L. Filmore, NBS Circular 568 (1956).

WASHINGTON, September 21, 1955.

Journal of Research of the National Bureau of Standards Vol. 56, No. 1, January 1956 Research Paper 2644

Thermal Decomposition of Polytetrafluoroethylene in Various Gaseous Atmospheres[1,2]

L. A. Wall and J. D. Michaelsen

The effects of various gaseous atmospheres on the thermal decomposition of polytetrafluoroethylene have been investigated in the range 450° to 500° C. Both catalysis and inhibition were observed. The inhibitory substances, chlorine, hydrogen, carbon tetrachloride, and toluene, all produced marked changes in the mechanism of polytetrafluoroethylene decomposition. Whereas the normal degradation reaction in a vacuum produces mainly monomer, the inhibited reactions give large fragments plus side reactions, such as the defluorination of the skeletal carbon structure. The results can be interpreted in terms of previous theoretical treatments of chain mechanisms for polymer decomposition and lead to the conclusion that, although the inhibited reactions produce little monomer and are highly random, the relatively high rates observed indicate induced decomposition by the inhibitory substances. Energetic considerations are discussed and appear consistent with the postulated mechanisms.

1. Introduction

The thermal decomposition of polytetrafluoroethylene in vacuum has been studied in some detail by Madorsky and coworkers [1][3]. Although Madorsky et al. report that the polymer degrades by a first-order rate law, close inspection of their data (fig. 1) reveals that this is only strictly true at temperatures above about 510° C, whereas below about 480° C the polymer degrades by a zero-order law.

The existence of the zero-order law governing the kinetics of degradation at temperatures lower than about 480° C has been confirmed by one of the present experiments, the data of which are plotted in figure 2. Here, the weight-loss-versus-time curve for the degradation performed in a flow system under nitrogen is given. The plot shows that after an initial slight dip the rate is constant up to about 40 percent of volatilization at 460° C. In the temperature range studied, however, the energy of activation obtained from extrapolated initial rates was 80 kcal, as reported by Madorsky [1].

During the degradation the polymer retains its rigid form to about 50-percent conversion, after which it softens. During this pyrolysis, close to 100 percent of the volatile matter is monomer.

Most polymer decompositions can be treated in terms of a mechanism analogous to polymerization involving four elementary processes: initiation, propagation, transfer, and termination [2]. In the case of this polymer, however, the characteristics of the rate versus conversion curves (fig. 1) and the type of products obtained from the decomposition lead one to the conclusion that a chain mechanism is operative and that little transfer is occurring. Therefore, only three of these reactions have been considered here:

$$P \xrightarrow{k_1} R{-}CF_2{-}CF_2\cdot + R_m{-}CF_2\cdot \quad (m=1 \text{ or } 2) \qquad (1)\ \text{Initiation}$$

$$R{-}CF_2{-}CF_2\cdot \xrightarrow{k_2} R\cdot + C_2F_4 \qquad (2)\ \text{Propagation}$$

$$2R{-}CF_2\cdot \xrightarrow{k_3} P \text{ or } 2P$$

$$\text{or} \quad R_m{-}CF_2\cdot \xrightarrow{k_4} \text{evaporation} \qquad (3)\ \text{Termination}$$

The P represents any size polymer, R is part of a polymer chain, and the k's are the specific rate constants.

The mechanism then is one in which a bond breaks, probably at the ends, forming radicals that unravel into monomer and eventually terminate by one or more of the processes listed.

The amount of unraveling per initiation or termination act is the kinetic chain length, γ, and a variation in this can influence the order of the rate with respect to mass, as shown in figure 3. Here are plotted theoretical curves, the upper two showing the over-all rate for this type of process, in which a polymer had an initial degree of polymerization of about 1,000 and a kinetic chain length of 10^4 and 10^3, respectively, with a given rate of initiation. With the same rate of initiation but now restricted to end initiation, and with little or no unraveling, i. e., $\gamma=1$, the dashed curve would apply, which has about 0.001 the initial rate of the upper curve. This dashed curve gives a zero-order rate with respect to mass, which would be the situation if complete inhibition could be produced.

The change in order of rate of degradation of polytetrafluoroethylene from zero to first order with increase in temperature may indicate an increase in

[1] Presented in part at the 126th Meeting of the American Chemical Society in New York, N. Y., September 12–17, 1954.

[2] This work was performed as a part of the research project on high-temperature-resistant polymers sponsored by the Ordnance Corps, Department of the Army.

[3] Figures in brackets indicate the literature references at the end of this paper.

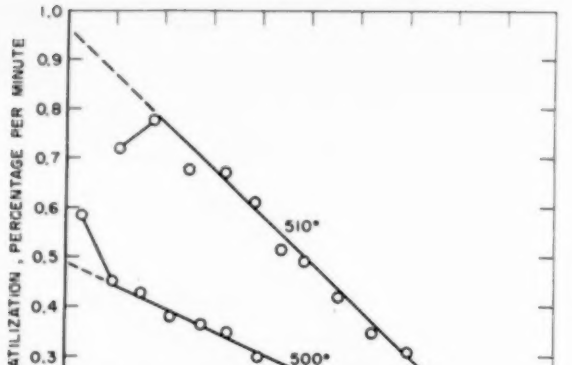

FIGURE 1. *Rate of thermal degradation of polytetrafluoroethylene in a vacuum as a function of percentage of volatilization [1].*

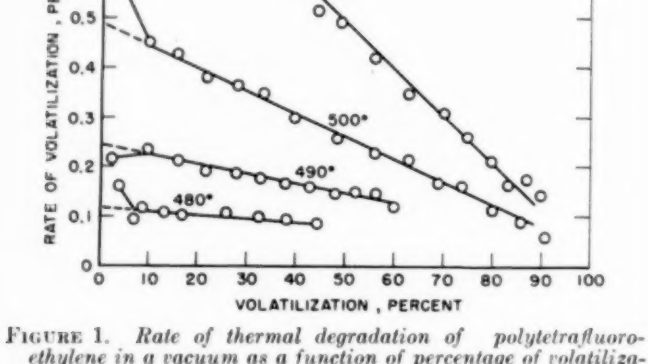

FIGURE 2. *Thermal degradation of polytetrafluoroethylene in flow system under nitrogen at 460° C.*

kinetic chain length from a value much lower than the degree of polymerization at temperatures of degradation below about 480° C to a value equal to or greater than the degree of polymerization at temperatures above 510° C. A possible alternate explanation could be that a surface effect is important at the lower temperature range, such that the rate is proportional to the surface area of the degrading polymer, whereas at high temperatures the rate eventually becomes proportional to the bulk of the material. However, in the experiments under gases reported here, surface effect does not appear to exist to any great extent because the surface area was varied in this study.

The curve with a maximum in figure 3 represents the behavior for a purely random degradation of a

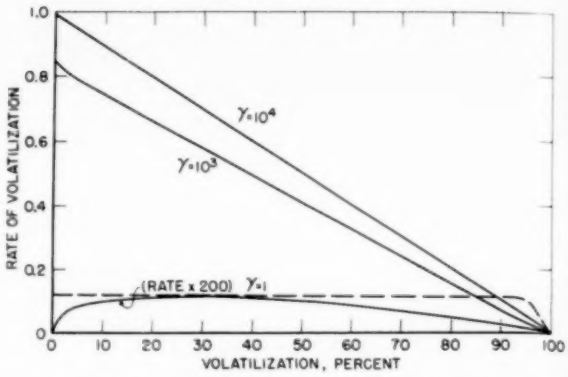

FIGURE 3. *Rate of volatilization as a function of conversion and kinetic chain length with random initiation (solid line) and end initiation (dashed line) [2].*

polymer. Random degradation may be the result of only random initiation, or of a high number of transfer reactions, if in either case a small number of depropagation or unraveling acts occur. A much slower over-all rate should result if the random effect is due to the initiation step alone.

Whenever a reaction proceeds by a chain mechanism it should be possible, in theory, to inhibit the over-all reaction by adding a reagent that would in effect make reaction 4 in the above mechanism more probable than is normal for the uninhibited reaction. Changing the history of the polymer in regard to catalyst and structural contaminants has previously been shown to have little effect on the rate of degradation [3]. However, in the thermal decomposition of hydrocarbons, various conditions of inhibition have been studied by Rice and Polly [4] and Hinshelwood and coworkers [5]. For gas-phase reactions inhibition has been shown to be produced by some gases, e. g., NO and CH_3CHCH_2. In solid polymers, and especially in polytetrafluoroethylene, one of the difficulties would be poor accessibility of the inhibitor to the radical chain carrier. This difficulty was borne out by the failure to alter appreciably the course of its degradation in over 40 experiments in which solid reagents that were considered to be potential inhibitors were intimately mixed with the polymer. On the other hand, gases can diffuse much more readily throughout a reaction medium and hence offered, on a priori considerations, the best possibility of influencing the course of the reaction.

2. Experimental Reagents

The polymer used was in the form of a water suspension obtained from E. I. duPont de Nemours & Co., Inc. and designated by them as TD-3. The suspension was frozen and then dried in a vacuum, and the powder so obtained was employed in the majority of the experiments.

The gases used were the purest obtainable from the Matheson Co., Inc. The toluene was Baker & Adamson's ACS grade.

3. Procedure

The rate of degradation was measured by determining the weight loss of the polymer after periodic heating under the various flowing gases. The sample of polymer was usually about 1g and was placed in a porcelain boat for heating. The boat was heated in a horizontally placed hard-glass tube surrounded by a brass furnace that covered about one-third of the tube. The gas and boat were introduced into one end of the tube, and the gas was exhausted at the other end. The boat was inserted into the tube via a female 34/45 standard-taper glass ground joint, after which the tube was capped with a male 34/45 standard-taper ground joint. A heavy nichrome wire passing through a small tube in the cap, and sealed with a rubber stopper, enabled the operator to move the porcelain boat while in the tube in and out of the furnace.

In a typical measurement the boat containing a weighed sample of polymer was placed in the unheated portion of the tube. The system was then thoroughly flushed with the gas under study and a steady flow maintained. The temperature of the furnace was brought to the desired level. The boat was then pushed into the furnace. The manually operated variable transformer sometimes had to be readjusted in order to maintain the desired temperature. Temperature equilibrium was usually reached about 3 to 4 min after the introduction of the boat into the furnace. The time at which the temperature reattained the desired value was taken as the zero time for that particular run. At the end of a given interval of time (usually 1 hr) the boat was withdrawn from the furnace into the unheated part of the tube. This time was taken as the end of the interval of pyrolysis. Experience showed that it made no difference whether the boat was then withdrawn from the tube and allowed to cool to room temperature in the air or left in the tube to cool.

The temperature of the furnace was measured by means of an iron-constantan thermocouple read on a potentiometer. The thermocouple was centered in the furnace by means of a thermocouple well, securely attached to the cap. The temperature was determined at a position above the boat and was steady to ± 2 deg C.

When pyrolyzed in a vacuum or under nitrogen, polytetrafluoroethylene retains its original form. In the experiments reported here the polymer, with one exception, became very fluid at the temperature of pyrolysis. Although the molecular weight of the polymer cannot be determined quantitatively, this change in viscosity from a solid to a very fluid liquid was taken as an indication of a very pronounced drop in molecular weight during the course of pyrolysis under the gases.

4. Results

The gases studied may be divided into three groups: (1) those exhibiting a strong catalytic effect on the rate of degradation, i.e., O_2, NO, H_2S, and SO_2; (2) those producing an initial inhibitory effect, i.e., H_2, Cl_2, CCl_4, and toluene; and (3) those that show neither effect, i.e., N_2 and benzotrifluoride. The rates under nitrogen (e.g., 0.017%/min at 457° C) are quite close to those observed previously in vacuum work (0.017%/min at 453° C) [1]. Consequently, results under nitrogen are used for comparison purposes.

TABLE 1. *Gaseous products from the decomposition of polytetrafluoroethylene under various gases*

Product	Gaseous atmosphere			
	O_2	H_2	Toluene	Cl_2
	Mole %	*Mole %*	*Mole %*	*Mole %*
Perfluoroethylene	------	33	45	[a]
Silicon tetrafluoride	19	34	9	[a]
Carbon dioxide	63	33	23	[a]
Carbon monoxide	18	------	------	[a]
Trifluoromethane	------	------	18	[a]
Perfluorocyclobutane	------	------	5	[a]

[a] Not identified. The products, besides an excess of chlorine atoms, showed ions in the mass spectrograph containing several chlorine atoms as well as oxygen and silicon. For example, the following ions were tentatively identified: CCl_3, $SiCl_3$, $SiCl_2F_2$, $OSiCCl_2$, and SiC_2Cl_4. The largest of these peaks, mass 161, was 11.7 percent of the maximum peak (mass 70, that is, Cl_2^{35}).

4.1. Catalytic Effect

The curves representing the degradation of polytetrafluoroethylene at 457° C under the various gases exhibiting a catalytic effect are shown in figure 4.

In the degradation under oxygen the polymer remained white and solid throughout the entire conversion. This fact, plus the catalytic effect and the absence of monomer in the products lead to the belief that the gas attacks the free radicals and increases, in effect, the rate of propagation. The analyses obtained from the mass spectra of the gases evolved from this experiment are listed in table 1.

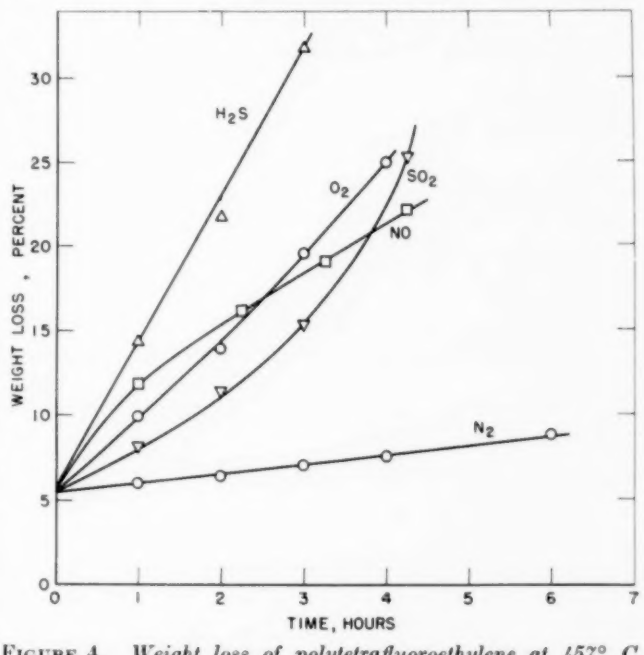

FIGURE 4. *Weight loss of polytetrafluoroethylene at 457° C. under various gases having a catalytic effect on the thermal degradation.*

The lack of monomer and the presence of SiF_4 and CO_2 are noted. A very small quantity ($<1\%$) of other silicon derivatives were also observed but were not identified. These results appear to indicate a reaction of the type:

$$\sim\!\sim\!CF_2\!-\!CF_2\cdot + O_2 \rightarrow \text{products.}$$

The primary products may consist of labile compounds, possibly CF_2O, that quickly decompose on the glass at the temperature of pyrolysis to give the observed compounds. There appears to be no attack on the polymer because this would be expected to result in a darkening of the polymer and/or a drop in molecular weight to give a residue of high fluidity at the temperature of pyrolysis.

When present at high concentrations in the thermal decomposition of hydrocarbons, nitric oxide has been shown [5] to catalyze the rate of decomposition. At the high concentrations used here, the nitric oxide also seems to have an over-all catalytic effect. The polymer darkened slightly initially, and as conversion increased, the residue became clear and very fluid. This, plus the fact that the rate starts to level off, would seem to indicate that not only an induced initiation by some transfer mechanism is taking place, but also some product is being formed that stabilizes the degrading free radicals or polymer.

In the experiment with hydrogen sulfide the polymer quickly blackened and became fluid at its temperature of pyrolysis. During the course of this experiment the apparatus became coated with sulfur.

As the apparatus was etched from other experiments, it was not known definitely whether or not hydrogen fluoride was produced here; it presumably was. These results would seem to indicate induced initiation and defluorination.

With sulfur dioxide the polymer became black and gelatinous. Again, this is indicative of induced decomposition and defluorination with no inhibition. The increasing rate of degradation as shown in figure 4 supports this.

4.2. Inhibition Effects

In figures 5, 6, and 7 are plotted the weight-loss-versus-time data for the thermal decomposition of polytetrafluoroethylene under hydrogen, chlorine, and toluene. Carbon tetrachloride also showed good inhibition initially, but as at later stages, the inhibition was much less effective than with the above three compounds, the system was not studied in detail.

It will be immediately noted on comparing these results with those obtained for the pyrolysis of polytetrafluoroethylene under nitrogen, figure 2, that the characteristics of the reaction have completely changed in that all the curves for the gas studies have a definite inflection point. Consequently, when the rate is plotted against conversion, figures 8, 9, and 10, it is seen that all the graphs have definite maxima and that initially the rates are much lower than those for the vacuum work, figure 1. These curves are typical of those obtained for mechanisms with large random components [2]. Random initiation or very

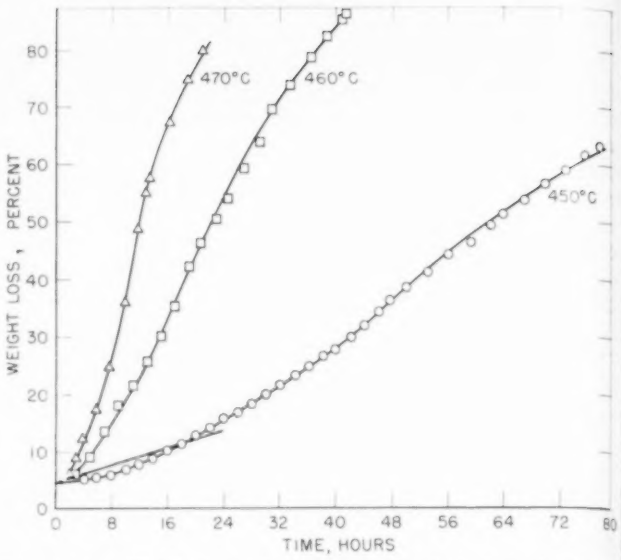

FIGURE 5. *Weight loss of polytetrafluoroethylene under hydrogen at several temperatures.*

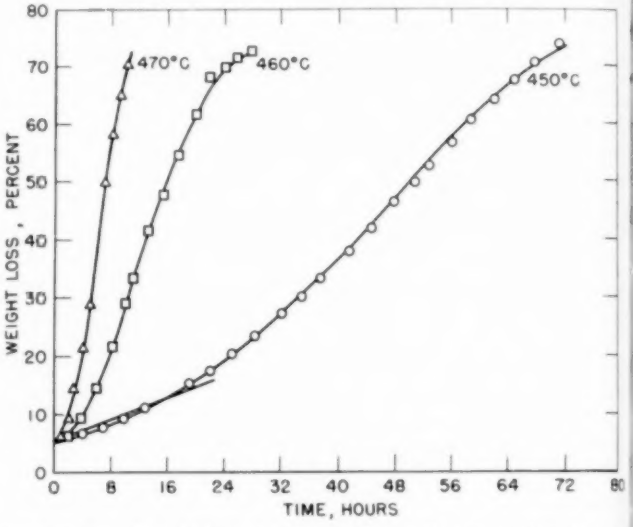

FIGURE 6. *Weight loss of polytetrafluoroethylene under chlorine at several temperatures.*

frequent transfer with short propagation and termination usually give rise to such results. It has been recently demonstrated that the thermal decomposition of polymethylene follows such a pattern [6]. This type of mechanism leads to a very fast drop in molecular weight, and this has been noted in these experiments, because the polymer quickly became very fluid.

The experiments with chlorine as the inhibitor did not show any consistent color change in the polymer. Also, an analysis of the polymer after 80-percent degradation showed a chlorine content of 0.6 percent by a microcombustion method. All this is compatible with the idea that the mechanism of the observed inhibition involves the combination of polymer radicals with the chlorine atoms produced. An analysis

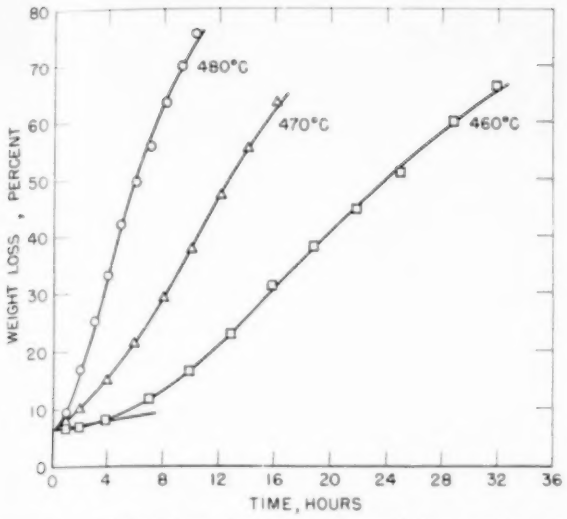

FIGURE 7. *Weight loss of polytetrafluoroethylene under toluene diluted with nitrogen at several temperatures.*

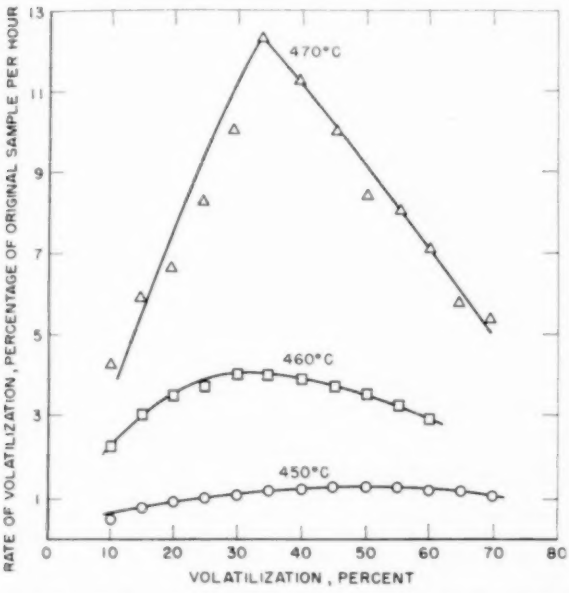

FIGURE 8. *Rate of volatilization of polytetrafluoroethylene under hydrogen as a function of conversion at several temperatures.*

of the gaseous products, table 1, is very complicated, consisting mostly of silicon, halogen, and carbon-containing compounds. These again would seem to result from the decomposition of labile primary products on the glass.

In the experiments with hydrogen there is, besides the molecular weight drop, a blackening of the polymer. At very high conversions (about 65%) the residue becomes hard. Concurrent with all this is an etching of the glass tube. An analysis of the gaseous products, table 1, shows that some monomer is produced, as well as carbon dioxide and silicon tetrafluoride. These results again indicate random degradation, but with the added feature of defluorination by hydrogen.

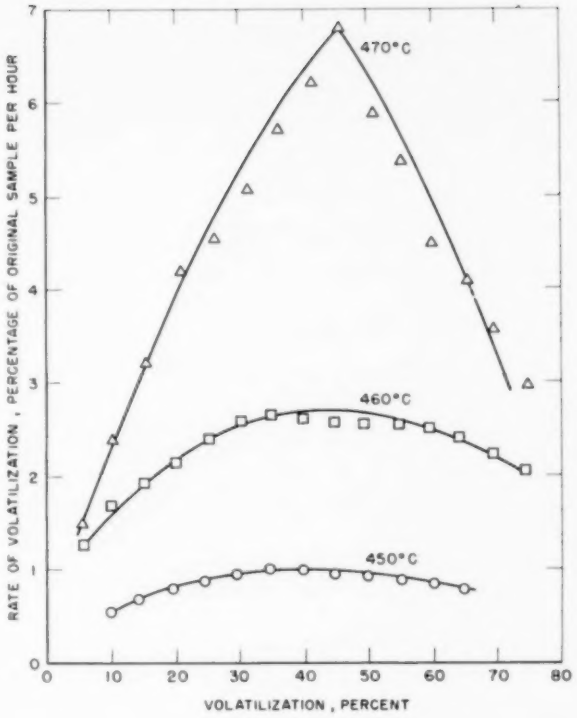

FIGURE 9. *Rate of volatilization of polytetrafluoroethylene under chlorine as a function of conversion at several temperatures.*

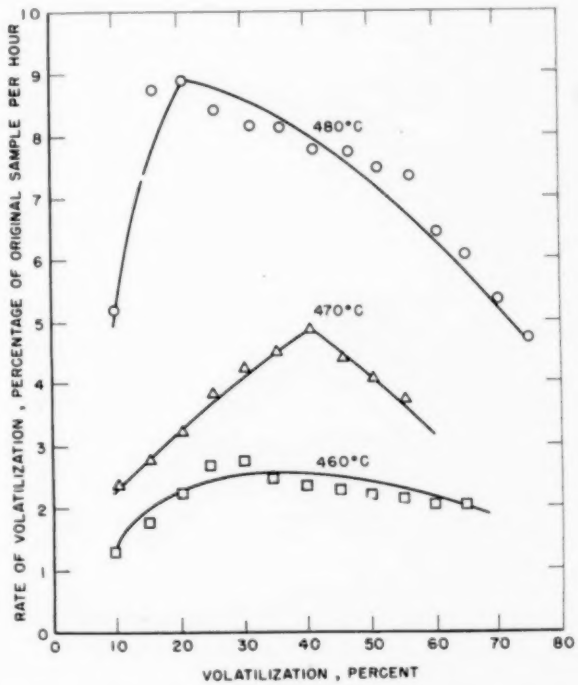

FIGURE 10. *Rate of volatilization of polytetrafluoroethylene under toluene diluted with nitrogen as a function of conversion at several temperatures.*

The experiments with toluene give results similar to those with hydrogen. However, defluorination is much more prevalent and may actually be rate determining, because the residue, after becoming liquid, soon hardens to a brittle mass at about 30-percent conversion. The analysis of gaseous products is given in table 1. Here again there is some monomer formed, as well as silicon tetrafluoride and carbon dioxide. The somewhat larger amount of monomer may mean relatively less effective reaction of the vapor with decomposing polymer free radicals.

5. Discussion

In any kinetic discussion some idea of the various bond strengths is valuable. However, the carbon-carbon-bond strength in fluorocarbons is in doubt. A value of 124 kcal for the carbon-carbon bond in hexafluoroethane has been reported by Dibeler, Reese, and Mohler [7] as obtained in electron-impact experiments. However, a recent, separate determination of the ionization potential of the perfluoromethyl radical by Lossing [8], using the electron-impact method, has lowered this value for hexafluoroethane to 95 kcal.

An analysis of the best thermochemical data on the subject would seem to favor a value about half way between these two extremes. Using the high and rather generally accepted value of the heat of sublimation of graphite, i. e., L (C)=170.6 kcal, together with the heat of formation of carbon tetrafluoride, 220 kcal [9, 10], an average carbon-fluorine bond of 116 kcal is obtained for this compound. Now in hydrocarbons the average carbon-hydrogen bond strength in ethane is about 8 percent less than those in methane. If in fluorocarbons the carbon-fluorine bond strengths drop off by approximately the same percentage in going from carbon tetrafluoride to hexafluoroethane, then the average carbon-fluorine bond strength in hexafluoroethane should be about 107 kcal. This, taken with the heat of formation of hexafluoroethane of 303 kcal, as obtained by Duus [9], gives a carbon-carbon bond strength for this fluorocarbon in the neighborhood of 112 kcal.

If the interpretation of the kinetic data along the lines of the existing theories is correct and polytetrafluoroethylene does decompose by end initiation with the average carbon-carbon bond strength being close to that in hexafluoroethane, e. g., 110 kcal, it should be possible to deduce the strength of the bond broken in the end initiation (see section 1), i. e., E_1. Taking the only value available for the molecular weight of polytetrafluoroethylene, i. e., 200,000 [11], and realizing that for end initiation to have a predominant effect on the kinetics, this rate of initiation must be 10 times faster at about 500° C than that for random initiation, it is found that there must be a difference of at least 15 kcal between the strength of the weak end bond and that of the average bond. This gives the value of 95 kcal, which was used for end initiation.

In the experiments described it appears that the various gases have in some cases altered the

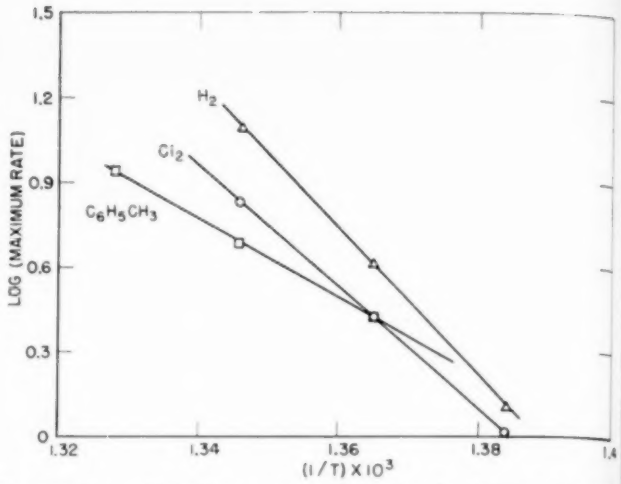

FIGURE 11. *Activation energy slopes for the thermal degradation of polytetrafluoroethylene under hydrogen, chlorine, and toluene.*

mechanism of the degradation of polytetrafluoroethylene. The gases that act as inhibitors have introduced a random quality to the over-all degradation.

In this random type of degradation as ascertained from the kinetic curves (fig. 8, 9, and 10), the maximum rates are the most dependable and the most significant from which to calculate energies of activation. The maximum rate of volatilization has been related [2] to the specific rate constant for a purely random reaction as follows:

$$[dC/dt]_{max}=k\frac{L}{e},$$

where C is conversion, t is time, k is a composite specific rate constant for the over-all reaction, e is the base for the natural logarithm, and L is the critical chain length for vaporization (i. e., the size for which rate of decomposition equals rate of vaporization) and is here assumed to be a constant. In terms of elementary chain mechanism and the total radical concentration R,

$$k=k_1+k_3\mathrm{R}=k_3(I/k_4)^{1/2} \qquad \text{(when } k_1 \text{ is small)},$$

where I is the rate of initiation of active centers, k_3 the rate constant for transfer, and k_4 the rate constant for termination.

Taking the maximum rate from the experimental curves as proportional to the specific rate constant and making Arrhenius-type plots of the data, straight lines are obtained, as shown in figure 11.

From the slopes of these lines energies of activation are obtained. In the case in which chlorine was the inhibiting gas, a value of 100 ±4 kcal is obtained. With hydrogen, a value of 118 ±4 kcal is obtained, and toluene gives 64 ±5 kcal.

The experimental results and theory can apparently be brought together if a mechanism of the following type is assumed, where, beside the three elementary reactions mentioned above, there is

$$A_2 \xrightarrow{k_1'} 2A\cdot \qquad (4)\ \text{Initiation.}$$

$$R{-}CF_2{-}R + A\cdot \xrightarrow{k_3} AF + P + RCF_2\cdot \qquad (5)\ \text{Transfer.}$$

$$R{-}CF_2{-}CF_2{-}R + A_2 \xrightarrow{k_5} R{-}CF{=}CF{-}R + 2AF \qquad (6)\ \text{Transfer.}$$

$$R{-}CF_2\cdot + A\cdot \xrightarrow{k_4''} R{-}CF_2{-}A \qquad (7)$$

$$R{-}CF_2\cdot + A_2 \xrightarrow{k_4'''} R{-}CF_2{-}A + A\cdot \qquad (8)$$

$$A\cdot + A\cdot + X \xrightarrow{k_4''''} A_2 + X \qquad (9)$$

(7), (8), (9) } Termination.

Here A_2 is the inhibiting gas, P and $R{-}CF_2\cdot$ are the polymer and polymer radicals, respectively, and X is the third body required for this reaction.

In the experiments with chlorine the low bond energy of this molecule should favor the formation of these atoms as the potential chain carriers. As the concentration of these atoms would be relatively high, the possibility of a chain transfer by reaction 5 and a molecular-weight drop would be increased, having an over-all effect of inducing the polymer decomposition. The lack of monomer in the gases evolved would seem to indicate that reaction 2 is suppressed, presumably owing to the termination of the polymer radicals by reactions 7 or 8, resulting in inhibition. The over-all chain termination would, then, seem to be by reaction 9, because the chlorine atoms would constitute the largest source of chain carriers. As the polymer is colorless throughout the degradation, reaction 6 would not likely be operative, as that would be expected to cause darkening of the polymer.

With this mechanism the over-all energy of activation would be expected to be related to those of the elementary steps as follows:

$$E = \tfrac{1}{2}E_1' + E_3 - \tfrac{1}{2}E_4''''$$

$$100 = \frac{57}{2} + E_3 - 0$$

$$E_3 = 71.5 \text{ kcal.}$$

Here 57 kcal is the dissociation energy of the chlorine molecule [12]. This rather high value for E_3 would seem to be the energy necessary for a chlorine atom to abstract a fluorine atom from the polymer, which reaction must be assumed in order to explain the high maximum rate and the molecular-weight drop.

When hydrogen is the inhibitor, the situation is slightly different. It is thought that the chain initiation step is the breaking off of a volatile fragment from the ends of the polymer, as shown by reaction 1, followed by unzipping of the polymer radical to give some monomer, reaction 2 (see table 1), but finally terminating by reaction 8. This mode of initiation of the reaction is assumed in place of hydrogen dissociation because the bond strength of hydrogen is higher than the 95 kcal of this reaction. Chain unzipping would be inhibited by reaction 8, and the hydrogen atom so formed probably induces further decomposition in the polymer by reaction 5. A side reaction such as reaction 6 would account for the darkening of the polymer but, due to the small mass of material vaporizing in this way, would probably not drastically affect the over-all rate. Final termination of the over-all chain reaction would seem to be most likely by reaction 7 if a steady state is truly obtained.

In this inhibition under hydrogen, the over-all energy of activation for this random process is broken down as follows:

$$E = \tfrac{1}{2}E_1 + E_3 - \tfrac{1}{2}E_4''$$

$$118 = \frac{95}{2} + E_3 - 0$$

$$E_3 = 70.5 \text{ kcal.}$$

These values obtained for the energy of activation for transfer, i. e., E_3, are high and constant within the experimental error of the experiment, e. g., 71 $\pm$4 kcal. As this step probably comprises two steps, one the abstraction of fluorine by a radical, and the other the breaking up of the polymer radical in a depropagation step, this high and apparently constant value is probably due to the propagation step E_2.

In the case of the toluene inhibition, an initial drop in molecular weight and the defluorination can be explained by the above reaction scheme, as in the case of hydrogen and chlorine. Here, formation of hydrogen atoms and benzyl radicals may be the most important initiation step (reaction 4), which in time should lead to chain transfer, reaction 5, and hence induced decomposition of the polymer. Termination by reactions 7 and 9, where benzyl radicals are important, would end the chain reaction. The observed inhibition could be explained by reactions 7 and 8. The presence of the defluorination by reaction 6, as evidenced by early hardening of the polymer, complicates the over-all rate. Therefore, it is not possible to identify the energy of activation obtained from the toluene experiments, i. e., 64 $\pm$5 kcal, as a single entity or a function of elementary energies of activation.

369131—56——3

6. References

[1] S. L. Madorsky, V. E. Hart, S. Straus, and V. A. Sedlak, J. Research NBS **51,** 327 (1953) RP2461.

[2] R. Simha, L. A. Wall, and P. J. Blatz, J. Polymer Sci. **5,** 615 (1950); R. Simha and L. A. Wall, J. Polymer Sci. **6,** 39 (1951); R. Simha and L. A. Wall, J. Am. Chem. Soc. **56,** 707 (1952).

[3] R. E. Florin, L. A. Wall, D. W. Brown, L. A. Hymo, and J. D. Michaelsen, J. Research NBS **53,** 121 (1954) RP2524.

[4] F. O. Rice and O. L. Polly, J. Chem. Phys. **6,** 273 (1938).

[5] L. A. K. Stavely, Proc. Roy. Soc. (London) [A] **162,** 557 (1937); L. A. K. Stavely and C. N. Hinshelwood, Nature **137,** 29 (1936); J. Chem. Soc. **1936,** 812, 818; Trans. Faraday Soc. **35,** 845 (1939); J. E. Hobbs and C. N. Hinshelwood, Proc. Roy. Soc. (London) [A] **167,** 439, 447 (1938); J. R. E. Smith and C. N. Hinshelwood, Proc. Roy. Soc. (London) [A] **180,** 237 (1942).

[6] L. A. Wall, S. L. Madorsky, D. W. Brown, S. Straus, and R. Simha, J. Am. Chem. Soc. **76,** 3430 (1954).

[7] V. H. Dibeler, R. M. Reese, and F. L. Mohler, J. Chem. Phys. **20,** 761 (1952).

[8] F. P. Lossing, private communication to V. H. Dibeler of the Mass Spectrometry Section, National Bureau of Standards.

[9] H. C. Duus, E. I. duPont de Nemours & Co., Inc., Wilmington, Del., presentation at the 126th Meeting of the American Chemical Society in New York, N. Y., September 15, 1954.

[10] R. S. Jessup, R. E. McCoskey, and R. A. Nelson, J. Am. Chem. Soc. **77,** 244 (1955); D. W. Scott, W. O. Good, and Guy Waddington, J. Am. Chem. Soc. **77,** 24[illegible] (1955).

[11] K. L. Berry and J. H. Peterson, J. Am. Chem. Soc. **73,** 5195 (1951).

[12] A. G. Gaydon, Dissociation energies and spectra of diatomic molecules (Dover Publications, Inc., New York, N. Y., 1950).

Washington, September 1, 1955.

Journal of Research of the National Bureau of Standards Vol. 56, No. 1, January 1956 Research Paper 2645

Abscissas and Weights for Gaussian Quadratures of High Order

P. Davis and P. Rabinowitz

Weights and abscissas are presented for the Gaussian quadrature rules of order $n=16$, 20, 24, 32, 40, 48. These constants were computed on Standards Automatic Computer by the method described and have passed a number of checks with about 20 places of decimals. Values of the weights and abscissas are also available for $n=64$, 80, and 96.

1. Introduction

Gaussian quadrature rules have hitherto been computed up to the case $n=16$ with 15 place accuracy [1].[1] In the work in the Numerical Analysis Section of the National Bureau of Standards, frequent use has been made of the rule $n=16$ and even of halving and quartering the interval for increased accuracy. For this reason, it is felt that the constants for rules of higher order will prove to be of use in working with electronic digital computers.

For further evidence of the practical utility of high-order rules, the reader may consult Hartree [2], Henrici [3], and Reiz [4]. Exact values of these quantities are also interesting in view of certain unsettled theoretical conjectures that have been made about distribution of the weights and abscissas [7].

2. Method of Computation

We deal with the Gaussian quadrature rule of order n on the interval $[-1,1]$:

$$\int_{-1}^{+1} f(x)dx = \sum_{k=1}^{n} a_{kn} f(x_{kn}). \tag{1}$$

The rule (1) holds exactly whenever f is a polynomial of degree $\leq 2n-1$. The abscissas $x_{kn}(k=1,2, \ldots, n)$ are the n zeros of the Legendre polynomial of order n: $P_n(x_{kn})=0$, whereas the weights are given by the expression

$$a_{kn}=\frac{k_{n+1}}{k_n}\frac{-1}{p_{n+1}(x_{kn})p'_n(x_{kn})}, \tag{2}$$

where $p_n x_n = k_n x_n + \ldots$ are the normalized Legendre polynomials. See, e. g., Szegö [5, p. 47]. Making use of the relationship

$$(1-x^2)P'_n(x)=n[P_{n-1}(x)-xP_n(x)], \tag{3}$$

we are able to derive from (2) the following alternate expression for the weights a_{kn}, which is useful for computation:

$$a_{kn}=\frac{2(1-x_{kn}^2)}{[nP_{n-1}(x_{kn})]^2} \qquad (k=1,2, \ldots, n). \tag{4}$$

[1] Figures in brackets indicate the literature references at the end of this paper.

To obtain a first approximation to the zeros of the Legendre polynomials, we make use of the following inequality derived by Szegö [6]: Let

$$x_{kn}=\cos\theta_{kn} \qquad (k=1,2, \ldots, n). \tag{5}$$

Then

$$\frac{j_k}{[(n+1/2)^2+c/4]^{1/2}}<\theta_{kn}<\frac{j_k}{(n+1/2)} \qquad (k=1,2, \ldots), \tag{6}$$

where j_k $(k=1,2, \ldots)$ are the successive zeros of the Bessel function $J_0(x)$ and $c=1-(2/\pi)^2$.

The first 150 values of j_k may be found in [8]. A preliminary computation of (6) with $n=16$ showed that the value of θ_{kn} is closer to the left-hand bound, and that five or six decimal places can be secured intially by employing

$$x_{kn}^{(1)}=\cos\frac{j_k}{((n+1/2)^2+c/4)^{1/2}} \tag{7}$$

as a first approximation to x_{kn}. The value $x_{kn}^{(1)}$ was successively improved by using the Newton formula

$$x_{kn}^{(t+1)}=x_{kn}^{(t)}-\frac{P_n(x_{kn}^{(t)})}{P'_n(x_{kn}^{(t)})}. \tag{8}$$

The derivative in (8) was computed from (3), whereas the Legendre polynomials themselves were computed from the recursion

$$\left.\begin{aligned} &nP_n(x)=(2n-1)xP_{n-1}(x)-(n-1)P_{n-2}(x)\\ &P_0(x)=1, \qquad P_1(x)=x. \end{aligned}\right\} \tag{9}$$

After the first approximation, the successive approximations were computed in double precision, and a shutoff value of $\epsilon=2^{-74}$ was employed in the iteration (8).

Although the abscissas and the weights are symmetric about $x=0$, all were computed independently. The starting values $x_{kn}^{(1)}$ for two symmetric points were different (cf. (7)). This served as one check of the accuracy of the computation. Additional checks were provided by computing the six quantities given in eq (10), page 37.

Abscissas	Weights
n = 2	
0.5773502691 89625764509	1.0000000000 0000000000
n = 4	
0.8611363115 94052575224	0.3478548451 3745385737
0.3399810435 84856264803	0.6521451548 6254614262
n = 8	
0.9602898564 97536231684	0.1012285362 9037625915
0.7966664774 13626739592	0.2223810344 5337447054
0.5255324099 16328985818	0.3137066458 7788728733
0.1834346424 95649804939	0.3626837833 7836198296
n = 16	
0.9894009349 91649932596	0.0271524594 1175409485
0.9445750230 73232576078	0.0622535239 3864789286
0.8656312023 87831743880	0.0951585116 8249278481
0.7554044083 55003033895	0.1246289712 5553387205
0.6178762444 02643748447	0.1495959888 1657673208
0.4580167776 57227386342	0.1691565193 9500253818
0.2816035507 79258913230	0.1826034150 4492358886
0.0950125098 37637440185	0.1894506104 5506849628
n = 20	
0.9931285991 85094924786	0.0176140071 3915211831
0.9639719272 77913791268	0.0406014298 0038694133
0.9122344282 51325905868	0.0626720483 3410906357
0.8391169718 22218823395	0.0832767415 7670474872
0.7463319064 60150792614	0.1019301198 1724043503
0.6360536807 26515025453	0.1181945319 6151841731
0.5108670019 50827098004	0.1316886384 4917662689
0.3737060887 15419560673	0.1420961093 1838205132
0.2277858511 41645078080	0.1491729864 7260374678
0.0765265211 33497333755	0.1527533871 3072585069
n = 24	
0.9951872199 97021360180	0.0123412297 9998719954
0.9747285559 71309498198	0.0285313886 2893366318
0.9382745520 02732758524	0.0442774388 1741980616
0.8864155270 04401034213	0.0592985849 1543678074
0.8200019859 73902921954	0.0733464814 1108030573
0.7401241915 78554364244	0.0861901615 3195327591
0.6480936519 36975569252	0.0976186521 0411388827
0.5454214713 88839535658	0.1074442701 1596563478
0.4337935076 26045138487	0.1155056680 5372560135
0.3150426796 96163374387	0.1216704729 2780339120
0.1911188674 73616309159	0.1258374563 4682829612
0.0640568928 62605626085	0.1279381953 4675215697

Abscissas	Weights
n = 32	
0.9972638618 49481563545	0.0070186100 0947009660
0.9856115115 45268335400	0.0162743947 3090567060
0.9647622555 87506430774	0.0253920653 0926205945
0.9349060759 37739689171	0.0342738629 1302143310
0.8963211557 66052123965	0.0428358980 2222668065
0.8493676137 32569970134	0.0509980592 6237617619
0.7944837959 67942406963	0.0586840934 7853554714
0.7321821187 40289680387	0.0658222227 7636184683
0.6630442669 30215200975	0.0723457941 0884850622
0.5877157572 40762329041	0.0781938957 8707030647
0.5068999089 32229390024	0.0833119242 2694675522
0.4213512761 30635345364	0.0876520930 0440381114
0.3318686022 82127649780	0.0911738786 9576388471
0.2392873622 52137074545	0.0938443990 8080456563
0.1444719615 82796493485	0.0956387200 7927485941
0.0483076656 87738316235	0.0965400885 1472780056
n = 40	
0.9982377097 10559200350	0.0045212770 9853319125
0.9907262386 99457006453	0.0104982845 3115281361
0.9772599499 83774262663	0.0164210583 8190788871
0.9579168192 13791655805	0.0222458491 9416695726
0.9328128082 78676533361	0.0279370069 8002340109
0.9020988069 68874296728	0.0334601952 8254784739
0.8659595032 12259503821	0.0387821679 7447201764
0.8246122308 33311663196	0.0438709081 8567327199
0.7783056514 26519387695	0.0486958076 3507223206
0.7273182551 89927103281	0.0532278469 8393682435
0.6719566846 14179548379	0.0574397690 9939155134
0.6125538896 67980237953	0.0613062424 9292893916
0.5494671250 95128202076	0.0648040134 5660103807
0.4830758016 86178712909	0.0679120458 1523390382
0.4137792043 71605001525	0.0706116473 9128677969
0.3419940908 25758473007	0.0728865823 9580405906
0.2681521850 07253681141	0.0747231690 5796826420
0.1926975807 01371099716	0.0761103619 0062624237
0.1160840706 75255208483	0.0770398181 6424796558
0.0387724175 06050821933	0.0775059479 7842481126
n = 48	
0.9987710072 52426118601	0.0031533460 5230583863
0.9935301722 66350757548	0.0073275539 0127626210
0.9841245837 22826857745	0.0114772345 7923453949
0.9705915925 46247250461	0.0155793157 2294384872
0.9529877031 60430860723	0.0196161604 5735552781
0.9313866907 06554333114	0.0235707608 3932437914
0.9058791367 15569672822	0.0274265097 0835694820
0.8765720202 74247885906	0.0311672278 3279808890
0.8435882616 24393530711	0.0347772225 6477043889
0.8070662040 29442627083	0.0382413510 6583070631
0.7671590325 15740339254	0.0415450829 4346474921
0.7240341309 23814654674	0.0446745608 5669428041
0.6778723796 32663905212	0.0476166584 9249047482
0.6288673967 76513623995	0.0503590355 5385447495
0.5772247260 83972703818	0.0528901894 8519366709
0.5231609747 22233033678	0.0551995036 9998416286
0.4669029047 50958404545	0.0572772921 0040321570
0.4086864819 90716729916	0.0591148396 9839563574
0.3487558862 92160738160	0.0607044391 6589388005
0.2873624873 55455576736	0.0620394231 5989266390
0.2247637903 94689061225	0.0631141922 8625402565
0.1612223560 68891718056	0.0639242385 8464818662
0.0970046992 09462698930	0.0644661644 3595008220
0.0323801709 62869362033	0.0647376968 1268392250

$$\left.\begin{aligned} &\sum_{k=1}^{n} a_{kn}=2, \qquad \sum_{k=1}^{n} a_{kn}x_{kn}=0, \qquad \sum_{k=1}^{n} a_{kn}x_{kn}^2=2/3 \\ &\sum_{k=1}^{n} a_{kn}x_n^3=0, \qquad \sum_{k=1}^{n} a_{kn}x_n^4=2/5, \\ &\sum_{k=1}^{n/2} x_{kn}^2=\frac{n(n-1)}{2(2n-1)}=-\frac{B_n}{A_n}, \end{aligned}\right\} (10)$$

where

$$P_n(x)=A_nx^n+B_nx^{n-1}+\ldots, \; n \text{ even}.$$

These checks were all met to within 2 units in the 20th decimal place. The first four checks in (10) were carried out on SEAC at the time of the computation, and the last two were made directly from the final tabulation.

In the tables only the abscissas lying between 0 and 1 have been listed.

The authors thank the Hand Computing Unit of the Bureau's Computation Laboratory for its assistance in checking these tables.

3. References

[1] A. N. Lowan, N. Davids, and A. Levinson, Table of the zeros of the Legendre polynomials of order 16 . . . , Bul. Am. Math. Soc. **48,** 739 (1942); reprinted in Tables of functions and of zeros of functions, NBS Applied Mathematics Series 37 (1954).
[2] D. R. Hartree, The evaluation of a diffraction integral, Proc. Cambridge Phil. Soc., p. 567 (1954).
[3] P. Henrici, Application of two methods of numerical analysis to the computation of the reflected radiation of a point source, J. Wash. Acad. Sci. **45,** 38 (1955).
[4] A. Reiz, On the numerical solution of certain types of integral equations, Arkiv Mat., Astron. Fysik **29a,** 1 (1943).
[5] G. Szegö, Orthogonal polynomials (New York, N. Y., 1939).
[6] G. Szegö, Inequalities for the zeros of the Legendre polynomials and related functions, Trans. Am. Math. Soc. **39,** 1 (1936).
[7] G. Szegö (written communication).
[8] British Association Mathematical Tables, vol. VI (Cambridge, 1937).

WASHINGTON, July 29, 1955.

Journal of Research of the National Bureau of Standards Vol. 56, No. 1, January 1956 Research Paper 2646

Behavior of Cements and Related Materials Under Hydrostatic Pressures up to 10,000 Atmospheres

C. E. Weir, C. M. Hunt, and R. L. Blaine

Compression studies were made on hardened cement pastes at 21° C and at pressures as high as 10,000 atmospheres. The effects of composition, age, moisture content, and water-cement ratio were studied. Compressibility of dried portland cement pastes appeared to proceed through a maximum with increased cure, the existence or location of the maximum being dependent on the water-cement ratio. Compression of both portland and aluminous cements increased with increasing evaporable water content. Portland cements with evaporable water contents in the range 17.5 to 32.4 percent exhibited a transition between 2,000 and 3,000 atmospheres. No similar effect occured in aluminous cement. Experiments indicated that the transition was attributable to hydrated lime formed in the portland cement. Average compressibilities of dried paste were 3.1×10^{-6} and 2.2×10^{-6} atm^{-1} between 1 and 5,000 atmospheres and between 5,000 and 10,000 atmospheres, respectively. Compression studies were also made with wet silica gel, hydrated tricalcium silicate, and dry and wet calcium hydroxide.

1. Introduction

In considering studies of the pore-size distribution in hardened cement pastes by the mercury porosimetry techniques [1, 2, 3][1] data are required on the magnitude of the compression of the cement when subjected to hydrostatic pressures. Normally the compression of the cement paste would be considered negligible, but a study by mercury porosimetry of the extremely small pores believed to exist in dried cement paste would require rather high pressures at which the change in volume of the paste might well be of significance.

Search of the literature revealed that while the elastic properties of concrete have been studied extensively, the measurements were conducted almost exclusively at low pressures and only rarely on neat cement [4]. However, the elastic properties of the rocks and minerals that may be used as aggregates in concrete have been investigated widely even at extreme conditions of temperature and pressure, primarily because of geological interest. The latter data have been compiled by Birch [5].

Because concrete is subjected to moderately high compressive stresses in many commercial applications it appears that there is little direct evidence—aside from successful usage—that the aggregate and the neat cement are compatible as regards compressibility. In order to obtain direct evidence on this question, as well as to evaluate the corrections required in high-pressure mercury porosimetry studies, preliminary data were obtained on the compression of hardened cement pastes with available high pressure equipment. These data immediately showed evidence of a transition at elevated pressures in wet cement and indicated the desirability of a detailed study of the compressibility of cement itself, irrespective of any immediate significance of the data in direct applications.

[1] Figures in brackets indicate the literature references at the end of this paper.

This paper contains the results of studies of the compression of neat cement pastes at pressures as high as 10,000 atm. Studies were made on the effects of cement type, water-cement ratio, water content, and length of cure. The compression characteristics of several pure materials of interest in connection with cement were also studied.

2. Experimental Method and Preparation of Specimens

2.1. Compression Measurements

The apparatus, experimental technique, and method of calculating the data have been described in detail [6]. An experiment consists in forcing a leakproof piston into the smooth bore of a high-pressure vessel containing the specimen immersed in a light petroleum distillate (Varsol). Readings of the depth of penetration of the piston are made at each 1,000 atm by means of a sensitive dial gage fastened to the piston, pressure in the vessel being measured by means of a calibrated manganin resistance gage immersed in the distillate. The apparatus was calibrated with steel bars having volumes similar to those of the specimens. The compressibility of steel has been measured by Bridgman [7]. The compression is defined as $-\Delta V/V_0$, where V_0 is the volume of the specimen at 1 atm, and ΔV is the change in the volume reckoned from the fiducial pressure of 2,000 atm; compressions at lower pressures, therefore, appear as negative values. All measurements described here were made with decreasing pressures, and frictional forces at the packing on the piston prevented the attainment of reasonable accuracy at pressures much below 2,000 atm. Values of compression reported at 1 atm are not experimental but are obtained by successive approximations. Values of V_0 were obtained by weighing in air before compression measurements and by hydrostatic weighing in distillate after the measurements.

2.2. Preparation and Treatment of Specimens

Test specimens were made by casting cement paste in paraffin-coated paper molds designed to yield a cylindrical specimen ½ in. in diameter and 4 in. long. Specimens were removed from the molds after 24 hr and cured at 21° C over water in closed glass containers. Cured specimens were dried in a vacuum at room temperatures with a dry-ice trap interposed between the specimen and the pump in an apparatus similar to that described by Copeland and Hayes [8]. During the initial 24 hr the drying was carried out at a pressure of approximately 1 to 2 mm of Hg. Following the initial 24-hr drying period, further drying was conducted at approximately 2×10^{-3} mm Hg. Cylindrical test specimens prepared in this manner were immersed in dry distillate until evolution of displaced air appeared to cease and were then subjected to a short evacuation at a pressure sufficiently low to cause the distillate to boil at room temperature. The resulting vacuum-impregnated specimens were used for test.

Certain materials studied could not be cast conveniently in cylindrical form. Such materials were packed into a thin-walled steel cylinder, which was open at one end, having dimensions ½ in. in diameter and 4 in. long. The material was impregnated with distillate, as previously described, prior to test.

2.3. Materials Studied

The materials studied included portland and aluminous cements, silica gel, tricalcium silicate, and calcium hydroxide.

a. Cements

The portland and aluminous cements studied in greatest detail had the compositions shown in table 1. The portland cement was denoted as cement A. This was a type-I (Federal Specification SS–C–192a) cement ground from clinker, the composition of which is given in the table. Limited studies were also conducted on other portland cements meeting the requirements of Federal Specification SS–C–192a for types I, II, III, IV, and V.

b. Silica Gel

The silica gel studied contained 205 percent of evaporable water, based on the dry weight of the sample. An additional 5.4 percent of water was removed by ignition at 1,000° C for 15 min. After an overnight evacuation at 100° to 110° C, the surface area of the material by low-temperature nitrogen adsorption was 749 m^2/g. This is a rather large surface area even for silica gel.

c. Tricalcium Silicate

The tricalcium silicate was prepared by heating and reheating of an intimately mixed paste of calcium carbonate and silica gel.

d. Calcium Hydroxide

The calcium hydroxide used was a reagent-grade product obtained commercially.

TABLE 1. *Compositions of cements studied*

Cement A[a] (portland cement, type I)			Aluminous cement	
Oxide	Percentage by weight	Calculated composition, percentage by weight	Oxide	Percentage by weight
CaO	65.13	$3CaO \cdot SiO_2$, 56%	CaO	36.8
SiO_2	22.62	$3CaO \cdot Al_2O_3$, 3%	SiO_2	8.6
Al_2O_3	4.41	$4CaO \cdot Al_2O_3 \cdot Fe_2O_3$, 16%	Al_2O_3	42.7
Fe_2O_3	5.33	$2CaO \cdot SiO_2$, 23%	Fe_2O_3	4.3
SO_3	0.10		SO_3	0.3
MgO	1.71		MgO	.8
Na_2O	0.04		FeO	6.2
K_2O	.28		TiO_2	0.4
Loss on ignition.[a]	.37		Gain on ignition.	.1
Insoluble residue.	.14		Insoluble residue.	1.7

[a] This is an analysis of clinker that was interground with different amounts of gypsum and blended to 1.8 percent of SO_3. Ignition loss of blended cement was 1.69 percent.

2.4. Determination of Volume and Cement Content of Specimens

The specimens were weighed in air before test and weighed in distillate after completion of the compressibility measurements. The volumes of the specimens at 1 atm, V_0, were calculated from the relationship

$$V_0 = \frac{w - w_v}{d_v}, \tag{1}$$

where w is the weight of the specimen in air, w_v is the weight of the specimen in distillate, and d_v is the density of the distillate.

The specimens were finally ignited in platinum crucibles at 1,050° C for 15 min, after first burning off the distillate in a flame. The cement content of the specimens, C, was calculated from the relationship

$$C = w_i(1+i), \tag{2}$$

where w_i is the ignited weight of the hydrated specimen, and i is the fractional ignition loss of the original cement.

3. Results and Discussion

3.1. General Considerations

Prior to a discussion of the experimental results it is advisable to consider details of the experiments that affect the experimental accuracy and the rigor with which the experimental data may be treated.

In many measurements on porous materials the failure to remove all air from the voids may introduce serious errors. However, in these studies the specimens were impregnated with distillate at reduced pressures. Under such conditions, if the whole void volume contains air trapped at the reduced pressure, the volume of the air at 1,000 atm will be quite small. Of still greater importance is the fact that the change in volume of the trapped air between 10,000 and 1,000 atm will be expected to produce a negligible error in these measurements. Two other factors tend to further decrease this small error. First, a large

quantity of air was displaced by distillate, and second, trapped air has been found to dissolve rapidly in the distillate at high pressure. Experimental evidence will be given to confirm the belief that any errors in compressibility arising from trapped air are negligible.

Penetration of distillate into the small voids in these experiments was accompanied by a rapid decrease in pressure with time. This effect occurred only when the specimen was initially subjected to high pressures and was absent on subsequent compressions. The rate of penetration was not measured but was observed to decrease with time and, although considerable time was allowed to attain equilibrium at the maximum pressure, it was most probable that slow penetration occurred during the initial measurement in each experiment.

Penetration of distillate into the specimens produced an apparent decrease in the quantity of liquid in the pressure vessel. The disappearance of liquid effectively increased the required displacement of the piston, so that in most instances the maximum stroke was exceeded before reaching 10,000 atm. Generally, more distillate was added to permit attainment of 10,000 atm, but in some instances measurements were made only to the maximum pressure attainable on the initial compression. In most of the latter instances the maximum was 9,000 atm, but in one instance it was only 8,000 atm.

The experimental error in these data is subject to some uncertainty. In general, with the techniques used here it has been concluded that the data may be reproduced to within ± 0.0004 in $-\Delta V/V_0$ [9]. Such precision is readily obtained when the correction terms [6] are kept reasonably small. In the present studies the correction terms were frequently undesirably large and were in general not subject to control because of the penetration of distillate into the specimen and variations in the real volume of the specimens. The actual volume of the specimen studied was likewise subject to some uncertainty arising from occasional loss of small fragments in handling prior to weighing hydrostatically.

Although this compilation of known sources of error is long, most of the errors involved are quite small and in many instances may mutually compensate. It is believed that each measured value of compression in these studies may be considered reliable to within ± 0.0008. The differences between data obtained with duplicate specimens may be somewhat greater than this and represent differences in the specimens themselves. Therefore, some of the conclusions based on small differences between different specimens are subject to some uncertainty.

3.2. Compression of Dried Cement Pastes of Different Ages and Water-Cement Ratios

Measurements were made on dry cement A before mixing it with water and after hydration for various periods of time. These specimens were prepared with nominal water-cement ratios 0.3, 0.5, and 0.7 to determine whether the distillate penetrated all the voids or whether a portion of the change in volume was due to compression of voids. The data on these specimens, which were all dried in a vacuum for 1 week, are given in tables 2 to 5.

All compressions as tabulated are based on the reference pressure of 2,000 atm, but may be calculated from 1 atm by adding to each value of the corresponding column the (positive) compression given at 1 atm. At the head of each column the nominal water-cement ratios are given. The actual water content was probably somewhat less than that indicated by the ratios given, which, however, serve to designate specimens differing significantly in total void content. Below each water-cement ratio are given in order the nonevaporable-water content based on the weight of the original cement, the density of the specimen, and the volume of the specimen at 1 atm.

TABLE 2. *Compression of hardened cement A paste cured for 1 week*

Nominal water-cement ratio	0.3	0.5		0.7
Nonevaporable water content, % of original cement	12.1	11.1	11.1	10.8
Density at 21° C, g/cm³	2.679	2.706	2.711	2.712
Volume of test specimen, cm³	8.361	5.869	5.702	4.737
Pressure	Compression, $-\Delta V/V_0$			
atm				
10,000	0.0193	0.0193	0.0176	0.0181
9,000	.0178	.0176	.0155	.0176
8,000	.0161	.0157	.0135	.0162
7,000	.0136	.0127	.0119	.0136
6,000	.0114	.0106	.0095	.0112
5,000	.0090	.0080	.0074	.0090
4,000	.0062	.0051	.0048	.0060
3,000	.0031	.0020	.0020	.0030
2,000	.0000	.0000	.0000	.0000
1,000	------	------	−.0016	------
1	−.006	−.005	−.005	−.006

TABLE 3. *Compression of hardened cement A paste cured for 1 month*

Nominal water-cement ratio	0.3	0.5	0.7
Nonevaporable water content, % of original cement	15.2	16.0	15.4
Density at 21° C, g/cm³	2.559	2.567	2.584
Volume of test specimen, cm³	8.951	6.550	5.211
Pressure	Compression, $-\Delta V/V_0$		
atm			
10,000	0.0255	0.0233	0.0217
9,000	.0211	.0214	.0199
8,000	.0195	.0185	.0175
7,000	.0169	.0155	.0148
6,000	.0136	.0129	.0125
5,000	.0107	.0097	.0089
4,000	.0077	.0064	.0061
3,000	.0036	.0025	.0050
2,000	.0000	.0000	.0000
1	−.008	−.006	−.006

369131—56——4

TABLE 4. *Compression of hardened cement A paste cured for 6 months*

Nominal water-cement ratio	0.3	0.5	0.7
Nonevaporable water content, % of original cement	16.7	20.1	32.8
Density at 21° C, g/cm³	2.557	2.456	2.333
Volume of test specimen, cm³	8.879	7.111	6.338
Pressure	Compression, $-\Delta V/V_0$		
atm			
10,000	0.0205	0.0224	0.0276
9,000	.0186	.0214	.0269
8,000	.0168	.0192	.0246
7,000	.0155	.0168	.0217
6,000	.0109	.0141	.0184
5,000	.0083	.0115	.0158
4,000	.0053	.0085	.0119
3,000	.0010	.0038	.0060
2,000	.0000	.0000	.0000
1	−.006	−.008	−.01

TABLE 5. *Compression of unhydrated cement A powder*

Density at 21° C, g/cm³	3.081[a]
Volume of test specimen, cm³	7.687
Pressure	Compression, $-\Delta V/V_0$
atm	
10,000	0.0166
9,000	.0150
8,000	.0130
7,000	.0113
6,000	.0089
5,000	.0070
4,000	.0053
3,000	.0034
2,000	.0000
1,000	−.0032
1	−.006

[a] Density by ASTM method C188–44 is 3.18 g/cm³.

In table 2, measurements are given for two specimens of water-cement ratio 0.5. The differences noted in data on these duplicates, particularly at the higher pressures, are believed to be larger than the experimental errors involved and, therefore, are indicative of differences in the specimens themselves.

The data in table 2 indicate very little difference in the compressions of cement pastes of different water-cement ratio after 1 week of curing. This strengthens the argument that the values obtained represent compression of the hydrated cement and do not reflect the compression of voids, except possibly submicroscopic pores believed to be present in all pastes regardless of the water-cement ratios. The differences in porosity of the specimens were quite evident from their behavior on initial compression. Time effects attributed to penetration of distillate into voids were observed, which were roughly proportional to the water-cement ratio, being extremely large in the specimens with a ratio of 0.7 and practically nonexistent in specimens with ratio 0.3.

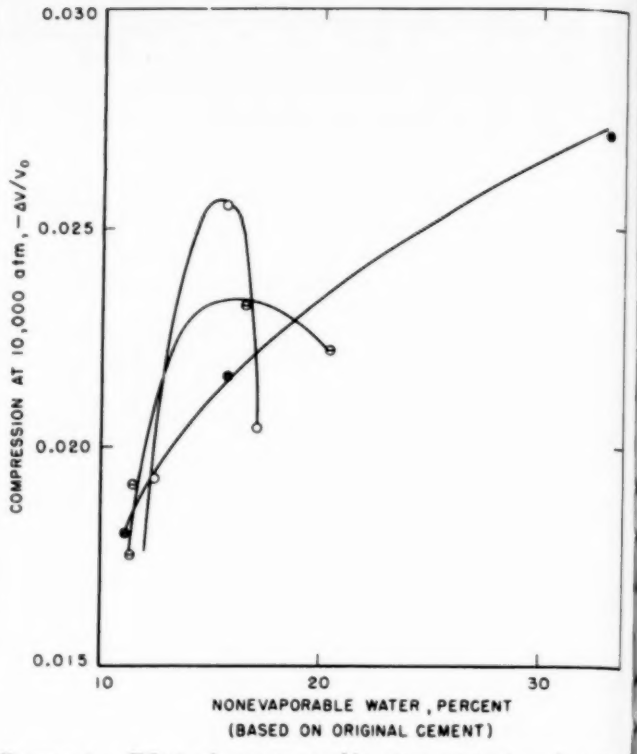

FIGURE 1. *Effect of nonevaporable-water content and water-cement ratio on compression.*

○, Water-cement ratio 0.3; ⊖, water-cement ratio 0.5; ●, water-cement ratio 0.7.

On comparing the compressions for the different curing periods shown in tables 2, 3, and 4, interesting differences may be noted. The data indicate that the compression initially increases with increased curing and then may reach a maximum and decrease with further curing, with the time of cure required to reach a maximum being dependent on the water-cement ratio. This behavior is illustrated in figure 1, where the compression at 10,000 atm is plotted against the nonevaporable water content. It will be noted that a well-defined maximum is shown for the lowest water-cement ratio; a similar maximum is absent in the highest water-cement ratio, whereas the intermediate water-cement ratio shows an intermediate behavior. It must be noted that the effects of curing period and water content shown in figure 1 are subject to some uncertainty caused by specimen-to-specimen variability. With these reservations in mind, however, the results suggest that the gel structure laid down in the first few weeks of hydration is being reinforced during subsequent hydration. This process is more marked at lower water-cement ratios, because there is not only less water but there is also less space for deposition of new gel [11]. At low water-cement ratio the rate of hydration is also slower in the later stages than in specimens of higher water-cement ratio. Possibly the maximum might be observed at all water-cement ratios if hydration were continued long enough.

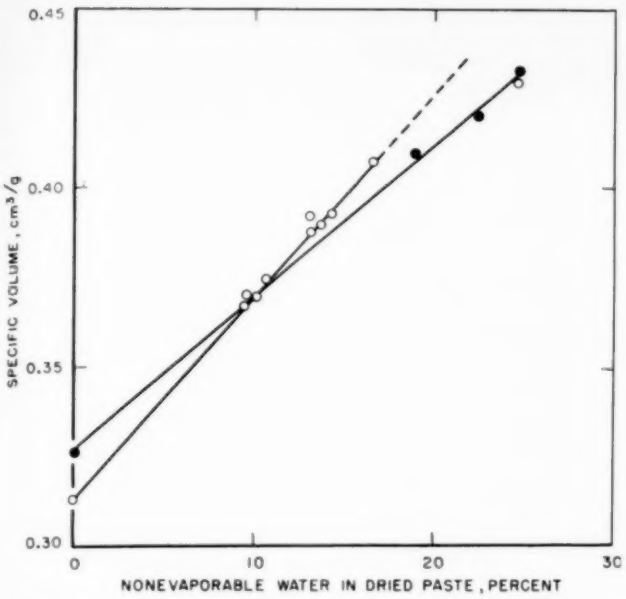

FIGURE 2. *Effect of nonevaporable-water content on specific volume of hydrated portland and aluminous cements.*

○, Portland cement; ●, aluminous cement.

The compression of the parent unhydrated cement is given in the data of table 5. This material was investigated as a powder and was studied in the steel cylinder as described previously. Although this material was investigated as a powder, the data are considered comparable with data obtained with cast cylinders. Evidence for the validity of this conclusion has been obtained in experiments comparing compressions of powdered and molded specimens of organic polymers [10].

Useful by-products of the compressibility measurements are density determinations on specimens that have been evacuated and then impregnated with distillate at a pressure of 10,000 atm. The values so obtained should represent a rather uniform penetration of the pore structure by the distillate. Powers and Brownyard [11] have expressed the volume of the solid phase in hydrated cement as the volumes of the original cement and the nonevaporable water according to the relationship

$$V_s = cv_c + w_n v_n, \tag{3}$$

where V_s is the volume of the solid phase, c the weight of the original cement, v_c the specific volume of the original cement, w_n the weight of nonevaporable water, and v_n the hypothetical specific volume of the nonevaporable water. In terms of specific volume of the solid phase, an equivalent relationship may be written as

$$v_s = x_c v_c + y_n v_n, \tag{4}$$

where, in addition to terms previously defined, v_s is the specific volume of the solid phase, and x_c and y_n are the weight fractions of cement and nonevaporable water, respectively. With the necessary relationship

$$x_c = 1 - y_n \tag{5}$$

eq (4) may be transformed into

$$v_s = v_c + (v_n - v_c)y_n. \tag{6}$$

From this equation a plot of y_n against v_s should yield a straight line of slope $(v_n - v_c)$ and intercept v_c on the v_s axis. Values of y_n the fraction of nonevaporable water in the dried specimen (expressed as percent), and v_s are plotted in figure 2. A linear relationship is obtained which by extrapolation gives the specific volume of unhydrated cement at zero water content. The experimental value for unhydrated cement in figure 2 was obtained with a Le Chatelier flask (ASTM standard method C188–44), because the value obtained after compression appeared to be high and an error in weighing was suspected. The nonevaporable water content of the portland cement specimen with the highest specific volume in figure 2 is also suspected to be in error, because it is greater than values for specimens prepared from the same cement and cured a year. Such an error might easily occur through the loss of a fragment of specimen which would be calculated as a loss of water. The nonevaporable water content of this specimen is given in table 4 as 32.8 percent of the weight of the original cement and is also plotted in figure 1. Powers and Brownyard give 20 to 25 percent, based on the weight of the cement, as a reasonable estimate for the nonevaporable water content of a specimen close to ultimate hydration [13]. The linearity observed below about 20-percent nonevaporable water in figure 2 offers strong evidence that the distillate penetrated the same domains of the structure irrespective of age or water-cement ratio. The exact dimensions of the finest pores in cement gel are somewhat conjectural but may be of the order of a few angstrom units in diameter [13,14]. It is doubtful if distillate penetrated all these ultrafine pores. However, penetration undoubtedly occurred in all pores whose size or number could be varied by changing the water-cement ratio.

From the slope of the line of figure 2 and the value of v_c, a value for the hypothetical specific volume of the nonevaporable water, v_n, was calculated. The value obtained was 0.87 ml/g. This value is higher than the 0.82 ml/g reported by Powers and Brownyard from measurements of density of a number of cements by helium displacement [11] or the value of 0.74 ml/g obtained by Copeland [12], using water as a displacement medium. This indicates that distillate did not penetrate the structure to the same extent as did helium or water. Another factor contributing to this difference may be the difference in the method of drying. These specimens were dried as ½- by 4-in. cylinders, whereas the specimens of Powers and Brownyard [11,15] and Copeland [8,12] were dried in granular form. Somewhat more water may be removed in the latter form.

3.3. Effect of Evaporable Water on Compression of Hydrated Cement

The effect of evaporable-water content on the compression of cement of a given age and water-cement ratio was most interesting. In these experiments six specimens of cement A mixed with a water-cement ratio of 0.5 were cured for 1 week. Following the curing period the specimens were dried in a vacuum for periods varying from 15 min to 1 week before the testing. The specimen dried for 1 week retained 10.9 percent of water, based on the weight of the cement used in preparing the specimen. Although more rigorous drying procedures might have removed a portion of this water, the 10.9 percent of water was arbitrarily taken to represent the nonevaporable-water content of all the specimens. The compression data obtained on these specimens are given in table 6, and the compression-pressure behavior is shown graphically in figure 3. In figure 3 the compressions of the specimens with evaporable-water contents of 2.2 and 5.2 percent were only slightly greater than the driest specimen. The specimens with evaporable-water contents of 17.5 percent or more, however, were highly compressible and the compression increased markedly with increasing water content. Although the increased compression extends over the whole pressure range, it will be noted in the three specimens of high moisture content that the curves are nearly parallel above about 5,000 atm.

TABLE 6. *Effect of evaporable water on compression of hardened cement A paste (1-week cure)*

Evaporable-water content, % of original cement	32.4	26.9	17.5	5.2	2.2	0
Density, g/cm³	1.951	2.100	2.270	2.580	2.650	2.735
Volume of test specimen, cm³	10.508	8.849	7.874	6.316	5.897	7.709
Pressure	Compression, $-\Delta V/V_0$					
atm						
10,000	0.0777	----	----	0.0219	0.0225	0.0182
9,000	.0733	0.0669	0.0465	.0198	.0204	.0172
8,000	.0690	.0628	.0426	.0178	.0182	.0151
7,000	.0641	.0579	.0375	.0148	.0153	.0126
6,000	.0589	.0524	.0323	.0122	.0127	.0102
5,000	.0528	.0442	.0272	.0095	.0100	.0074
4,000	.0445	.0376	.0216	.0064	.0068	.0048
3,000	.0326	.0253	.0130	.0025	.0029	.0017
2,000	.0000	.0000	.0000	.0000	.0000	.0000
1,000	−.0168	−.0120	−.0127	----	----	----
1	−.03	−.02	−.02	−.006	−.006	−.005

Compressibility—the slope of the curves—is less affected by moisture content above 5,000 atm even at high evaporable-water content. Below about 4,000 atm a rapid change in compression is observed at the higher moisture contents, and the compression in this region of pressures is a strong function of the water content. Below 4,000 atm the sigmoid shape of the compression curve clearly indicates that a transition is occurring. The transition is not sharp and appears to occur principally between 2,000 and 3,000 atm. Large thermal effects are associated

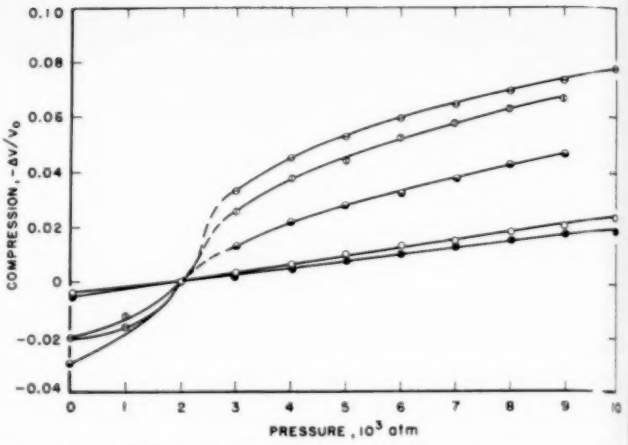

FIGURE 3. *Effect of evaporable-water content on the compression of hydrated portland cement A, type I.*

⊖, 32.4 percent of evaporable water; ◍, 26.9 percent of evaporable water; ◒, 17.5 percent of evaporable water; ○, 2.2 and 5.2 percent of evaporable water; ●, 0 percent of evaporable water.

with this transition and these are readily observed experimentally [9] in their effect on the pressure. From the experimental observations of the thermal effects it is concluded that the transition is not occurring below 2,000 atm but that it persists to pressures as high as 4,000 atm. No experimental evidence was found for any comparable discontinuity at the lower moisture contents, and it is concluded that the phenomenon requires moisture.

The transition is completely analogous to a phase transition produced isobarically by changing the temperature, i. e., freezing point. The fact that this transition occurs over a rather wide pressure interval is understandable because in a complex material such as cement many other substances may enter into the phase change. In this respect it is analogous to the freezing of an impure material.

A different picture of the process may be obtained by considering the compression isobarically in relation to the evaporable water content. Isobars at a few representative pressures are given in figure 4. The broken lines in figure 4 represent compressions calculated for ideal mixtures of water and dry paste and converge on the compression axis with the corresponding experimental isobars. The calculated compressions were based on the known compression of water [16] and dry paste (the specimen containing no evaporable water in table 6) and their respective volume fractions. Significant divergence of the calculated and experimental curves appears at pressures of 3,000 atm and higher and approximately 10 percent or more evaporable moisture. At 1,000 atm the calculated and measured data are in substantial agreement over the whole moisture range. It will also be noted that divergence of calculated and measured values increases rapidly with increasing moisture content but is relatively insensitive to changing pressure at a given moisture content at the higher pressures. These observations are consistent with the behavior to be expected from a transition centered between 2,000 and 3,000 atm.

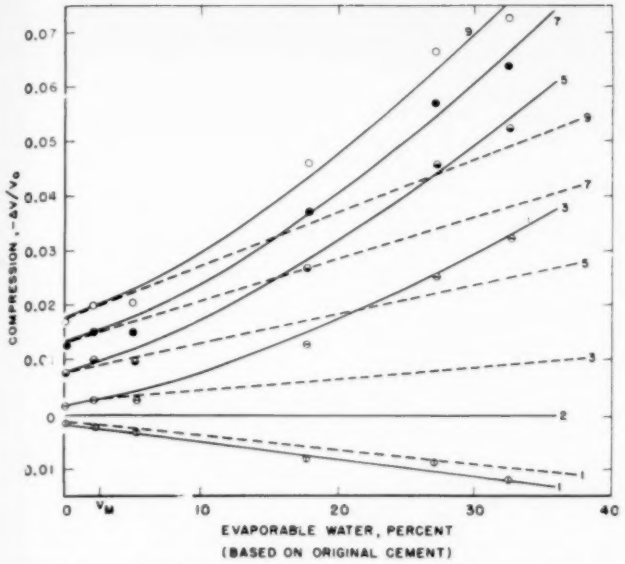

FIGURE 4. *Calculated and measured isobars for portland cement as functions of evaporable-water content.*

Digits at right of each isobar denote the presence in kiloatmospheres. ———, Measured; — — — —, calculated.

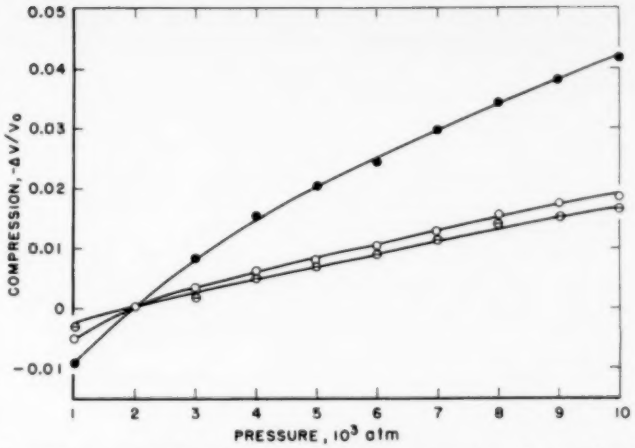

FIGURE 5. *Calculated and measured compressions for portland cement as affected by nonevaporable-water content.*

●, Calculated (unhydrated cement and mixture of 10.9 percent of liquid water); ○, measured (hydrated cement with 10.9 percent of nonevaporable water); ⊖, measured (unhydrated cement).

Water-vapor sorption measurements have been made on separate specimens of hardened paste prepared from the same cement and cured 1 week over water. If the adsorption of water vapor by hydrated cement is a multilayer adsorption process, in the range of relative humidity over which the Brunauer-Emmett-Teller (BET) equation applies, V_m is the amount of water theoretically required to cover the total surface of the hydrated cement with a layer of water 1 molecule thick. A V_m value of 2.8 percent of evaporable water was calculated from such data by the BET equation [17]. From figure 4 it is noted that the correlation between the experimental and calculated compressions deviates appreciably above an evaporable water content 2 or 3 times V_m.

The data at low moisture contents are of interest in connection with questions concerning the nature of this water. Within the experimental errors no essential differences exist between calculated and measured compressions at low moisture contents as shown in figure 4. Although the experimental points at 5.2 percent of evaporable water are indicated as lying somewhat below the calculated curves, there is some doubt as to whether this is of real significance. However, all data shown in figure 4 are based on evaporable-water content, and all specimens are considered to contain 10.9 percent of nonevaporable water. The compression curve for the specimen containing 10.9 percent water has been compared with a similar curve for unhydrated cement and also with a curve calculated for a mixture of unhydrated cement and 10.9 percent of water, assuming the specific volume of nonevaporable water to be 0.87 ml/g. These results are shown in figure 5. Similar curves could be made from the data in tables 2 to 5. Although all the compression curves would not coincide as closely with the unhydrated cement as the specimen shown in figure 5, all results would show that the experimental compressions were much less than those calculated for corresponding mixtures of unhydrated cement and water. Thus compressibility measurements confirm what would seem evident from other considerations, namely, that nonevaporable water is accommodated differently in the structure of hydrated cement than evaporable water.

Before describing the experiments that were conducted to ascertain the source of the transition observed in hydrated portland cement containing large amounts of evaporable water, it is of interest to consider certain possible explanations for the phenomenon. Water is known to freeze to ice VI at approximately 8,700 atm at room temperature [18]. Liquid water in cement will exist in a solution which will be expected to freeze at still higher pressures. A marked reduction of this freezing point by some 6,000 atm is not expected. It has been proposed, however, that adsorbed moisture and water present in fine capillaries are subject to extreme surface forces and, therefore, normally exist under high hydrostatic pressure [19]. Such concepts have frequently been advanced in connection with theories of bound water which will not be reviewed here. A small increase in external hydrostatic pressure on such tightly bound water might exceed the freezing pressure and produce the transition observed here. However, such an explanation should lead to observations of a transition even at low moisture contents at which it appears to be completely absent. In addition, no similar effects were observed in studies on fibrous polymers containing as much as 30 percent of moisture [20]. It has been suggested, also, that the high hydrostatic pressure might rupture small particles of cement as a result of nonhydrostatic forces at grain boundaries, thereby producing an apparent transition. However, all data reported here were obtained on decreasing pressure and in these studies measurements may be made only

in this direction because of penetration of distillate into the voids upon compression. However, additional observations indicated that the transition was completely reversible, and it is difficult to conceive of a reversible but destructive physical phenomenon. Furthermore, as later data will show, a cement with no detectable transition has been studied. This fact alone essentially eliminates the forementioned explanations for the transition.

From the data already presented it appears that some hydrated material in cement produced the observed transition. The wide pressure range of the transition is attributed to the fact that hydrated cement is not a pure substance.

3.4. Source of the Transition in Hydrated Cement Containing Large Amounts of Evaporable Water

A number of experiments were performed to study the transition in detail and to ascertain the material responsible for the phenomenon. In order to determine whether the transition disappeared permanently once the sample was dried, or whether it could be regenerated by rewetting, the following experiment was performed with three specimens prepared from cement A, nominal water-cement ratio 0.5, cured 1 week. The first specimen was tested immediately following the 1-week cure, with most of its evaporable water intact. The other two specimens were dried in vacuum for 1 week and one was tested in the dried condition. The last specimen was rewet in liquid water and tested immediately. The results obtained in these experiments are shown graphically in figure 6. It is apparent that the transition appearing in the original specimen is eliminated by drying and regenerated on rewetting the dried specimen. Whatever the source of the transition, it must arise from a material formed rapidly in the presence of water.

Compressibility measurements were made on hardened aluminous-cement pastes containing different amounts of evaporable water. This was done with the idea that some structural similarity might exist between the hydrated tricalcium aluminate of portland cement and some of the hydrated compounds in aluminous cement paste [21]. No transition was observed with hydrated aluminous cement containing large amounts of evaporable water. These data will be discussed in the next section.

Compression measurements made on silica gel containing a large amount of evaporable water showed no transition within the pressure range investigated. A specially prepared cement containing no gypsum was hydrated and observed to exhibit a small transition on compression. These data, together with those on the silica gel, are only qualitative and are not given in tabular form. The graphical data, however, are shown in figure 7. It is concluded that neither gypsum nor calcium sulfoaluminates were involved in the transition.

Further studies were made using a specimen of tricalcium silicate mixed with approximately an equal weight of water and cured for 1 week. Analysis of part of the specimen showed that it contained 9.9 percent of nonevaporable water, expressed as percentage of the tricalcium silicate. The compression data showed a very strong transition between 2,000 and 3,000 atm, as shown in figure 7. The transition here is much sharper than observed in the cements but occurs in the same pressure interval. On drying and remeasuring the test specimen, the transition disappeared as in the hydrated cements.

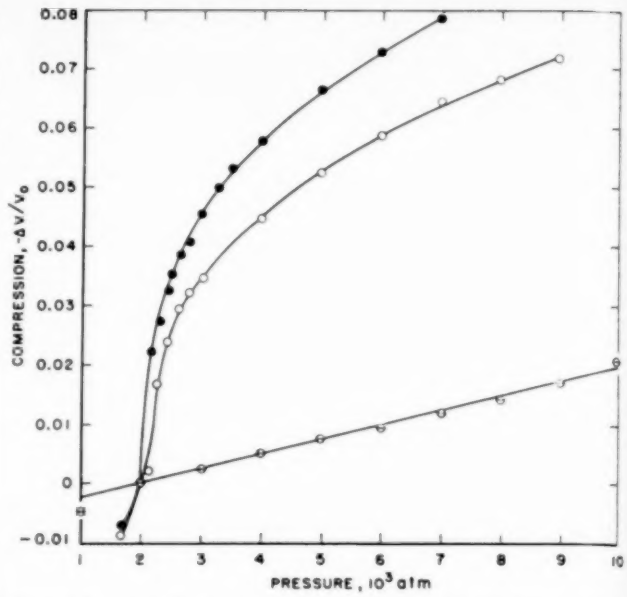

FIGURE 6. *Effect of drying and rewetting on the transition in hydrated portland cement.*

○, Original moisture content; ⊖, dried in a vacuum, ●, dried in a vacuum and rewet.

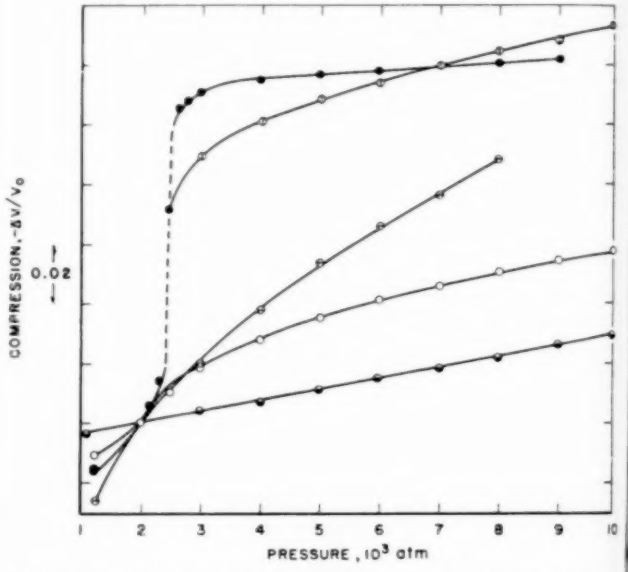

FIGURE 7. *Comparison of compressions of various materials.*

①, Hydrated tricalcium silicate containing evaporable water; ○, hydrated gypsum-free cement containing evaporable water; ●, $Ca(OH)_2$ (containing water); ▬, $Ca(OH)_2$ (dry); ⊖, silica gel (containing water).

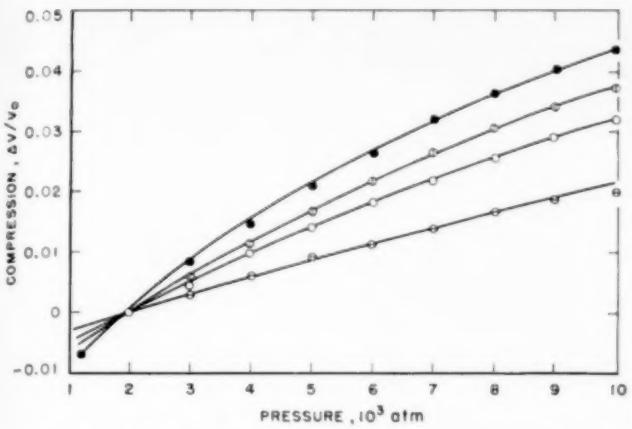

FIGURE 8. *Effect of evaporable water on compression of hydrated aluminous cement.*

●, 21.2 percent of evaporable water; ◐, 18.1 percent of evaporable water; ○, 15.8 percent of evaporable water; ⊖, 0 percent of evaporable water.

As free $Ca(OH)_2$ is one of the hydration products of tricalcium silicate and other cement compounds [22], a final experiment was performed on $Ca(OH)_2$ in the wet and dry states. A very strong transition was observed in the wet lime, which was completely absent in the dried material. The graphical data on wet $Ca(OH)_2$ are given in figure 7. It will be noted that the transition in this material occurs at approximately the same pressure and is noticeably sharper than that in the tricalcium silicate.

Although the transition in wet cement is extended over a pressure interval, the major portion of the volume change occurs at essentially the same pressure at which the transition takes place in wet $Ca(OH)_2$. The chance of finding two different materials having similar transition temperatures at 1 atm is quite small. The chance of finding different materials having the same transition pressure at a given temperature is remote because pressure-induced transitions are less common than those of thermal origin. It may be concluded, therefore, that the discontinuity in volume observed in hydrated cement containing appreciable evaporable water arises from wet $Ca(OH)_2$, which is liberated in the hydration of portland cement. The system $Ca(OH)_2$-H_2O has been investigated under pressure in additional experiments reported elsewhere, and it has been concluded that the transition arises from the formation of a hydrate of $Ca(OH)_2$ [23].

3.5. Aluminous Cement

The aluminous cements occur in a different region of the CaO-SiO_2-Al_2O_3 system from portland cements [22]. The compounds $5CaO{\cdot}3Al_2O_3$, $CaO{\cdot}3Al_2O_3$, and $3CaO{\cdot}5Al_2O_3$ are believed to constitute the major portion of aluminous cements instead of the compounds $2CaO{\cdot}SiO_2$, $3CaO{\cdot}SiO_2$, $3CaO{\cdot}Al_2O_3$, and $4CaO{\cdot}Al_2O_3{\cdot}Fe_2O_3$, which are believed to exist in portland cements [22, 24]. Aluminous cements hydrate more rapidly than portland cements, with a corresponding more rapid evolution of heat. Free lime is not one of the final end products of hydration in the aluminous cements, as in portland cement [25].

Studies made on aluminous cement included the effects of evaporable water and length of cure. Compression data on these specimens are given in tables 7 and 8 and are shown in part in figure 8. The specimen of highest evaporable water content in table 7 received no drying treatment; the driest specimen was dried in vacuum for 1 week, and had a nonevaporable-water content of 29.2 percent. In figure 8 it is observed that the compression increases with evaporable-water content, but from observations during the measurements it was evident that there was no transition similar to that observed in the portland cements. In general, it was found that the compressibility of the hydrated aluminous cement was somewhat higher than that of the hydrated portland cement, but part of this difference may arise from a somewhat higher nonevaporable-water content in the aluminous-cement pastes.

TABLE 7. *Effect of evaporable-water content on compression of hardened aluminous-cement paste cured for 1 week*

Evaporable-water content, % of original cement	21.2	18.1	15.8	0.0
Density, g/cm³	2.092	2.131	2.173	2.390
Volume of test specimen, cm³	9.894	9.642	9.180	7.327
Pressure	Compression, $-\Delta V/V_0$			
atm				
10,000	0.0436	0.0373	0.0319	0.0202
9,000	.0402	.0340	.0290	.0186
8,000	.0364	.0307	.0257	.0167
7,000	.0321	.0267	.0220	.0142
6,000	.0267	.0218	.0182	.0116
5,000	.0211	.0168	.0142	.0091
4,000	.0148	.0113	.0102	.0061
3,000	.0086	.0052	.0057	.0032
2,000	.0000	.0000	.0000	.0000
1,220	−.0068	-------	−.0064	-------
1	−.014	−.012	−.01	−.006

TABLE 8. *Compression of hardened aluminous-cement paste*

Cure	1 day	1 month	7½ month
Nonevaporable-water content, % of original cement	23.7	33.2	37.5
Density at 21° C, g/cm³	2.446	2.318	2.263
Volume of test specimen, cm³	7.027	7.708	8.348
Pressure	Compression, $-\Delta V/V_0$		
atm			
10,000	0.0136	0.0385	0.0268
9,000	.0122	.0350	.0284
8,000	.0102	.0317	.0254
7,000	.0084	.0281	.0223
6,000	.0065	.0246	.0182
5,000	.0047	.0200	.0138
4,000	.0028	.0156	.0094
3,000	.0018	.0088	.0042
2,000	.0000	.0000	.0000
1,000	−.0017	----------	−.0052
1	−.003	−.015	−.003

The measured specific volumes of the specimens of aluminous-cement pastes have been plotted in accordance with eq (6). The value for the unhydrated cement was obtained with the Le Chatelier flask because no compression measurements were made on this material. The graph of these data is shown in figure 2 and again indicates a linear relationship. The slope of the line, which is somewhat less than that found for portland cement, yields a value of 0.75 ml/g for the hypothetical specific volume of the nonevaporable water as compared to the 0.87 ml/g found for portland cement by the same method. This difference suggests that on hydration the system, aluminous cement plus water, undergoes a greater contraction than portland cement. Lea and Desch [22] have cited the work of Le Chatelier [26] and Gessner [27] in support of a similar conclusion.

A graph of the isobars of aluminous cement similar to figure 4 for the portland cement is not included because the number of specimens was limited. However, experimental compression values were lower than values computed on the assumption that the compressions of dried paste and evaporable water were additive. This is quite different from moist portland-cement paste and adds support to the view that hydrated aluminous cement undergoes no transition like that produced in hydrated portland cement, or if any such transition occurs while the paste is under pressure, it is greatly reduced in extent.

According to the data in table 8 the compression increases with hydration up to 1 month, but it is less than the maximum at 7½ months. In other words, aluminous cement also shows a maximum similar to the ones shown in figure 1. The initial increase in compression is considerably greater than was found in the portland cement, but at least a portion of the effect may arise from the greater nonevaporable-water content in aluminous cement.

3.6. Compression of Different Types of Portland Cement

In these studies measurements were made on hydrated cements of different types mixed with a water-cement ratio of 0.5. Results obtained with specimens cured 1 week and vacuum dried 1 week are given in table 9. Measurements on specimens cured 1 month and longer are given in tables 10 and 11. These cements showed differences in rate of hydration, as evidenced by their different moisture contents after drying. However, the correlation between degree of hydration and compression was only fair, which suggests other factors also play a part in determining the behavior of hydrated cement under pressure. Hydrated type II cement was consistently a little less compressible than the others.

The compressions of only the types II and V cements were measured at three ages so that plots similar to the ones shown in figure 1 could be made. Such plots are not given for these specimens, but it is evident that the type V cement had a maximum similar to those shown in figure 1, and the type II merely showed curvature.

TABLE 9. *Compression of hardened pastes of various types of cements (1-week cure)*

Type of cement	I	II	III	IV	V
Nonevaporable water content, % of original cement	15.0	11.9	17.3	12.0	10.8
Density at 21° C, g/cm³	2.597	2.683	2.524	2.697	2.705
Volume of test specimen, cm³	6.422	5.745	6.538	6.271	5.956
Pressure	Compression, $-\Delta V/V_0$				
atm					
10,000	0.0189	.....	0.0211	0.0170	0.0170
9,000	.0177	0.0121	.0192	.0160	.0160
8,000	.0155	.0107	.0167	.0139	.0139
7,000	.0136	.0091	.0144	.0119	.0119
6,000	.0111	.0077	.0118	.0095	.0099
5,000	.0086	.0052	.0088	.0072	.0074
4,000	.0054	.0035	.0059	.0044	.0047
3,000	.0033	.0012	.0030	.0031	.0024
2,000	.0000	.0000	.0000	.0000	.0000
1,260	.....	−.0018	−.0032	−.0025	−.0020
1	−.006	−.005	−.006	−.005	−.005

TABLE 10. *Compression of hardened pastes of various types of cements (1-month cure)*

Type of cement	II	IV	V
Nonevaporable water content, % of original cement	16.9	18.2	12.8
Density at 21° C, g/cm³	2.518	2.525	2.657
Volume of test specimen, cm³	6.769	6.829	6.354
Pressure	Compression, $-\Delta V/V_0$		
atm			
10,000	.....	0.0207	0.0232
9,000	.....	.0194	.0196
8,000	0.0151	.0173	.0170
7,000	.0131	.0149	.0145
6,000	.0105	.0124	.0118
5,000	.0091	.0097	.0091
4,000	.0057	.0069	.0059
3,000	.0029	.0036	.0029
2,000	.0000	.0000	.0000
1	−.006	−.007	−.006

TABLE 11. *Compression of hardened pastes of various types of cements (7½-month cure)*

Type of cement	I	II	V
Nonevaporable water content, % of original cement	25.9	21.7	20.0
Density at 21° C, g/cm³	2.367	2.433	2.481
Volume of test specimen, cm³	7.687	7.373	6.782
Pressure	Compression, $-\Delta V/V_0$		
atm			
10,000	0.0237	0.0177	0.0190
9,000	.0220	.0175	.0186
8,000	.0203	.0161	.0166
7,000	.0176	.0144	.0144
6,000	.0146	.0120	.0124
5,000	.0114	.0089	.0096
4,000	.0080	.0057	.0069
3,000	.0046	.0029	.0038
2,000	.0000	.0000	.0000
1,000	−.0048	−.0039	−.0017
1	−.008	−.006	−.006

3.7. Compressibility and Elastic Constants of Cement

The coefficient of compressibility, β, is defined by means of the relationship

$$\beta = -dV/V_0 dP, \tag{7}$$

where V_0 is the volume at 1 atm and dV/dP the infinitesimal change in volume divided by the infinitesimal change in pressure. Values of β can be obtained as the slopes of the $-\Delta V/V_0$ versus P curves shown. For most of the dried cements β decreases with increasing pressure only slightly and, therefore, average compressibilities above and below 5,000 atm have been calculated from the equation

$$\beta = -\Delta V/V_0 \Delta P, \tag{8}$$

where ΔV represents the change in volume between the maximum or minimum pressure and 5,000 atm, and ΔP the corresponding change in pressure. Average compressibilities calculated from eq (8) are given for a number of cements in tables 12 to 14.

Table 12 contains data for dried specimens and shows the decrease in average compressibility with increasing pressure. Average compressibilities below 5,000 atm show a maximum with increasing curing time only for hydrated cement A, of water-cement ratio 0.3, whereas the corresponding data above 5,000 atm exhibit the maximum for all water-cement ratios for which the comparison could be made. Table 13 contains corresponding data for specimens of various evaporable-water contents. The marked difference in compressibilities noted above and below 5,000 atm at the higher moisture contents is directly attributable to the transition occurring in these specimens. Where such a disparity in compressibility is effected by pressure changes of this order of magnitude, it is most probable that a transition of some sort is involved. In such cases no real significance is attached to the compressibility, which is averaged over the pressure interval containing the transition. In table 14 corresponding data are given for the aluminous cements.

On averaging the data for the dry hydrated portland cement specimens of tables 12 and 13 regardless of age, water-cement ratio, or type of cement, an average compressibility of 3.1×10^{-6} atm^{-1} is obtained below 5,000 atm and the corresponding value above 5,000 atm is 2.2×10^{-6} atm^{-1}. The standard deviations of these figures are $0.7\times$

TABLE 12. *Average compressibility of hydrated cements after vacuum drying for 1 week*

Curing period	Average compressibility, 10^{-6}/atm	
	1 to 5,000 atm	5,000 to 10,000 atm
Cement A: Water-cement ratio 0.3		
1-week	3.0	2.1
1-month	3.7	3.0
6-month	2.9	2.6
Cement A: Water-cement ratio 0.5		
1-week	2.6	2.2
1-month	3.1	2.7
6-month	3.9	2.2
Cement A: Water-cement ratio 0.7		
1-week	3.0	1.8
1-month	3.0	2.5
6-month	5.2	2.4
Type I cement: Water-cement ratio 0.5		
1-week	2.9	2.1
7½-month	3.9	2.5
Type II cement: Water-cement ratio 0.5		
1-week	2.0	1.8
1-month	3.0	2.0
7½-month	3.0	1.8
Type III cement: Water-cement ratio 0.5		
1-week	3.0	2.0
Type IV cement: Water-cement ratio 0.5		
1-week	2.4	2.0
1-month	3.1	2.2
Type V cement: Water-cement ratio 0.5		
1-week	2.5	1.9
1-month	3.0	2.8
7½-month	3.1	1.9

TABLE 13. *Average compressibility of hydrated cement A containing different amounts of evaporable water*

(water-cement ratio 0.5; 1-week cure)

Evaporable water	Compressibility, 10^{-6}/atm	
	1 to 5,000 atm	5,000 to 10,000 atm
Percent		
32.4	14.6	5.0
26.9	12.8	5.7
17.5	9.4	4.8
5.2	3.1	2.5
2.2	3.2	2.5
0	2.5	2.2

TABLE 14. *Average compressibility of hydrated aluminous cement of different age and evaporable-water content*

(Water-cement ratio 0.5)

Curing period	Evaporable water	Compressibility, 10^{-6}/atm	
		1 to 5,000 atm	5,000 to 10,000 atm
	Percent		
1 day	0	1.5	1.8
1 week	21.2	7.0	4.5
Do	18.1	5.8	4.1
Do	15.8	4.8	3.5
Do	0	3.0	2.2
1 month	0	7.0	3.7
7½ months	0	4.6	3.2

10^{-6} atm^{-1} and 0.3×10^{-6} atm^{-1}, respectively. The single specimen of unhydrated cement powder had a compressibility of 2.8×10^{-6} atm^{-1} below 5,000 atm and 1.6×10^{-6} atm^{-1} above 5,000 atm.

From the average compressibility and one other elastic constant, the elastic moduli may be calculated from the well-known relationships [5]

$$E=3(1-2\nu)/\beta \tag{9}$$

$$G=3(1-2\nu)/2\beta(1+\nu), \tag{10}$$

where E is Young's modulus, ν Poisson's ratio, and G the shear modulus. Poisson's ratios were determined by sonic measurements on pastes made from cement A cured 1 week. They ranged from 0.27 for a specimen of nominal water-cement ratio 0.25 to a value of 0.31 for a specimen of nominal water-cement ratio 0.7. Adams and Williamson [28] have concluded that Poisson's ratio for plutonic rocks is approximately 0.27. These rocks are silicates and have essentially the same compressibility as hydrated portland cement. In table 15 elastic constants are

TABLE 15. *Elastic constants for the hydrated cements, estimated from compressibility measurements, assuming Poisson's ratio=0.27*

	1 to 5,000 atm	5,000 to 10,000 atm
Young's modulus	4.5×10^5 atm 6.6×10^6 lb/in.^{2} 4.6×10^5 kg/cm^2	6.3×10^5 atm 9.3×10^6 lb/in^2 6.5×10^5 kg/cm^2
Modulus of shear	1.8×10^5 atm 2.6×10^6 lb/in.^{2} 1.9×10^5 kg/cm^2	2.5×10^5 atm 3.7×10^6 lb/in.^{2} 2.6×10^5 kg/cm^2
Compressibility	3.1×10^{-6} atm^{-1} 2.1×10^{-7} in.^{2}/lb 3.0×10^{-6} cm^2/kg	2.2×10^{-6} atm^{-1} 1.5×10^{-5} in.^{2}/lb 2.1×10^{-6} cm^2/kg

given for dried cement pastes. The values for Young's modulus and shear modulus have been computed from the average value of compressibility, assuming a Poisson's ratio of 0.27. It may be noted that these elastic constants of cement are nearly the same order of magnitude as corresponding constants of the more compressible rocks, many of which are used as aggregates in concrete [5, 28].

The authors are indebted to E. T. Carlson at the Bureau for the specimen of tricalcium silicate, also to R. C. Valore, S. Spinner, and T. W. Reichart for the determinations of Poisson's ratio by sonic methods, and to Vernon Dantzler for technical assistance.

4. References

[1] H. L. Ritter and L. C. Drake, Ind. Eng. Chem. **17,** 782 (1945).
[2] L. C. Drake and H. L. Ritter, Ind. Eng. Chem. **17,** 787 (1945).
[3] L. C. Drake, Ind. Eng. Chem. **41,** 780 (1949).
[4] F. O. Slate, Comprehensive bibliography of cement and concrete 1925–1947, p. 160–162 (Joint Highway Research Project, Engineering Experiment Station, Purdue University, Lafayette, Ind.).
[5] F. Birch, J. F. Schairer, and H. C. Spicer, Handbook of physical constants, Geol. Soc. America Special Paper No. 36 (Jan. 31, 1942).
[6] C. E. Weir, J. Research NBS **45,** 468 (1950) RP2160.
[7] P. W. Bridgman, Proc. Am. Acad. Arts Sci. **74,** 11 (1940).
[8] L. E. Copeland and J. C. Hayes, ASTM Bul. No. 184, p. 70 (1953).
[9] C. E. Weir, J. Research NBS **52,** 247 (1954) RP2496.
[10] C. E. Weir (unpublished data).
[11] T. C. Powers and T. L. Brownyard, Proc. Am. Concrete Inst. **43,** 669–712 (1947); Bulletin No. 22, Portland Cement Assn. (March 1948).
[12] L. E. Copeland (personal communication from manuscript Submitted to The Journal of the American Concrete Institute).
[13] T. C. Powers and T. L. Brownyard, Proc. Am. Concrete Inst. **43,** 971–992 (1947). Bulletin No. 22, Portland Cement Association (March 1948).
[14] S. Giertz-Hedstrom, Proceedings of the symposium on the chemistry of cements (Stockholm 1938, published by the Royal Swedish Institute for Engineering Research).
[15] T. C. Powers and T. L. Brownyard, Proc. Am. Concrete Inst. **43,** 249 (1946); Bulletin No. 22, Portland Cement Assn. (March 1948).
[16] L. H. Adams, J. Am. Chem. Soc. **53,** 3769 (1931).
[17] S. Brunauer, P. H. Emmett, and E. Teller, J. Am. Chem. Soc. **60,** 309 (1938).
[18] International Critical Tables, **IV** (McGraw-Hill Book Co., New York, N. Y., 1928).
[19] H. F. Winterkorn, Soil Sci. **56,** 109–115 (1943).
[20] C. E. Weir, J. Research NBS **49,** 135 (1952) RP2349.
[21] G. Assarsson, Proceedings of the symposium on the chemistry of cements (Stockholm 1938, published by the Royal Swedish Institute for Engineering Research).
[22] F. M. Lea and C. H. Desch, The chemistry of cement and concrete (Edward Arnold & Co., London, 1935).
[23] C. E. Weir, J. Research NBS **54,** 37 (1955) RP2562.
[24] R. H. Bogue, The chemistry of portland cement (Reinhold Publishing Corp., New York, N. Y., 1947).
[25] H. Lafuma, Rev. Gen. Sci. Appl. **1,** 66 (1952), reference from Chem. Abstracts **46,** 11617g.
[26] H. LeChatelier, Le Ciment **32,** 82 (1927).
[27] H. Gessner, Kolloid Zeit. **46,** 207 (1928); **47,** 65, 160 (1929).
[28] L. H. Adams and E. D. Williamson, J. Franklin Inst. 195, 475 (1923).

WASHINGTON, May 3, 1955.

Journal of Research of the National Bureau of Standards Vol. 56, No. 1, January 1956 Research Paper 2647

Formulas for Inverse Osculatory Interpolation

Herbert E. Salzer [1]

Formulas for inverse osculatory interpolation are obtained by inversion of Hermite's formula. They cover the cases for $n=2(1)7$, where n is the number of points required in direct osculatory interpolation. The formulas provide an improved means for inverse interpolation in the case where the first derivative is either tabulated alongside the function or is easily obtained.

The author has previously given inverse interpolation formulas [1, 2] [2] for finding $x=x_0+ph$ from $f(x)$, in terms of $f_i \equiv f(x_i)$, where the $x_i \equiv x_0+ih$ are equally spaced at intervals of h. Those formulas were obtained by the inversion of Lagrange's interpolation formula. As the Hermite osculatory interpolation formula [3, 4, 5] in terms of the function and its first derivative at preassigned points x_i is more accurate than the Lagrangian formula, inverse interpolation formulas obtained from the inversion of Hermite's formula would be expected to be more efficient than the corresponding formulas obtained from Lagrange's formula.

There are many tables where the first derivative is either tabulated alongside the function (e. g., Bessel functions of the first or second kind, which give $J_1(x)=-J_0'(x)$ [6, 7] or $Y_1(x)=-Y_0'(x)$ [8], respectively, or probability functions [9]), or where the derivative is very easy to obtain (e. g., tables of the more elementary functions and their integrals, such as tables of sine, cosine, or exponential integrals [10, 11]). In all such tables, and in many others, the user will find the inverse interpolation formulas given below to be particularly convenient, especially when the tabular interval h is too large for sufficiently accurate inverse interpolation, using the formulas in terms of the functional values alone.

These present formulas give p in terms of $f(x_0+ph) \equiv f$, $f(x_i) \equiv f_i$, and $f'(x_i) \equiv f_i'$ for $x_i \equiv x_0+ih$ at equally spaced intervals h, where the i ranges from $-[(n\text{-}1)/2]$ to $[n/2]$, for $n=2(1)7$, where n is the number of points required in direct osculatory interpolation. Although the direct interpolation formula for $n=6$ and $n=7$ is of the 11th- and 13th-degree accuracy, respectively, the inversion formula for p that is given below does not go beyond the 10th- degree terms (and in most practical problems it is very rarely that one will go that far; in fact, the first few terms will usually suffice). Thus we do not use the coefficient of p^{11} in the 6-point Hermite formula nor the coefficients of p^{11}, p^{12}, and p^{13} in the 7-point Hermite formula. For every n, we define $r=(f-f_0)/hf_0'$, and corresponding to $n=2(1)7$, quantities s, t, u, v, w, x, y, z, and $\bar{z}$ are defined as follows:

$$n=2$$

$$s=(-3\{f_0-f_1\}-h\{2f_0'+f_1'\})/hf_0',$$

$$t=(2\{f_0-f_1\}+h\{f_0'+f_1'\})/hf_0',$$

$$u=v=w=x=y=z=\bar{z}=0.$$

$$n=3$$

$$s=\left(f_{-1}-2f_0+f_1+\frac{h}{4}\left\{f'_{-1}-f'_1\right\}\right)\Big/hf_0',$$

$$t=\left(-\frac{5}{4}\left\{f_{-1}-f_1\right\}-\frac{h}{4}\left\{f'_{-1}+8f_0'+f'_1\right\}\right)\Big/hf_0',$$

$$u=\left(-\frac{1}{2}\left\{f_{-1}-2f_0+f_1\right\}-\frac{h}{4}\left\{f'_{-1}-f'_1\right\}\right)\Big/hf_0',$$

$$v=\left(\frac{3}{4}\left\{f_{-1}-f_1\right\}+\frac{h}{4}\left\{f'_{-1}+4f_0'+f'_1\right\}\right)\Big/hf_0',$$

$$w=x=y=z=\bar{z}=0.$$

[1] Present address, Diamond Ordnance Fuze Laboratory, Department of Defense, Washington, D. C.

[2] Figures in brackets indicate the literature reference at the end of this paper.

$$n=4$$

$$s=\left(\frac{1}{108}\left\{56f_{-1}-297f_0+216f_1+25f_2\right\}+\frac{h}{18}\left\{2f'_{-1}-18f'_0-18f'_1-f'_2\right\}\right)\Big/hf'_0,$$

$$t=\left(-\frac{1}{108}\left\{124f_{-1}-27f_0-108f_1+11f_2\right\}-\frac{h}{36}\left\{8f'_{-1}+63f'_0-f'_2\right\}\right)\Big/hf'_0,$$

$$u=\left(\frac{1}{54}\left\{25(f_{-1}-f_2)+135(f_0-f_1)\right\}+\frac{h}{36}\left\{f'_{-1}+72f'_0+63f'_1+4f'_2\right\}\right)\Big/hf'_0,$$

$$v=\left(\frac{1}{108}\left\{59f_{-1}-54f_0-27f_1+22f_2\right\}+\frac{h}{36}\left\{7f'_{-1}+18f'_0-9f'_1-2f'_2\right\}\right)\Big/hf'_0,$$

$$w=\left(-\frac{1}{108}\left\{52f_{-1}+81f_0-108f_1-25f_2\right\}-\frac{h}{36}\left\{5f'_{-1}+36f'_0+27f'_1+2f'_2\right\}\right)\Big/hf'_0,$$

$$x=\left(\frac{1}{108}\left\{11(f_{-1}-f_2)+27(f_0-f_1)\right\}+\frac{h}{36}\left\{f'_{-1}+9f'_0+9f'_1+f'_2\right\}\right)\Big/hf'_0,$$

$$y=z=\bar{z}=0.$$

$$n=5$$

$$s=\left(\frac{1}{108}\left\{7(f_{-2}+f_2)+128(f_{-1}+f_1)-270f_0\right\}+\frac{h}{72}\left\{(f'_{-2}-f'_2)+32(f'_{-1}-f'_1)\right\}\right)\Big/hf'_0,$$

$$t=\left(-\frac{1}{864}\left\{31(f_{-2}-f_2)+1408(f_{-1}-f_1)\right\}-\frac{h}{144}\left\{(f'_{-2}+f'_2)+64(f'_{-1}+f'_1)+360f'_0\right\}\right)\Big/hf'_0,$$

$$u=\left(-\frac{1}{288}\left\{41(f_{-2}+f_2)+256(f_{-1}+f_1)-594f_0\right\}-\frac{h}{96}\left\{3(f'_{-2}-f'_2)+64(f'_{-1}-f'_1)\right\}\right)\Big/hf'_0,$$

$$v=\left(\frac{1}{1152}\left\{91(f_{-2}-f_2)+1792(f_{-1}-f_1)\right\}+\frac{h}{192}\left\{3(f'_{-2}+f'_2)+128(f'_{-1}+f'_1)+396f'_0\right\}\right)\Big/hf'_0,$$

$$w=\left(\frac{1}{144}\left\{13(f_{-2}+f_2)+32(f_{-1}+f_1)-90f_0\right\}+\frac{h}{48}\left\{(f'_{-2}-f'_2)+12(f'_{-1}-f'_1)\right\}\right)\Big/hf'_0,$$

$$x=\left(-\frac{1}{576}\left\{29(f_{-2}-f_2)+272(f_{-1}-f_1)\right\}-\frac{h}{96}\left\{(f'_{-2}+f'_2)+24(f'_{-1}+f'_1)+60f'_0\right\}\right)\Big/hf'_0,$$

$$y=\left(-\frac{1}{864}\left\{11(f_{-2}+f_2)+16(f_{-1}+f_1)-54f_0\right\}-\frac{h}{288}\left\{(f'_{-2}-f'_2)+8(f'_{-1}-f'_1)\right\}\right)\Big/hf'_0,$$

$$z=\left(\frac{1}{3456}\left\{25(f_{-2}-f_2)+160(f_{-1}-f_1)\right\}+\frac{h}{576}\left\{(f'_{-2}+f'_2)+16(f'_{-1}+f'_1)+36f'_0\right\}\right)\Big/hf'_0,$$

$$\bar{z}=0.$$

$$n=6$$

$$s=\left(\frac{1}{3000}\left\{76f_{-2}+2375f_{-1}-8500f_0+5000f_1+1000f_2+49f_3\right\}\right.$$
$$\left.+\frac{h}{600}\left\{3f'_{-2}+150f'_{-1}-400f'_0-600f'_1-75f'_2-2f'_3\right\}\right)\Big/hf'_0,$$

$$t=\left(-\frac{1}{108000}\left\{3327f_{-2}+169500f_{-1}-8000f_0-168000f_1+2625f_2+548f_3\right\}\right.$$
$$\left.-\frac{h}{3600}\left\{21f'_{-2}+1500f'_{-1}+8600f'_0+1200f'_1-75f'_2-4f'_3\right\}\right)\Big/hf'_0,$$

$$u=\Big(-\frac{1}{21600}\Big\{943f_{-2}-2050f_{-1}-62550f_0+45200f_1+17575f_2+882f_3\Big\}$$
$$-\frac{h}{1440}\Big\{13f'_{-2}+260f'_{-1}-2400f'_0-2960f'_1-445f'_2-12f'_3\Big\}\Big)\Big/hf'_0,$$

$$v=\Big(\frac{1}{86400}\Big\{5729f_{-2}+121400f_{-1}-16000f_0-118400f_1+6175f_2+1096f_3\Big\}$$
$$+\frac{h}{2880}\Big\{37f'_{-2}+1720f'_{-1}+5140f'_0+1120f'_1-155f'_2-8f'_3\Big\}\Big)\Big/hf'_0,$$

$$w=\Big(\frac{1}{144000}\Big\{1274f_{-2}-84875f_{-1}-189000f_0+175000f_1+92750f_2+4851f_3\Big\}$$
$$+\frac{h}{14400}\Big\{36f'_{-2}-2175f'_{-1}-19800f'_0-20100f'_1-3600f'_2-99f'_3\Big\}\Big)\Big/hf'_0,$$

$$x=\Big(-\frac{1}{144000}\Big\{5743f_{-2}+50125f_{-1}-22000f_0-46000f_1+10625f_2+1507f_3\Big\}$$
$$-\frac{h}{4800}\Big\{39f'_{-2}+925f'_{-1}+1900f'_0+100f'_1-225f'_2-11f'_3\Big\}\Big)\Big/hf'_0,$$

$$y=\Big(\frac{1}{14400}\Big\{172f_{-2}+3275f_{-1}+3900f_0-4600f_1-2600f_2-147f_3\Big\}$$
$$+\frac{h}{480}\Big\{f'_{-2}+45f'_{-1}+200f'_0+180f'_1+35f'_2+f'_3\Big\}\Big)\Big/hf'_0,$$

$$z=\Big(\frac{1}{86400}\Big\{351f_{-2}+750f_{-1}-4000f_0+2625f_2+274f_3\Big\}$$
$$+\frac{h}{2880}\Big\{3f'_{-2}+30f'_{-1}-20f'_0-120f'_1-45f'_2-2f'_3\Big\}\Big)\Big/hf'_0,$$

$$\bar{z}=\Big(-\frac{1}{432000}\Big\{1066f_{-2}+10625f_{-1}+9000f_0-13000f_1-7250f_2-441f_3\Big\}$$
$$-\frac{h}{14400}\Big\{8f'_{-2}+175f'_{-1}+600f'_0+500f'_1+100f'_2+3f'_3\Big\}\Big)\Big/hf'_0.$$

$n=7$

$$s=\Big(\frac{1}{36000}\Big\{157(f_{-3}+f_3)+4968(f_{-2}+f_2)+43875(f_{-1}+f_1)-98000f_0\Big\}$$
$$+\frac{h}{1200}\Big\{(f'_{-3}-f'_3)+54(f'_{-2}-f'_2)+675(f'_{-1}-f'_1)\Big\}\Big)\Big/hf'_0,$$

$$t=\Big(-\frac{1}{108000}\Big\{167(f_{-3}-f_3)+8667(f_{-2}-f_2)+192375(f_{-1}-f_1)\Big\}$$
$$-\frac{h}{3600}\Big\{(f'_{-3}+f'_3)+81(f'_{-2}+f'_2)+2025(f'_{-1}+f'_1)+9800f'_0\Big\}\Big)\Big/hf'_0,$$

$$u=\Big(-\frac{1}{648000}\Big\{7339(f_{-3}+f_3)+213786(f_{-2}+f_2)+631125(f_{-1}+f_1)-1704500f_0\Big\}$$
$$-\frac{h}{21600}\Big\{47(f'_{-3}-f'_3)+2403(f'_{-2}-f'_2)+20925(f'_{-1}-f'_1)\Big\}\Big)\Big/hf'_0,$$

$$v=\Big(\frac{1}{1296000}\Big\{5206(f_{-3}-f_3)+249831(f_{-2}-f_2)+2517750(f_{-1}-f_1)\Big\}$$
$$+\frac{h}{129600}\Big\{94(f'_{-3}+f'_3)+7209(f'_{-2}+f'_2)+125550(f'_{-1}+f'_1)+340900f'_0\Big\}\Big)\Big/hf'_0,$$

$$w=\Big(\frac{1}{5184000}\Big\{52109(f_{-3}+f_3)+1310016(f_{-2}+f_2)+1525875(f_{-1}+f_1)-5776000f_0\Big\}$$
$$+\frac{h}{172800}\Big\{337(f'_{-3}-f'_3)+15648(f'_{-2}-f'_2)+88275(f'_{-1}-f'_1)\Big\}\Big)\Big/hf'_0,$$

$$x=\Big(-\frac{1}{5184000}\Big\{18493(f_{-3}-f_3)+772368(f_{-2}-f_2)+4174125(f_{-1}-f_1)\Big\}$$
$$-\frac{h}{518400}\Big\{337(f'_{-3}+f'_3)+23472(f'_{-2}+f'_2)+264825(f'_{-1}+f'_1)+577600f'_0\Big\}\Big)\Big/hf'_0,$$

$$y=\Big(-\frac{1}{1728000}\Big\{6217(f_{-3}+f_3)+117408(f_{-2}+f_2)+72375(f_{-1}+f_1)-392000f_0\Big\}$$
$$-\frac{h}{57600}\Big\{41(f'_{-3}-f'_3)+1584(f'_{-2}-f'_2)+6675(f'_{-1}-f'_1)\Big\}\Big)\Big/hf'_0,$$

$$z=\Big(\frac{1}{1728000}\Big\{2209(f_{-3}-f_3)+70584(f_{-2}-f_2)+272625(f_{-1}-f_1)\Big\}$$
$$+\frac{h}{172800}\Big\{41(f'_{-3}+f'_3)+2376(f'_{-2}+f'_2)+20025(f'_{-1}+f'_1)+39200f'_0\Big\}\Big)\Big/hf'_0,$$

$$\bar{z}=\Big(\frac{1}{5184000}\Big\{2783(f_{-3}+f_3)+38592(f_{-2}+f_2)+14625(f_{-1}+f_1)-112000f_0\Big\}$$
$$+\frac{h}{172800}\Big\{19(f'_{-3}-f'_3)+576(f'_{-2}-f'_2)+2025(f'_{-1}-f'_1)\Big\}\Big)\Big/hf'_0.$$

For every n, the formula for p is the following:

$$p=r-r^2s+r^3(2s^2-t)+r^4(-5s^3+5st-u)+r^5(14s^4-21s^2t+3t^2+6su-v)+r^6(-42s^5+84s^3t$$
$$-28st^2-28s^2u+7tu+7sv-w)+r^7(132s^6-330s^4t+180s^2t^2+120s^3u-12t^3-72stu-36s^2v+4u^2$$
$$+8tv+8sw-x)+r^8(-429s^7+1287s^5t-990s^3t^2-495s^4u+495s^2tu+165st^3+165s^3v-45t^2u$$
$$-45su^2-90stv-45s^2w+9uv+9tw+9sx-y)+r^9(1430s^8-5005s^6t+5005s^4t^2+2002s^5u$$
$$-1430s^2t^3-2860s^3tu-715s^4v+55t^4+660st^2u+330s^2u^2+660s^2tv+220s^3w-55tu^2-55t^2v$$
$$-110suv-110stw-55s^2x+5v^2+10uw+10tx+10sy-z)+r^{10}(-4862s^9+19448s^7t-24024s^5t^2$$
$$-8008s^6u+10010s^3t^3+15015s^4tu+3003s^5v-1001st^4-6006s^2t^2u-2002s^3u^2-4004s^3tv$$
$$-1001s^4w+286t^3u+858stu^2+858s^2tw+858st^2v+858s^2uv+286s^3x-22u^3-132tuv-66t^2w$$
$$-66sv^2-132suw-132stx-66s^2y+11vw+11ux+11ty+11sz-\bar{z})+\cdots.$$

[1] H. E. Salzer, A new formula for inverse interpolation, Bul. Am. Math. Soc. **50,** 513 (1944).

[2] H. E. Salzer, Inverse interpolation for eight-, nine-, ten-, and eleven-point direct interpolation, J. Math. Phys. **24,** 106 (1945).

[3] T. Fort, Finite differences, p. 85 (Clarendon Press, Oxford, England, 1948).

[4] J. F. Steffensen, Interpolation, p. 33 (Williams & Wilkins, Baltimore, Md., 1927).

[5] H. E. Salzer, New formulas for facilitating osculatory interpolation, J. Research NBS **52,** 211 (1954) RP2491.

[6] National Bureau of Standards, Table of the Bessel functions $J_0(z)$ and $J_1(z)$ for complex arguments (Columbia University Press, New York, N. Y., 1943; 2d ed. 1947).

[7] Harvard Computation Laboratory, The annals of the computation laboratory of Harvard University **III,** Tables of the Bessel functions of the first kind of orders zero and one (Harvard University Press, Cambridge, Mass., 1947).

[8] National Bureau of Standards, Table of the Bessel functions $Y_0(z)$ and $Y_1(z)$ for complex arguments (Columbia University Press, New York, N. Y., 1950).

[9] Tables of normal probability functions, NBS AMS23 (1953); Tables of the error function and its derivative, NBS AMS41 (1954).

[10] Tables of sine, cosine, and exponential integrals, NBS MT5; NBS MT6 (1940).

[11] Table of sine and cosine integrals for arguments from 10 to 100, NBS AMS32 (1954).

WASHINGTON, September 27, 1955.

U. S. GOVERNMENT PRINTING OFFICE: 1956

Recent Publications of the National Bureau of Standards

Journal of Research of the National Bureau of Standards, volume 55, No. 5, November 1955 (RP2626 to RP2632 incl.). Annual subscription $4.00.

Technical News Bulletin, volume 39, No. 11, November 1955. 10 cents. Annual subscription $1.00.

Basic Radio Propagation Predictions for February 1956. Three months in advance. CRPL-D 124. Issued November 1955. 10 cents. Annual subscription $1.00.

Research Papers

Journal of Research, volume 55, number 5, November 1955. Single copies of the Journal vary in price. Single copies of Research Papers appearing in the Journal are not available for sale. The Superintendent of Documents, U. S. Government Printing Office, Washington 25, D. C., will reprint 100 or more copies of a Research Paper. Request for the purchase price should be mailed promptly to that office.

RP2626. Properties of piezoelectric ceramics in the solid-solution series lead titanate-lead zirconate-lead oxide: tin oxide and lead titanate-lead hafnate. B. Jaffe, R. S. Roth, and S. Marzullo.

RP2627. Heat capacity, heats of fusion and vaporisation, and vapor pressure of decaborane ($B_{10}H_{14}$). George T. Furukawa and Rita P. Park.

RP2628. Preparation of titanium tetrachloride of high purity. W. Stanley Clabaugh, Robert T. Leslie, and Raleigh Gilchrist.

RP2629. Liquid-vapor phase equilibrium in solutions of oxygen and nitrogen at pressures below one atmosphere. George T. Armstrong, Jack M. Goldstein, and D. Ellis Roberts.

RP2630. Precise measurement of wavelengths in infrared spectra. Earle K. Plyler, Lamdin R. Blaine, and Eugene D. Tidwell.

RP2631. Ideal gas thermodynamic functions of the isotopic hydrogen sulfides. Lester Haar, Joe C. Bradley, and Abraham S. Friedman.

RP2632. Measurement of field distortion in free-air ionisation chambers by analog method. William Miller and Robert J. Kennedy.

Miscellaneous Publications

M216. Report of the 40th National Conference on Weights and Measures. 70 cents.

Publications in Other Journals

Absorption by concrete of X-rays and gamma-rays. R. E. Foster. BuDocks Technical Digest No. 56, May 1955.

Paper milk containers. M. W. Jensen. Scale Journal (176 W. Adams St., Chicago 3, Ill.) 41, No. 12, 8 (Sept. 1955).

Distribution of electrons scattered by gold. L. Marton, J. Arol Simpson, and T. F. McCraw. Phys. Rev. (57 E. 55th St., New York 22, N. Y.) 99, No. 2, 495 (July 1955).

Physiological monitor for anesthesia. S. R. Gifford and H. P. Broida. Electronics (330 W. 42d St., New York 36, N. Y.) 28, No. 10, 180 (Oct. 1955).

Crazing of acrylic resins. W. T. Sweeney, G. M. Brauer, and I. C. Schoonover. J. Dental Research (International Assoc. for Dental Res., C. V. Mosby Co., St. Louis 3, Mo.) 34, No. 3, 306 (June 1955).

Atomic flames: spectra, "temperatures," and products. R. E. Ferguson and H. P. Broida. Fifth Symposium (International) on Combustion published by Reinhold Publishing Corp. (430 Park Ave., New York 22, N. Y.) 754 (1955).

Information theory aspects of propagation through time-varying media. Joseph Feinstein. J. Appl. Phys. (57 E. 55th St., New York 22, N. Y.) 26, No. 2, 219 (Feb. 1955).

Nonlinear theory of space-charge wave in moving, interacting electron beams with application to solar radio noise. Hari K. Sen. Phys. Rev. (57 E. 55th St., New York 22, N. Y.) 97, No. 4, 849 (Feb. 1955).

Temperature control during mixing of rubber compounds. Frank L. Roth, George E. Decker, and Robert D. Stiehler. Rubber World (386 4th Ave., New York 16, N. Y.) 132, 482 (July 1955).

Generation of Coulomb wave functions by means of recurrence relations. Irene A. Stegun and Milton Abramowitz. Phys. Rev. (57 E. 55th St., New York 22, N. Y.) 98, No. 6, 1851 (June 1955).

Publications for which a price is indicated are available only from the Superintendent of Documents, U. S. Government Printing Office, Washington 25, D. C. (foreign postage, one-third additional). Reprints from outside journals are not available from the National Bureau of Standards but can often be obtained from the publishers.

UNITED STATES
GOVERNMENT PRINTING OFFICE
DIVISION OF PUBLIC DOCUMENTS
WASHINGTON 25, D. C.

OFFICIAL BUSINESS

PENALTY FOR PRIVATE USE TO AVOID
PAYMENT OF POSTAGE, $300
(GPO)

Journal of Research of the National Bureau of Standards Vol. 56, No. 1 January 1956

Contents

		Page
Dielectric constant of water from 0° to 100° C. C. G. Malmberg and A. A. Maryott.	RP2641	1
A calorimeter for measuring the power in a high-energy X-ray beam. John McElhinney, Bernard Zendle, and Steve Domen.	RP2642	9
Pyrochlore-type compounds containing double oxides of trivalent and tetravalent ions. Robert S. Roth.	RP2643	17
Thermal decomposition of polytetrafluoroethylene in various gaseous atmospheres. L. A. Wall and J. D. Michaelsen.	RP2644	27
Abscissas and weights for Gaussian quadratures of high order. P. Davis and P. Rabinowitz.	RP2645	35
Behavior of cements and related materials under hydrostatic pressures up to 10,000 atmospheres. C. E. Weir, C. M. Hunt, and R. L. Blaine.	RP2646	39
Formulas for inverse osculatory interpolation. Herbert E. Salzer.	RP2647	51-54

Single copies of the above Research Papers are not available for sale, but the Superintendent of Documents, U. S. Government Printing Office, Washington 25, D. C., will reprint 100 or more copies, and request for the purchase price should be mailed promptly to that Office.

[A list of recent NBS publications is given on page 3 of the cover.]

For sale by the Superintendent of Documents, U. S. Government Printing Office, Washington 25, D. C. Price 60c (single copy). Subscription price: $4.00 a year; $1.25 additional for foreign mailing. Single copies vary in price.

UNITED STATES GOVERNMENT PRINTING OFFICE, WASHINGTON : 1956